Dynamics of Passive Scalars and Probe Particles in Driven Diffusive Systems

Sakuntala Chatterjee

Department of Theoretical Physics

Tata Institute of Fundamental Research

Mumbai, India.

A thesis submitted for the degree of

Doctor of Philosophy

January, 2008

Declaration

I state that the work embodied in this thesis forms my own contribution to the research work carried out under the guidance of Prof. Mustansir Barma. This work has not been submitted for any other degree to this or any other University or body. Whenever references have been made to previous works of others, it has been clearly indicated.

(signature of the supervisor) (signature of the candidate)

Acknowledgements

First of all, I would like to thank Mustansir for his patient guidance over the last five years. His emphasis on perfection and strong sense of ethics have had a deep influence on me. His care and constant encouragement have made my thesis work much easier and pleasant.

I am indebted to Deepak for many illuminating discussions and useful suggestions. I also thank him for many insightful comments during seminars. It was very nice to have Kedar around. Quite often I found his questions and comments in seminars extremely useful. I also thank him for his friendliness. Special thank goes to Vikram for organising "Monday Meetings" regularly and making this seminar series more coherent.

I would like to thank all the office staff in our department for their support and their readiness to help.

I am grateful to Anindya for managing all our computers so efficiently. I also thank him for being a wonderful friend.

I am lucky to have found many good friends in TIFR. They have made my stay here really enjoyable through their love and affection.

Finally, I would like to thank my parents and relatives for their unconditional love and support, without which nothing would have been possible.

to my parents

Contents

Synopsis

A wide variety of physical processes, ranging from turbulent fluids to sandpiles and moving traffic, falls under the class of "driven diffusive systems" where an external drive is applied to constantly maintain the system in a nonequilibrium steady state. In certain driven diffusive systems, it is natural to identify two coupled sub-systems (or fields) which interact with and may influence each other. Consider fluorescent dye carried by a turbulent jet or dust particles moving in air. In such situations the density field of the dye (dust) is coupled to the velocity field of the fluid jet (air). However, these advected substances are 'passive', *i.e.* they have a negligible effect on the fluid flow. In other words, the coupling is one way. In other type of situations, the coupling works both ways. For example, introduction of tracer particles to probe a medium sometimes results in a coupled system where dynamical evolution of both the 'probe particles' and the medium get strongly affected by each other. In this thesis, we have investigated both these kinds of coupling by studying simple models which we describe below.

A broad field of research, which deals with the first kind of coupling, is the field of "passive scalar" where the dynamics of a nonequilibrium driving field strongly affects that of the other (passive) scalar field with no back-effect from the latter. In many situations, the passive scalar field spreads out in space to reach a homogeneous state. However, in certain cases, (*e.g.* when the driving field describes the velocity of a compressible fluid) the advected passive scalar field may show a clustering tendency [1, 2]; we have considered one such example here. The specific system we study consists of hard-core particles sliding under gravity on a one dimensional fluctuating interface; the instantaneous force on the particles is then proportional to the local slope of the surface [3]. Earlier studies of static properties of this system show that starting from a randomly disordered state, the sliding particles evolve towards a state with long-ranged order [3]. However, this is an unusual kind of ordered state where strong fluctuations are always present giving rise to a broad distribution of order parameter even in the thermodynamic limit.

We have carried out a dynamical characterisation of this new kind of ordered state. To our knowledge, the dynamics of passive scalars in general, has not been explored systematically, and our study adds to the relatively sparse work on this important question [4]. We have obtained results for auto-correlation and space-time correlation functions in steady state and aging correlations in the approach to steady state. We find that both types of correlation functions follow a scaling description. In steady state, these scaling forms show a strong dependence on the system size L, as reminiscent of ordinary phase-ordered systems [5]. However, in contrast to a linear decay normally expected for phase-ordered systems [5] in the limit of small argument, the scaling function of steady state auto-correlation decays with a cusp. It is therefore interesting to understand the nature of phase-ordering present in the steady state. As mentioned above, strong fluctuations are present in the steady state and do not decrease even in thermodynamic limit [3]. The question then arises in what sense is the system in an ordered state, if strong fluctuations drive it between macroscopically different configurations on a relatively rapid time-scale? We have addressed this by studying the variation of the length of the largest particle cluster present in the system and show that the corresponding probability distribution provides an unequivocal signal of ordering.

The second type of coupling is more frequently encountered. For instance, quite often the driven system is not really 'passive' but produces a back-effect on the driving system. For example, useful information about a complex system is often obtained by introducing probe particles into it. Although it is generally assumed that for low enough concentration of the probe particles the medium is not strongly affected by their presence, in certain cases this assumption can break down. The probe particles can indeed produce a strong effect on the medium even when present in a vanishingly low concentration. At the same time, the medium may also induce correlations between the probe particles. We have demonstrated this for a class of models of probe particles in one dimension which evolve through

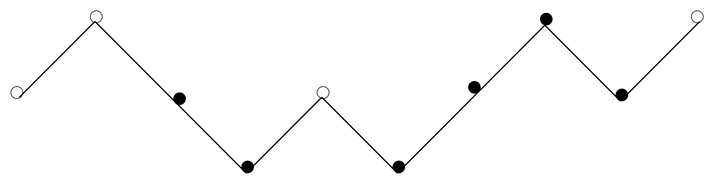

Figure 1: *Hard-core particles(shown by solid circle) sliding towards the local valleys. The hollow circles represent the empty sites or holes.*

moves that violate detailed balance. In our model, these nonequilibrium probes are found to produce a drastic effect on a medium which is initially in equilibrium: even when a single such probe is present, the system develops a macroscopic density gradient and evolve towards a nonequilibrium current-carrying steady state. However, if the medium is initially in a nonequilibrium state, the effect is less drastic. The density perturbation created by a single probe does not extend through macroscopic distances, but depending on the kinematics of the probe and the medium, may either decay as a power law, or as an exponential [6]. This gives rise to an interesting phase diagram (fig 3). For a finite density of probes, we have monitored time-dependent correlations involving the displacement of the tagged probe particles. We have found that the above phase diagram for a single probe has important consequences on the dynamical properties of the macroscopic number of probe particles.

The two problems discussed above are described in more detail below.

Dynamics of Passive Scalars

The specific passive scalar model we have considered consists of a set of hard-core particles sliding downwards (under gravity) on an independently fluctuating one dimensional surface (see fig 1). The driving field in this case is the fluctuating slope of the surface and the passive scalar field is the density field of the sliding particles. The passive scalar field undergoes diffusion and also gets advected (carried along) by the driving field. We have considered two kinds of surface evolutions—dynamical rules in one kind respect symmetry under reflection about the reference axis (Edwards-Wilkinson or EW surface [7]) while the other kind violates this symmetry (Kardar-Parisi-Zhang or KPZ surface [8]). Using the mapping between the KPZ interface and the vorticity-free Burgers fluid [8], the particles sliding on the KPZ interface can be equivalently described as passive scalars advected by a noisy Burgers flow.

To monitor dynamical correlations of the density fluctuation of the particles, we performed Monte Carlo simulation on a discrete lattice model. The hard-core particles are represented by the variables $\{\sigma_i\}$, each of which can take a value $+1$ or -1 according as the i-th site is occupied or empty. We measured auto-correlation and space-time correlation functions in steady state and aging correlations in the approach to steady state. We have also done analytical calculations on a coarse-grained surface model explained below.

Due to gravity the particles tend to slide down into local valleys of the surface. Therefore, it is plausible that the dynamics of hills and valleys of the interface may provide insight into the dynamics of the particles. To this end, we define a coarse-grained depth model (CD model) as follows [3]. Consider the variable $s_i(t)$ defined as $s_i(t) = sgn[h_i(t) - \langle h(t)\rangle]$, where $h_i(t)$ is the height of the interface at the i-th site at time t and $\langle h(t)\rangle$ is the average height $\frac{1}{L}\sum_{i=1}^{L} h_i(t)$. The variable $s_i(t)$ can take the values $+1$, -1 or 0, depending on whether the position of the i-th site is above, below or at the average level. In other words, $s_i(t)$ gives a coarse-grained description of the surface by labeling 'highlands' and 'lowlands'. For an EW interface, the dynamics is tractable and we obtain an analytic expression for time-dependent correlations of $s_i(t)$, using the arc-sine law for Gaussian variables [9]. These results might be expected to be close to those of the sliding particles density, in the extreme adiabatic limit, when the surface evolves infinitely more slowly than the particles. As a matter of fact, we find that they also describe qualitatively the particle behavior even when the surface movement and the particle movement occurs at comparable time-scale. In this strongly nonequilibrium case, before the particles can fill in the lowest valleys, the interface evolves, often causing the valleys to turn over. For a system of size L, the lifetime of a typical deep valleys is $\sim L^z$ which is therefore the time-scale over which the macroscopic state of the system changes, in contrast to an exponential time-scale for regular phase ordering. This implies that the system always undergoes strong fluctuations, despite the clustering tendency among the particles. This gives rise to an unusual kind of fluctuation dominated phase-ordering (FDPO) and below we summarise our results for the dynamics of this new ordered state. We have performed Monte Carlo simulation for measuring various functions of the density field $\sigma_i(t)$ and the CD variable $s_i(t)$. We have been able to analytically calculate the correlation functions of $s_i(t)$ for an EW surface.

Auto-correlation in Steady State

We have measured the steady state auto-correlation $A(t, L)$ involving the density variable $\langle \sigma_i(0)\sigma_i(t)\rangle$ of the particles and the CD variables $\langle s_i(0)s_i(t)\rangle$ for the surface. Here, the averaging is done over different initial configurations drawn from the steady state ensemble. We find that $A(t, L)$ is a scaling function of t/L^z, where z is the surface dynamic exponent. In this limit of small scaling argument, the scaling function decays with a cusp [see fig 2]: $m^2 \left[1 - b\left(\frac{t}{L^z}\right)^{\beta}\right]$. For a customary phase-ordering system, the steady state auto-correlation is expected to decay linearly. The presence of a cusp ($\beta < 1$) is one manifestation of the unusual kind of phase-ordering. The constant m is a measure of the long-range order present in the system. Table 1 summarises the values of m and β for different cases. These values correspond to the case when the system is half-filled. Our measurement for other values of filling fractions show that the cusp exponent β remains same while the value of the intercept changes.

For small time $t \lesssim 1$ which falls outside the scaling regime, the auto-correlation function shows a linear drop with a slope $\sim L^{\delta}$ [see table 1]. Using the mapping between a typical configuration of one-dimensional EW or KPZ interface and the trajectory of a one-dimensional random walker with L steps, it can be argued that for CD model $\delta = 1/2$.

Auto-correlation in Aging Regime

In the aging regime, *i.e.* during the approach towards steady state, the system does not have time translational invariance. The aging auto-correlation $\mathcal{A}(t_1, t_2)$, defined as $\langle \sigma_i(t_1)\sigma_i(t_1 + t_2)\rangle$ for the particles and as $\langle s_i(t_1)s_i(t_1 + t_2)\rangle$ for the CD variables, does not depend only on the time difference t_2 but also on t_1 [5]. In

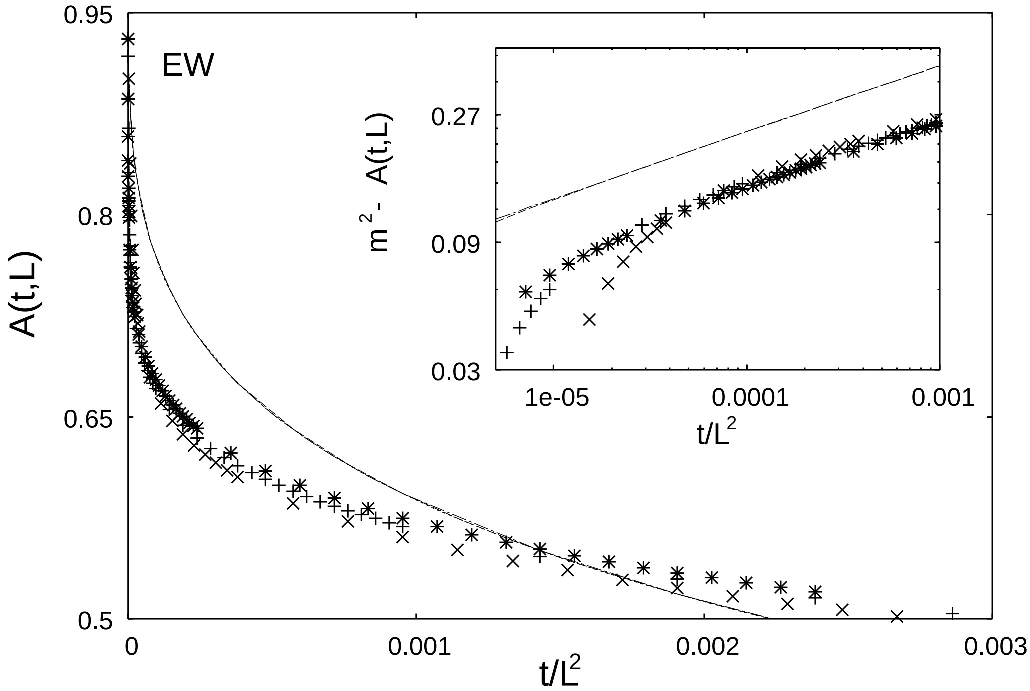

Figure 2: *Numerical results for scaled auto-correlation function for the particles sliding on an EW surface are shown by discrete points. The continuous line shows exact calculation in CD model for EW surface. In both cases we used* $L = 512, 1024, 2048$*. The cusp exponent is shown in the inset.*

fact $\mathcal{A}(t_1, t_2)$ is found to be a scaling function of t_1/t_2. In the limit when $t_1 \gg t_2$, the scaling function decays with a cusp, as in steady state, only the system size L is replaced by $t_1^{1/z}$, meaning that locally the system has reached steady state over a length scale of $t_1^{1/z}$. In the opposite limit $t_2 \gg t_1$, we find $\mathcal{A}(t_1, t_2) \sim (t_1/t_2)^{\gamma}$, as expected for a phase-ordering systems.

Space-time Correlation in Steady State

The space-time correlation $G(r, t, L)$ defined in steady state as $\langle \sigma_i(0)\sigma_{i+r}(t)\rangle$ for the particles and $\langle s_i(0)s_{i+r}(t)\rangle$ for the CD variables, does not show any L-independent scaling between r and t. Rather, it is a function of the scaled variables $\xi = r/L$ and $\tau = t/L^z$. With ξ held fixed, the scaling function shows an interesting non-monotonic behavior with τ. For $\tau = 0$, this scaling function

	Surface Model		Particle Model	
	EW	KPZ	EW	KPZ
m^2	1.0	1.0	0.82 ± 0.03	0.75 ± 0.04
β	0.25	0.31 ± 0.02	0.22 ± 0.02	0.18 ± 0.01
δ	0.5	0.5	0.26 ± 0.005	0.15 ± 0.005
γ	0.75	0.84 ± 0.02	0.69 ± 0.02	0.82 ± 0.04

Table 1: *The values of relevant exponents and intercepts for dynamical characterization of surface model and particle model*

corresponds to spatial (equal-time) correlation and for $\tau \gg \xi^z$, it decays like the auto-correlation function, as expected.

Largest Cluster in Steady State

In steady state, large clusters are present in the system and the cluster size distribution follows a power law. Because of strong fluctuations these clusters undergo large changes in their lengths, associated with the fact that the macroscopic state of the system keeps changing over a time-scale $\sim L^z$. The question arises: if the lifetime of a macrostate is so much smaller than an exponential, in what sense, can we call such a state a "ordered phase"? We have addressed this question by studying the largest cluster $l_{max}(t)$ present in the system at time t. We show that in steady state $l_{max}(t)$ fluctuates strongly, thereby changing the macrostate of the system, but it continues to remain substantially above its disordered state value ($\sim \log L$). In other words, the system manages to retain its ordered character despite strong steady state fluctuations.

Dynamics of Nonequilibrium Probes in Driven Diffusive Systems

In this problem, we aim to understand how the dynamical evolution of a medium gets affected by the presence of some special kind of probe particles in the low dilution limit, and the influence of the medium on the probe dynamics itself.

We have considered medium which can be described by simple one dimensional lattice models of nonequilibrium (driven) systems and their equilibrium counterparts. We have mainly considered two different kinds of nonequilibrium probe particles—shock tracking probes (STPs) and directed probe particles (DPPs). The exchange rules are:

$$
\begin{aligned}
&Medium: \qquad && +- \xrightarrow{1} -+ \\
& && -+ \xrightarrow{q} +- \\
& && \\
&Probe: && 0- \xrightarrow{1} -0 \\
& && +0 \xrightarrow{w} 0+
\end{aligned}
\tag{1}
$$

where '+' denotes a particle, '−' denotes a hole and '0' denotes a probe. STPs exchange with the particles and holes of the medium in opposite directions but with equal rates, *i.e.* $w = 1$. For a DPP on the other hand, these two rates are different—we consider $w < 1$. Both these types of probes tend to settle in the regions of strong density variations or 'shocks'. However, depending on the system under study, the density profile around a probe can be qualitatively different. In the low concentration limit of the probes, different behaviors are found—ranging from diverging correlation lengths and power law decays to effects which are felt over macroscopic distances throughout the system. We relate these differences to an interesting interplay between the equilibrium and nonequilibrium characteristics of the medium and the probe particles. We summarise our results for these different systems below.

Probes in an Initially Equilibrium Medium

STPs and DPPs are found to produce a strong effect on a medium that is initially in an equilibrium state. We have considered a medium described by symmetric exclusion process (SEP), which correspond to $q = 1$ in Eq 5.1. Throughout the top thick line shown in fig 3, our numerical simulation shows that introduction of even a single probe gives rise to a macroscopic density gradient across the system and a (small) current. This can be explained as follows. Presence of even a single nonequilibrium probe in an equilibrium diffusive medium would

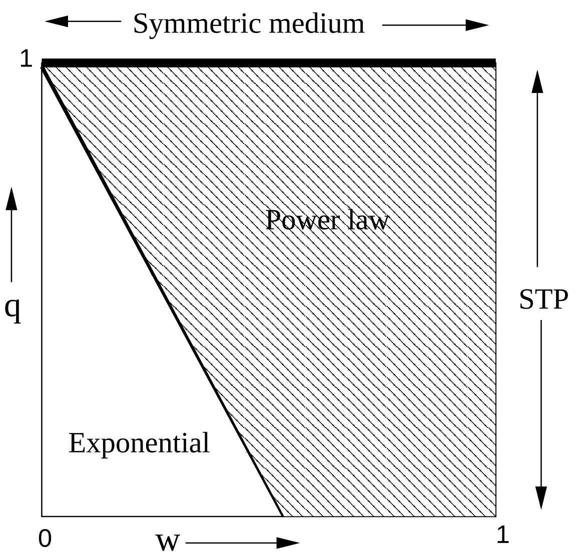

Figure 3: *Phase diagram for nonequilibrium probes in a nonequilibrium medium. The x-axis refers to properties of the probe and the y-axis refers to properties of the medium.*

imply that the resulting steady state should have nonequilibrium characteristics, *i.e.* there should be a current in the system. Now, the only way a diffusive system can support a current is by maintaining a concentration gradient. When several such probes are introduced, we find that the medium induces a strong attraction among the probes and they phase separate. We have found that these conclusions remain valid for other class of symmetric medium, described by the Kawasaki model [10] or the symmetric version of k-hop model [11].

Probes in an Initially Nonequilibrium Medium

Interesting effects are observed for a medium that is initially maintained in a nonequilibrium steady state by some external drive. We are primarily interested in the case when the medium can be described by an asymmetric simple exclusion processes (ASEP), which corresponds to $q < 1$. When DPPs are introduced in such a medium, depending on the exchange rates q for the medium and w for the probes, qualitatively different effects are found and this gives rise to an interesting phase diagram [fig 3]. Earlier studies [6, 12] of this model in presence of a single

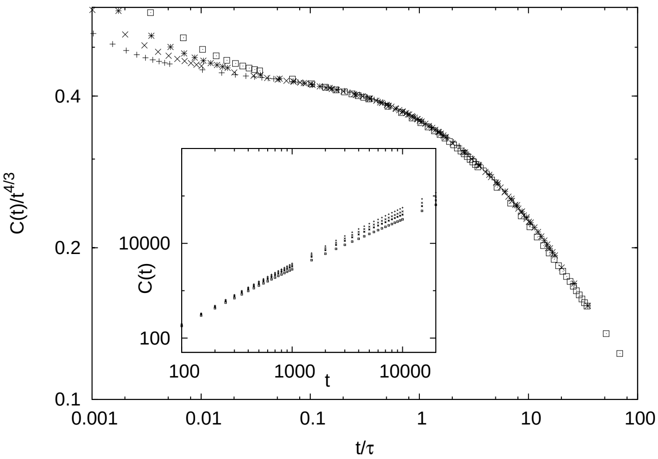

Figure 4: *Scaling collapse for mean square displacement $C(t)$ of tagged STPs for $q = 0$ for probe density $\rho_0 = 0.08, 0.1, 0.12, 0.15$ (moving upwards) and system size $L = 131072$. Inset shows the unscaled data.*

probe show that in the unshaded part of the phase diagram, the effect produced by a single probe is short-ranged—the density profile around the probe decays exponentially over a finite length scale; in the shaded region of the phase-diagram, the density profile around the single probe relaxes as a power law. These two regions of the phase diagram are separated by a critical line along which the density profile around a single probe shows the same power law decay as found in the shaded region. We have calculated the the slope of this critical line using mean field theory. In [13] a macroscopic number of probes has been considered for $w = 1$, $q = 0$ and a correlation length is found which diverges strongly in the limit of low probe concentration.

We have studied the dynamical properties of a macroscopic number of probes for general values of q and w. Our numerical simulations show that in the shaded region of the phase-diagram, the mean squared displacement $C(t)$ of the tagged probes undergoes a crossover from a superdiffusive regime at early times to a diffusive regime at late times. The crossover time-scale τ diverges in the limit of low probe concentration and enters into a scaling description of several dynamical properties of the probes. In fig 4 the scaling collapse of $C(t)$ is shown for $w = 1$ and $q = 0$. No such diverging time-scale is found for the unshaded region of the phase diagram where the effect is short-ranged. We have also investigated other types of driven diffusive systems described by the k-hop model [11] and the partially asymmetric variation of Katz-Lebowitz-Spohn model [14]. We find that in all these cases, dynamics of STPs always associates a diverging time-scale which allows for scaling description of dynamical correlation functions. DPPs on the other hand, may give rise to short ranged or long-ranged effect depending on the properties of the medium and probe itself. However, mapping out the full phase-diagram for these systems needs further detailed study.

Bibliography

[1] K. Gawedzki and M. Vergassola, *Physics D* **138**, 63 (2000). i

[2] A.Nagar, M. Barma and S.N. Majumdar, *Phys. Rev. Lett* **94**, 240601 (2005). i

[3] D. Das, M. Barma and S.N. Majumdar, *Phys. Rev. E* **64**, 046126 (2001). i, ii, iv

[4] D. Mitra and R. Pandit, *Phys. Rev. Lett* **95**, 144501 (2005). ii

[5] A.J. Bray *Adv. Phys. 51*, 481 (2002). ii, v

[6] K. Mallick *J. Phys. A: Math. Gen* **29**, 5375 (1996). iii, ix

[7] S.F. Edwards and D.R. Wilkinson *Proc. R. Soc. London, Ser. A* **381**, 17 (1982). iii

[8] E. Medina, T. Hwa and M. Kardar *Phys. Rev. A* **39**, 3053 (1989). iv

[9] W. Feller *An Introduction to Probability Theory and Its Application* vol I (John Wiley & Sons, 1970). iv

[10] K. Kawasaki in *Phase Transitions and Critical Phenomena* vol II (Academic Press, 1972), edited by C. Domb and M. Green. ix

[11] P.M. Binder, M. Paczuski and M. Barma *Phys. Rev. E* **49**, 1174 (1994) ix, xi

[12] T. Sasamoto *Phys. Rev. E* **61**, 4980 (2000). ix

[13] B. Derrida, S.A. Janowsky, J.L. Lebowitz and E.R. Speer *J. Stat. Phys.* **73**, 813 (1993). x

[14] S. Katz, J.L. Lebowitz and H. Spohn *J. Stat. Phys.* **34**, 497 (1984). xi

Chapter 1

Introduction

Driven Diffusive Systems

The term "driven diffusive systems" describes a wide variety of physical systems ranging from turbulent fluids to sand-piles and moving traffic. These are systems out of equilibrium under the influence of an external drive. In these multiparticle systems, individual particles have a diffusive motion apart from an overall systematic drift. Because the the system is constantly driven from outside, it never attains equilibrium, but in the long time limit, goes towards a nonequilibrium steady state. In this nonequilibrium steady state, the detailed balance does not hold, (*i.e.* the probability that the system goes from one particular configuration C to another configuration C' is not same as the probability of going from C' to C). Such non-equilibrium systems are beyond the scope of Boltzmann-Gibbs framework. As a result, much of the intuition developed from equilibrium statistical physics does not work for these non-equilibrium driven systems. For example, the arguments based on the competition between energy and entropy often fail dramatically [1].

One important question for these driven systems is the form of the steady state measure $P(C)$ [2]. Further, the study of correlation functions of the dynamical variables and also their average values shed light on the steady state properties of such a system. Finally, in order to explore the relaxation of the system, static and dynamic characterisations are also carried out during its approach towards the steady state.

In the absence of any general framework for the statistical description of these nonequilibrium driven systems, one usually investigates specific model systems, and these studies sometimes yield an understanding about general behavior of systems in the same universality class. For example, flowing grains on a sandpile [3], river networks [4], biological evolution of interacting species—all these systems have been modelled and are known to exhibit self-organised criticality which is characterised by power law distribution of the size of avalanches (number of correlated events).

Another class of models involve growth of materials on the top of substrates. The fluctuations of the surface height follow a scaling description [5].

$$\langle [h(x,t) - h(x',t')]^2 \rangle \approx |x - x'|^{2\chi} \ Y\left(\frac{|t-t'|}{|x-x'|^z}\right) \tag{1.1}$$

where $h(x,t)$ is the height of the surface at point x at time t and Y is a scaling function. The roughness exponent χ and the dynamic exponent z characterise the universality class for similar growth processes [5]. In section 2.1.1 of chapter 2 we discuss in more detail about this class of models.

In order to understand many generic properties of driven diffusive systems, simple particle hopping models on a lattice prove to be extremely useful. The simplest such model is 'asymmetric simple exclusion process' (ASEP) which describes hard-core particles on a lattice (a lattice gas) with a preferential direction of motion. This model has been intensively studied and provides useful insight into several aspects of driven diffusive systems. Fortunately, in one dimension, ASEP allows for many exact calculations. Recently, Prähofer and Spohn have even calculated the *complete scaling function* for dynamical correlation function for density [7]. Several variants of the ASEP have been successfully used to model systems like vehicular traffic flow [8] and movement of motor-proteins along micro-tubules inside a cell [9].

Although no phase transition is possible for an equilibrium system in one dimension, driven diffusive systems often show phase transition in one dimension and interesting phase diagrams are obtained. For instance, in an ASEP in an

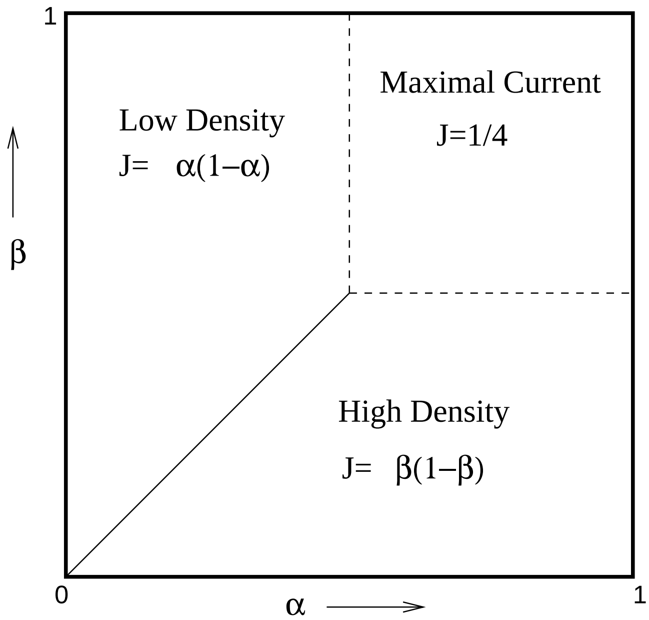

Figure 1.1: *Phase diagram for 1-d ASEP in an open chain with injection rate α and extraction rate β. The macroscopic density and the bulk current J characterise different phases. The solid line represents a first order phase transition while the dashed lines correspond to continuous transitions.*

open chain, by changing the boundary rates of injection (α) and extraction (β), one can induce transitions between steady state phases with different macroscopic densities and currents [6]. These different phases are summarised in the phase diagram shown in fig 1.

Even in absence of any boundary effect, driven diffusive systems may show interesting bulk phase separation in one dimension. In [10] a closed chain with three kinds of particles (also known as ABC model) was considered where an asymmetric exchange takes place between two unlike particles. In this one dimensional system with local dynamics, a phase separation of the three species takes place, although for an equilibrium system in one dimension with short ranged interaction, no phase separation is possible. In [28] Lahiri *et al.* studied a system of two coupled lattice gases used to model sedimenting colloidal crystals. They found that by changing the coupling parameter, it is possible to have a strong phase separation in the steady state. Another completely different kind of phase ordering had been observed by Das *et al.* [24, 25]. They considered a set of hard-core particles sliding locally downwards (under gravity) on a one dimensional fluctuating surface and found that in steady state the particles show an unconventional phase ordering where strong fluctuations are always present. This is called fluctuation dominated phase ordering (FDPO) [25]. In chapter 2 and 3 of this thesis we will have a detailed discussion on various properties of FDPO.

Coupled Driven Diffusive Systems

In this thesis, we are interested in the situation when two such driven diffusive systems are coupled together. Several examples of such coupled systems are found in nature. It is an interesting question to ask how the properties of the individual systems are affected by the coupling present. Consider the example of ant trails [11]. Ants move preferentially along the direction of increasing pheromone density and while doing so they drop pheromones for other ants to follow. The density fields of the pheromone and the ants therefore constitute a two-way coupled system and this coupling results in interesting patterns in the ant traffic [11]. Sedimentation of colloidal crystals in viscous fluids [28], motion of a polymer in a random medium or a vortex line in a superconductor with randomly distributed impurities [29] are other examples of coupled driven systems.

Quite often this bidirectional coupling gives rise to many complications. Consider the example of sedimentation—the settling of heavier particles in a lighter fluid. Due to viscous damping, when a given particle is slowed down by the fluid, its momentum does not disappear but produces disturbances in the fluid which affect the motion of other particles [12, 13]. This makes the full description of sedimentation a challenging problem [14].

Passive Scalars vs Probe Particles

In certain situations, for example, when (i) the coupling itself is weak or (ii) the sizes of the two coupled systems are not comparable, the bidirectional coupling can be expected to be effectively unidirectional. We will mainly be interested in the second scenario. Consider a fluorescent dye carried by a turbulent jet or smoke particles dispersed in air [15]. Here, the density field of the dye (smoke) gets advected by the velocity field of the jet (air). But if the amount of advected substance (smoke or dye) present is much smaller than the total bulk of the fluid, then the back-effect produced on the fluid is negligible. Under such circumstances, it is safe to treat the density field of the advected substance to be the driven or 'passive' field and the velocity field of the fluid to be the driving field. Such systems belongs to the class of 'passive scalar advection'.

However, under certain circumstances, it is possible to have bidirectional coupling, even when condition (*ii*) is satisfied. For example, introduction of tracer particles to probe a medium sometimes results in a coupled system where dynamical evolution of both the probe particles and the medium get strongly affected by each other.

In this thesis, we have investigated two kinds of coupling. We have considered simple models in one dimension describing passive scalar advection and probe particles in a medium. In the remaining part of this chapter, we include a general discussion on these two topics and summarise the relevant earlier results.

1.1 Passive Scalar Advection

Spreading and Clustering

As mentioned above, the problem of passive scalar advection is described by two fields: one driving field and one driven or passive field. In many earlier studies, the driving field was taken to be the velocity field of a fluid and the driven field is the density field of the advected substance. In the examples of fluorescent dye carried by a turbulent jet or smoke particles dispersed in air, the advected substance spreads out in space under the influence of the driving field. In certain other types of situations, the driving field may induce a clustering tendency and the advected particles may clump together—as seen in air bubbles in water or dust particles in air [16, 17]. Earlier studies reveal that such an effect may be observed if the passive scalar flow has low inertia or high viscosity or if the driving fluid is highly compressible.

Earlier Studies on Passive Scalar Clustering

Deutsch [18] and later Wilkinson and Mehlig [19] investigated the clustering properties of the passive scalar as the inertia and viscosity of the passive scalar flow is changed. The effect of the driving fluid was modelled by a random force with rapidly decaying correlations. In [18] Deutsch showed that if the mass of the passive particle is below some critical value, the probability that two particles will be found at an infinitesimal distance away from each other in the long time limit is 1, implying that the neighboring particles aggregate. The value of the critical mass depends on the viscosity and also on the form of the two-point force-force correlation function. The above probability, which serves as the order parameter in this case, changes discontinuously across the critical point.

Wilkinson and Mehlig investigated the above clustering transition as the viscosity is changed [19]. As viscosity exceeds a certain threshold, which depends on the mass and the form of the force-force correlator, the particles aggregate. The associated phase transition is characterised by the fraction of initial conditions for which the separation between a pair of infinitesimally close trajectories approaches zero in the long time limit. This order parameter jumps from 0 to 1 as the viscosity exceeds its critical value. In the aggregated phase, the two-point density-density correlation function shows a divergence near the origin, indicating a strong clustering between the particles.

In [18] and [19] damped motion of inertial particles in a random force field was considered and it was found that path coalescence mechanism gives rise to a clustering transition in low inertia and high viscosity regime. However, when the correlation time of the force field approaches zero, path coalescence can exist if and only if the force field describes a predominantly potential flow. A more general case was considered in [20] where the driving field has both a potential component as well as a solenoidal component. It was found that in two dimension, the particles cluster onto a network of caustic lines. Thus even when no path coalescence occurs, there is a significant density inhomogeneity.

Falkovich *et al.* showed in [21] that in presence of turbulent vortices inside the cloud cores, the advected inertial droplets are driven outwards due to centrifugal force. This gives rise to a jet of droplets and concentration inhomogeneity, both of which increase the mean collision rate between the droplets. As a result, large aggregates form due to coalescence of droplets of different sizes.

Clustering of passive scalars may also be observed in case the driving field is compressible. Gawędzki and Vergassola studied the effect of compressibility on passive scalars in [17]. In their model, the fluid velocity was chosen to have a Gaussian distribution with correlation properties that incorporate the compressibility of the fluid. They found that when the compressibility is low, the trajectories of the fluid particles separate explosively (*i.e.* two infinitesimally close trajectories reach an $O(1)$ separation in finite time). However, when the compressibility increases beyond a threshold, the trajectories collapse implosively and the advected passive particles clump together. The two point density-density correlation function for passive particle density shows a divergence for small separation—an indication of strong clustering.

Passive Sliders on Fluctuating Surface

In our model of passive scalar advection, the driving field represents the fluctuating height field of a one dimensional surface. The time evolution of the surface is described by Edwards-Wilkinson (EW) or Kardar-Parisi-Zhang (KPZ) equation. The passive scalar field in our case is the density field of a set of hard-core particles sliding downwards (under gravity) along the local slope of the surface. Nagar *et al.* studied the same model in absence of the hard-core constraint [22]. Note that in their model, when the underlying surface is of KPZ type, the problem maps onto non-interacting passive scalars advected by perfectly compressible Burgers fluid. Nagar *et al.* found that driven by the surface fluctuations, the passive particles go towards a strongly clustered state. The spatial correlation function of particle density is a scaling function of r/L, where r is the spatial separation and L is the system size. The scaling function shows a divergence near the origin, as found in [17].

When the hard-core constraint is imposed, instead of a strongly clustered state, the passive particles now show a new kind of ordered state where strong fluctuations are always present. This is called fluctuation dominated phase-ordering (FDPO) [25]. Das *et al.* investigated static properties of this model in [24, 25].

They found that spatial correlation function of particle density in steady state is a scaling function of r/L, as expected for phase-ordered systems. The scaling function, however, decays with a cusp, as opposed to a linear decay for ordinary phase-ordered systems. In chapter 2 we will discuss their main results in detail.

This model is in fact a special case of Lahiri-Ramaswamy (LR) model [28] which describes a colloidal crystal that is steadily sedimenting through a viscous fluid. The magnitude of the local settling velocity of a region of the crystal depends on its concentration and the direction of the local settling velocity depends on its 'tilt', *i.e.* the orientation, relative to the applied force (gravity) of the principal axis of the local particle distribution. In [28], such a system was modelled by a driven lattice gas describing the coupled dynamics of the concentration and the tilt field. With the variation of the coupling parameters, an interesting phase-diagram results. FDPO has been found along one particular line of this phase diagram where one coupling parameter vanishes and the system becomes semi-autonomous.

Dynamics of Passive Scalars

In this thesis, we study dynamical properties of the hard-core passive sliders on a fluctuating surface. To our knowledge, the dynamics of passive scalars has not been explored systematically and our study adds to the relatively sparse work on this important question [26, 22]. We have measured dynamical correlation functions of the density fluctuations of the passive sliders—auto-correlation and space-time correlation in steady state and aging correlation during approach towards steady state. The steady-state correlation functions show a scaling with the system size which indicates that the system has a long-ranged order in steady state. However, as in [24, 25], the scaling functions show cusp singularities and are significantly different from those in ordinary phase-ordered systems [27], which implies an unusual kind of ordering.

1.2 Probe Particles in a Driven Diffusive Medium

Earlier Studies on Two-Way Coupled Systems

Although the field of passive scalar advection is quite interesting and often describes physical systems, a more realistic situation however, corresponds to the case when the coupling works both ways. There have been earlier studies on such coupled driven diffusive systems, dynamical evolutions of both of which affect each other. Ertaş and Kardar in [29] have considered fluctuations of a stretched string, *e.g.* a vortex line or a polymer moving with a uniform velocity through a random medium. They model the longitudinal and transverse motion of the string by a pair of coupled nonlinear equations. In [30] Barabasi has considered a generalised version of these equation allowing for additional coupling terms. Both these studies focus on the variation of the critical exponents as the coupling parameters are changed. In a relatively recent study, the coupled system of ant-trails and pheromone density has been considered where this two-way coupling gives rise to interesting patterns in the ant traffic [11]. LR model, mentioned in the last section, is another example of bidirectional coupling.

Probe Particles

In all the above examples, the coupling between the two systems is rather strong and this substantially changes the properties of both the systems, as expected. However, in certain cases, even when the two systems are expected to be semi-autonomously coupled and the properties of the driving system are supposed to remain unchanged, it is found that the coupling is in fact bidirectional and both the systems are substantially affected by each other. For example, introduction of tracer particles to probe the properties of a system may sometimes give rise to such two-way coupling.

In many situations, useful information about a complex system is obtained by injecting probe particles and monitoring their motion, after they have come to a steady state with the system. Dynamics of probe particles may yield information about visco-elastic properties of a cell-interior [31], sol-gel transition in a polymer solution [32] or correlations present in bacterial motion [33]. In all these examples, it is generally assumed that if the concentration of the probe particles is sufficiently low, then the system properties are not affected too much by their presence, *i.e.* the coupling between the probe particles and the surrounding medium is unidirectional. In this thesis, we consider one example where this assumption breaks down.

Nonequilibrium Probes

We show that the probe particles can indeed produce a strong effect on the medium even when present in a vanishingly low concentration. At the same time, the medium may also induce correlations between the probe particles [34, 35]. We have demonstrated this for a class of nonequilibrium probe particles in one dimension which evolve through moves that do not satisfy detailed balance. The medium is taken to be described by simple lattice gas models of equilibrium and non-equilibrium systems in one dimension and the effect produced by the probes is qualitatively different in the two cases. The nonequilibrium probes are found to strongly affect a medium which is initially in equilibrium—even a single probe gives rise to a macroscopic effect. However, for a medium which is initially in a current-carrying nonequilibrium state, the effect produced by a single probe is less drastic. Depending on the kinematics of the probe and the medium, this effect may be short-ranged or long-ranged [36] and this gives rise to an interesting phase diagram. We have investigated dynamical properties of the composite system for finite density of probes. We have found that the above phase diagram for a single probe has important consequences on the dynamical properties of a macroscopic number of probe particles.

In chapter 2 we describe our results on static and dynamic correlation functions of the passive sliders on a fluctuating surface and discuss how the scaling forms of these correlation functions indicate the presence of FDPO. In chapter 3 we study this FDPO state in detail and discuss how such a state can be characterised as an ordered state despite the presence of strong fluctuations. A brief discussion of our results on passive scalars has been included in chapter 4.

In chapter 5 we introduce the general model we examine to study the dynamics of nonequilibrium probe particles in driven diffusive medium. In chapter 6 we consider the probe particles in an initially equilibrium medium and describe how the probes produce a macroscopic effect on the medium. Statics and dynamics of the probes in nonequilibrium medium are considered in chapter 7 and full phase diagram (obtained under the variation of the properties of the probe and the medium) is discussed. Chapter 8 deals with probes in an interacting driven diffusive medium and we show that even in presence of the interaction, the scaling properties of the system remain the same as in the non-interacting case, in contradiction with some recent results. We conclude our discussion on probes in driven diffusive systems in chapter 9.

In chapter 10 of this thesis, we study a simple model which shows hysteresis. We consider an asymmetric simple exclusion in one dimension under the influence of a bias which is a periodic function of time. The time-dependence of the bias gives rise to interesting crossover effects in the dynamical correlation functions of the system. By mapping the particle-hole configuration on an interface between the up-down spin phases of a two dimensional Ising model, we show that for a bias that varies sinusoidally with time, the system shows hysteresis and for this simple model it is possible to obtain the hysteresis curve analytically.

At the end of this thesis, we include few appendices where we provide derivation of some earlier results, which we have used in our thesis. In appendix A we discuss the mapping between exclusion process and fluctuating surfaces. In appendix B we show the calculation of sign-sign correlation function of a Gaussian variable. Appendix C contains an outline of calculation of static correlation function of nonequilibrium probe particles (second class particles in this case) in an ASEP. In appendix D we describe the derivation of the steady state measure of KLS model in one dimension. Finally, appendix E contains a description of an algorithm for generating steady state ensemble for second class particles in an ASEP.

Chapter 2

Dynamics of Passive Scalars

In this chapter, we discuss our results on the dynamics of passive scalars. The specific system we have considered consists of hard-core particles sliding under gravity along the local slope of a one dimensional fluctuating interface. The driving field in our case is the fluctuating height field of the surface and the passive field is the density of the sliding particles.

We have done Monte Carlo simulations on a lattice model which involves both the height field and the density field and also analytical calculations on a related simpler model which involves only the height field. In the next section, we describe both these models in detail. In section 2.2, we summarise the earlier studies on static properties of this system. Then we discuss our results on dynamics. We have studied dynamical properties of this system both in steady state and during the approach towards steady state. We are mainly interested in the scaling properties of the dynamical correlation functions of particle density. Study of the steady state dynamics involves the measurement of the auto-correlation function and space-time correlation function in steady state which we discuss in section 2.3. In steady state, the particles show an unconventional phase-ordering which is governed by strong fluctuations. Like any phase-ordered state therefore, the scaling forms of the steady state correlation functions of the density variable show a strong dependence on the system size L [see Eq. 2.7 and 2.11] —even though fluctuations of the underlying height field show L-independent power law scaling [5]. In section 2.4 we discuss auto-correlation function in aging regime.

2.1 Description of the Model

We study a system of hard-core passive sliders on a one dimensional fluctuating surface. In the following subsection, we give a general description of this system where we discuss the time-evolution equation for the height field of the surface and the density field of the passive particles. In section 2.1.2, we describe the lattice model on which we perform numerical simulations to monitor several dynamical correlation functions involving the density fluctuations of the sliding particles. We have also calculated these correlation functions analytically on a relatively simple coarse-grained surface model which we describe in section 2.1.3.

2.1.1 Surface Fluctuation and Particle Movement

The dynamical evolution of the systems consists of two parts—fluctuation of the underlying surface and movement of the sliding particles.

Surface Fluctuations: A surface with no overhangs is completely specified by the height $h(x,t)$ at point x at time t. The evolution of the height field is taken to be described by the Kardar-Parisi-Zhang (KPZ) equation [37].

$$\frac{\partial h}{\partial t} = \nu_1 \frac{\partial^2 h}{\partial x^2} + \lambda \left(\frac{\partial h}{\partial x}\right)^2 + \eta_1(x,t) \tag{2.1}$$

The first term represents the smoothening effect of surface tension ν_1, and $\eta_1(x,t)$ is a white noise with zero average and $\langle \eta_1(x,t)\eta_1(x',t')\rangle = \Gamma\delta(x-x')\delta(t-t')$. Notice that if $\lambda = 0$, the equation has an $h \to -h$ symmetry and describes the Edwards-Wilkinson (EW) model [38].

However, if $\lambda \neq 0$, $h \to -h$ symmetry is not preserved, reflecting the fact that the interface moves in a preferred direction. Positive values of λ imply that the surface is moving downward and $\lambda < 0$ yields a surface which moves upward [see appendix A]. This non-linear term captures the growth along the local normal to the interface. Let v be the growth velocity along the local normal and δh be the change in the local height in time δt. Then according to the fig 2.1, $\delta h = [(v\delta t)^2 + \left(v\delta t\frac{\partial h}{\partial x}\right)^2]^{1/2}$. Expanding for $\left|\frac{\partial h}{\partial x}\right| \ll 1$ one obtains the quadratic non-linearity with $\lambda = v/2$.

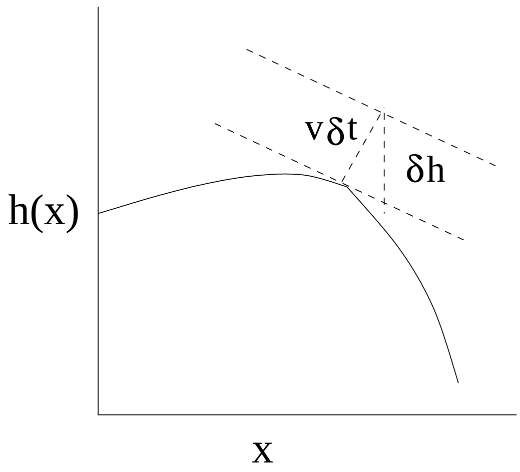

Figure 2.1: *The origin of non-linear term in the KPZ equation: the growth occurs along the local normal.*

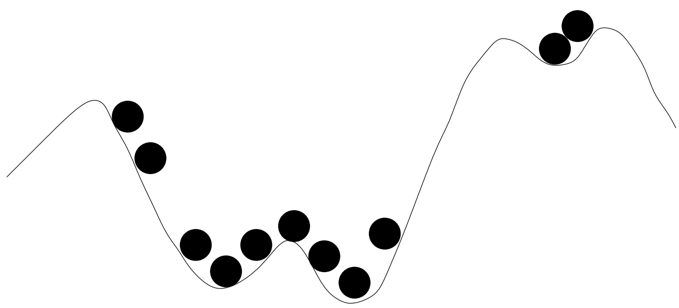

Figure 2.2: *Hard-core passive sliders on a fluctuating surface*

The height-height correlation function has a scaling form for large separations in space and time [39] :

$$\langle [h(x,t) - h(x',t')]^2 \rangle \approx |x - x'|^{2\chi} \ Y \left(\frac{|t - t'|}{|x - x'|^z} \right) \tag{2.2}$$

Here f is a scaling function and χ and z are the roughness and dynamic exponents, respectively, with values which depend on the surface dynamics. For an EW interface $\chi = 1/2$, $z = 2$ while for a KPZ interface $\chi = 1/2$, $z = 3/2$.

Particle Movement: The hard-core particles slide downwards along the local slope $\left(\frac{\partial h}{\partial x}\right)$ of the interface, as shown in fig 2.1.1.

In the over-damped limit, their velocity is proportional to the local gradient of height. The equation governing the evolution of particle density can be derived from the continuity equation $\frac{\partial\rho(x,t)}{\partial t} = -\frac{\partial J(x,t)}{\partial x}$. The local current $J(x,t)$ has a systematic part $\rho(1-\rho)(-\frac{\partial h}{\partial x})$ (which represents the current flowing down the slope, from an occupied site to a neighboring empty site), a diffusive part $-\nu_2\frac{\partial\rho}{\partial x}$ (driven by local density inhomogeneity) and a stochastic part $\eta_2(x,t)$ represented by a Gaussian white noise. The time-evolution equation for the density fluctuation $\tilde{\rho} = \rho - \rho_0$ is then

$$\begin{aligned}\frac{\partial\tilde{\rho}}{\partial t} &= \nu_2\frac{\partial^2\tilde{\rho}}{\partial x^2} + 2\rho_0(1-\rho_0)\frac{\partial^2 h}{\partial x^2} - (1-2\rho_0-2\tilde{\rho})\left(\frac{\partial\tilde{\rho}}{\partial x}\right)\left[1-2\left(\frac{\partial h}{\partial x}\right)\right] + \\ &\qquad 2(1-2\rho_0)\tilde{\rho}\frac{\partial^2 h}{\partial x^2} - 2\tilde{\rho}^2\frac{\partial^2 h}{\partial x^2} + \frac{\partial\eta_2(x,t)}{\partial x}\end{aligned} \tag{2.3}$$

We will not analyze this equation directly; rather we will study the particle dynamics by performing numerical simulations on a lattice model, whose long distance and long time properties are expected to be described by Eqs.(2.2) and (2.3). We introduce the lattice model below.

2.1.2 Lattice Model

The 1-d interface of length L, consists of discrete surface elements; the slope of the surface elements between the i-th and $(i+1)$-th site is $\tau_{i+\frac{1}{2}}$, which can take the value $+1$ or -1. Accordingly the height at site i is given by $h_i = \sum_{j=1}^{i}\tau_{j-\frac{1}{2}}$. The dynamics follows that of the single-step model [40, 41] which involves stochastic corner flips with exchange of adjacent τ's; the transition /\ to \/ occurs with a rate p_1 while \/ to /\ with rate q_1. As in [40, 41], we take $p_1 = q_1 = 1$ to represent an EW surface and $p_1 = 1$, $q_1 = 0$ for a KPZ surface. The overall slope $\mathcal{T} = \frac{1}{L}\sum_{i=1}^{L}\tau_{i+\frac{1}{2}}$ is conserved and in our case we will consider $\mathcal{T} = 0$, meaning that the interface is untilted.

The hard-core particles are represented by variables $\{\sigma_i\}$ each of which takes a value $+1$ or -1 according as the i-th site contains a particle or a hole. The deviation from half-filling $\mathcal{S} = \frac{1}{L}\sum_{i=1}^{L}\sigma_i$ is conserved. A particle and hole on adjacent sites $(i, i+1)$ exchange with rates that depend on the intervening local slope $\tau_{i+\frac{1}{2}}$; thus the moves $\bullet\backslash\circ \to \circ\backslash\bullet$ and $\circ/\bullet \to \bullet/\circ$ occurs at rate p_2 while the inverse moves occur at rate q_2. In the case when the particles are sliding

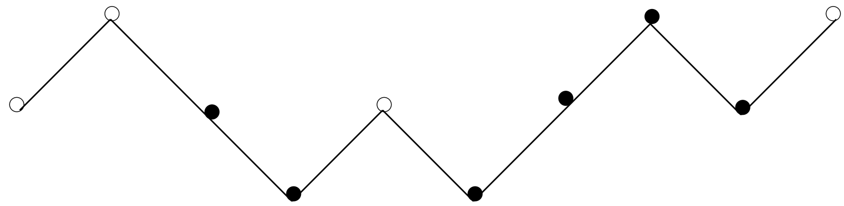

Figure 2.3: *Hard-core particles(shown by solid circle) sliding towards the local valleys. The hollow circles represent the empty sites or holes.*

downwards along gravity, we have $q_2 < p_2$. We have considered $p_2 = 1$ and $q_2 = 0$. In fig 2.3, a typical configuration is shown.

Because of the hard-core exclusion between the particles, in a half-filled system with the above update rules, one has particle-hole symmetry, *i.e.* any correlation function involving the density variable remains invariant, when the particle density is replaced by the hole density. This implies that the correlation measured in an advection process (with $\lambda > 0$, when the surface is moving downward along the same direction as the particles) is exactly same as that in an anti-advection process ($\lambda < 0$, *i.e.* the surface moves upwards, opposite to the particle movement). This is an important difference from the case of non-interacting particles, where the correlations in advection and anti-advection show qualitatively different behavior.

2.1.3 Coarse-grained Depth (CD) Model

From the above dynamical rules, it follows that the movement of particles depends on the fluctuations of the underlying interface. Due to gravity the particles tend to slide down into local valleys. However, in the non-equilibrium system under consideration, before the particles can fill in the lowest valley, the interface evolves, often causing the valley to turn over. [1]

Nevertheless, it is useful to consider the adiabatic limit where the interface moves infinitely more slowly than the particles, in which case the particles have

[1]Note that if a large number of particles are trapped into a valley which is large but not the deepest, then the time-scale over which the particles will come out of this valley to go to the deepest valley is $\sim exp(L^2)$, while the deepest one will evolve over a time-scale $\sim L^z$.

ample time to explore the landscape and eventually settle in the deepest valleys. It seems plausible that the dynamics of hills and valleys of the interface may provide insight into the dynamics of the particles. This motivates the definition of a coarse-grained depth model (CD model) as follows [24, 25]. Consider the variable $s_i(t)$ defined as $s_i(t) = sgn[h_i(t) - \langle h(t)\rangle]$, where $\langle h(t)\rangle$ is the average height at time t: $\langle h(t)\rangle = \frac{1}{L}\sum_{i=1}^{L} h_i(t)$. The variable $s_i(t)$ can take values $+1$,-1 or 0, depending on whether the position of the i-th site is above, below or at the average level. In other words, $s_i(t)$ gives a coarse-grained description of the surface by labeling 'highlands' and 'lowlands'.

For an EW interface, the dynamics is tractable and we obtain an analytic expression for time-dependent correlations of $s_i(t)$. These results might be expected to be close to those of $\sigma_i(t)$ in the extreme adiabatic limit. As a matter of fact, we find that they also describe qualitatively the particle model even in the strongly non-equilibrium case.

2.2 Static Properties

In [24, 25] Das *et al.* have studied the static properties of this model. They have found that the particles tend to cluster in the valleys of the surface. In steady state, this clustering tendency gives rise to a phase-ordered state. But this is an unconventional phase-ordered state which supports strong fluctuation. Below we summarise their main results.

- **Cluster Size Distribution:** In the steady state of the sliding particles (SP) model, the particle and hole cluster size distributions decay as a power law, as opposed to an exponential distribution for a disordered state. The probability to find a particle (hole) cluster of length l, for large l, is

$$P(l) \sim l^{-\theta} \tag{2.4}$$

  with a system size dependent cut-off. The exponent θ depends on the details of the dynamical rules.

  In case the underlying surface is of EW type, the size distribution of particle clusters and hole clusters are identical and $\theta = 1.69 \pm 0.02$. For a KPZ

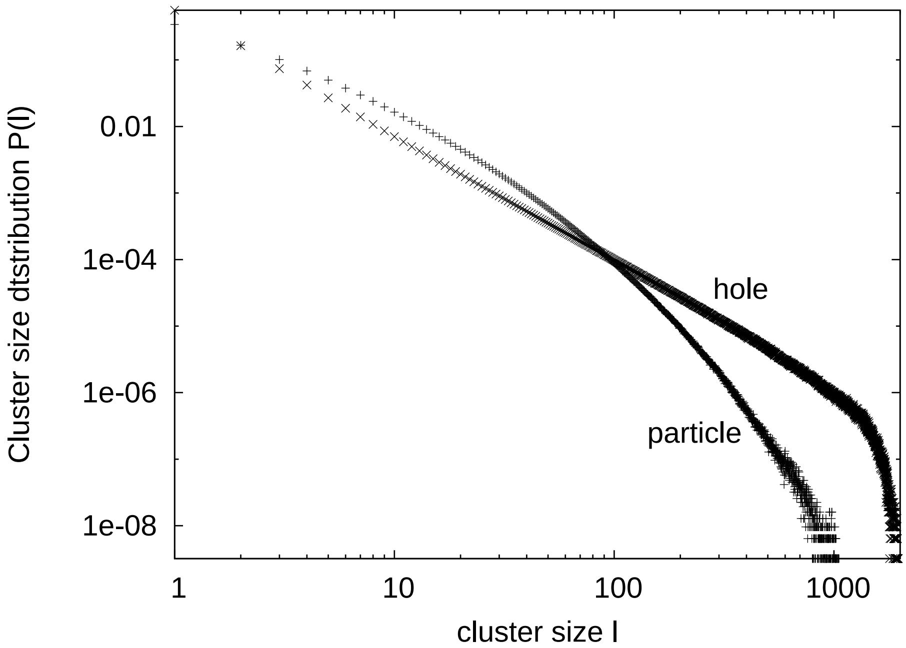

Figure 2.4: *Cluster size distribution for particles and holes on a KPZ surface. The system size* $L = 4096$.

interface, $P(l)$ for particle and hole clusters are different as shown in fig 2.4. A KPZ surface has an overall motion in one direction, and hence the upward motion of the holes and the downward motion of the particles are no longer symmetrical. A hole cluster size distribution in this case still shows a power law with exponent $\theta = 1.87 \pm 0.03$. For particle clusters, however, the distribution deviates from a power law for large l. Note that the exponent θ being less than 2, the average cluster size diverges with the system size.

- **Density-Density Correlation Function:** The two point density-density correlation function in steady state for a system of size L is defined as

$$C(r, L) = \frac{1}{L} \sum_{i=1}^{L} \langle \sigma_i(t) \sigma_{i+r}(t) \rangle \tag{2.5}$$

In the limit of $r \to \infty$, $L \to \infty$ with r/L fixed, $C(r, L)$ is found to be a scaling function of r/L. Such a scaling form is found for phase-ordered systems where because of the presence of macroscopic domains, the typical length scale is $\sim L$. The scaling function has a finite intercept m^2, and for small argument it decays with a cusp:

$$\begin{aligned} C(r,L) &= f\left(\frac{r}{L}\right) && (2.6)\\ &= m^2\left[1 - a\left(\frac{r}{L}\right)^{\alpha}\right], \quad \left(\frac{r}{L} \ll 1\right) && (2.7) \end{aligned}$$

The intercept m^2 is a measure of the long-ranged order (LRO) present in the system. This is because $\langle \sigma_i(t)\sigma_{i+r}(t)\rangle$ for an infinite system, factorises for sufficiently large but *finite* r and approaches a non-zero constant in presence of true LRO. Now for a very large system of size L, in terms of the scaled variable r/L, this short-ranged decay of $C(r,L)$ corresponds to $r/L \to 0$. In other words, the non-zero constant m^2 can be read off from the intercept of $C(r,L)$ vs r/L plot. We show the $C(r.L)$ data for particles on a KPZ surface in fig 2.5 and summarise the values for m^2 and α in table 2.1.

For an ordinary phase-ordered system, the scaling function for two point correlation decays linearly. The structute factor $\mathcal{S}(k,L)$, defined as the Fourier transform of $C(r,L)$, decays quadratically $\mathcal{S}(k,L) \sim (kL)^{-2}$. This is known as Porod law [42, 27]. But in Eq. 2.7 the scaling function decays with a cusp ($\alpha < 1$) and as a result $\mathcal{S}(k,L) \sim (kL)^{-(1+\alpha)}$. This indicates that the steady state shows an unusual phase-separation.

- **<u>Broad Distribution of Order Parameter:</u>** A suitable order parameter for this system is the first Fourier component of the density profile. Consider

$$Q(k) = \left| \frac{1}{L}\sum_{j=1}^{L} e^{ikj} n_j \right| \qquad (2.8)$$

with $k = 2\pi m/L$, m being a positive integer and $n_j = (1+\sigma_j)/2$. The order parameter is defined as $Q(2\pi/L)$. The distribution of this order parameter remains broad even as $L \to \infty$ which implies that strong fluctuations do not die out even in the thermodynamic limit. From the time-series of this

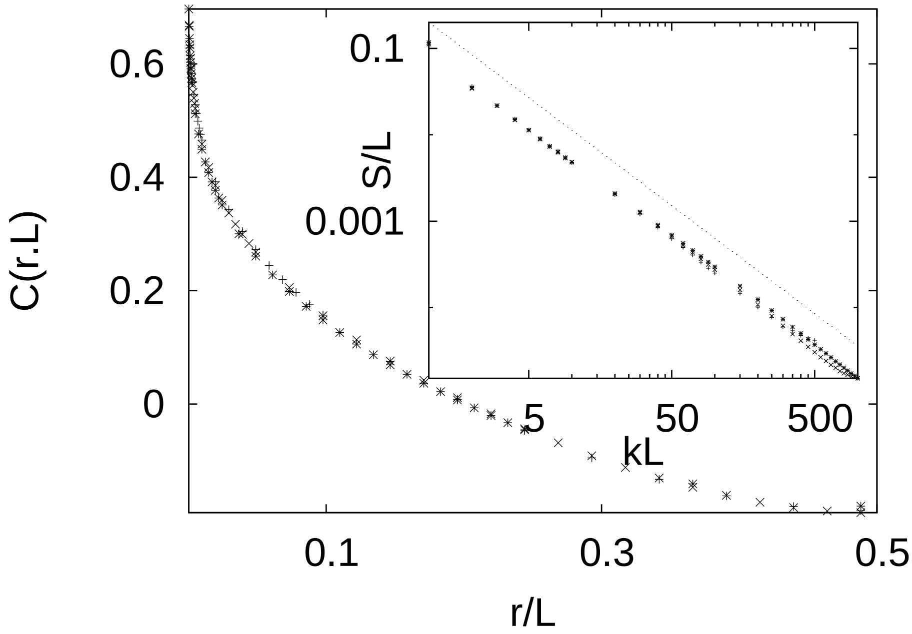

Figure 2.5: *Scaled* $C(r.L)$ *for SP model on a KPZ surface for* $L = 1024, 2048, 4096$. *The cusp exponent* α *has been estimated in the inset from the scaled plot for the structure factor* S.

order parameter in steady state, it is seen to fluctuate strongly and often becomes zero, as shown in fig 2.6. However, this does not mean that the system becomes disordered. Time-series of higher order Fourier components of the density profile shows that a dip in the first Fourier component (*i.e.* the order parameter) is always accompanied by a simultaneous rise in the value of the second or third Fourier component [see fig 2.6]. This implies that whenever a single large cluster breaks up (making the first Fourier component small), two or three macroscopic clusters appear in its place (causing the second or third Fourier component to go up). Thus the system manages to retain its ordering even in the presence of strong fluctuations. This is known as fluctuation dominated phase-ordering (FDPO) [24].

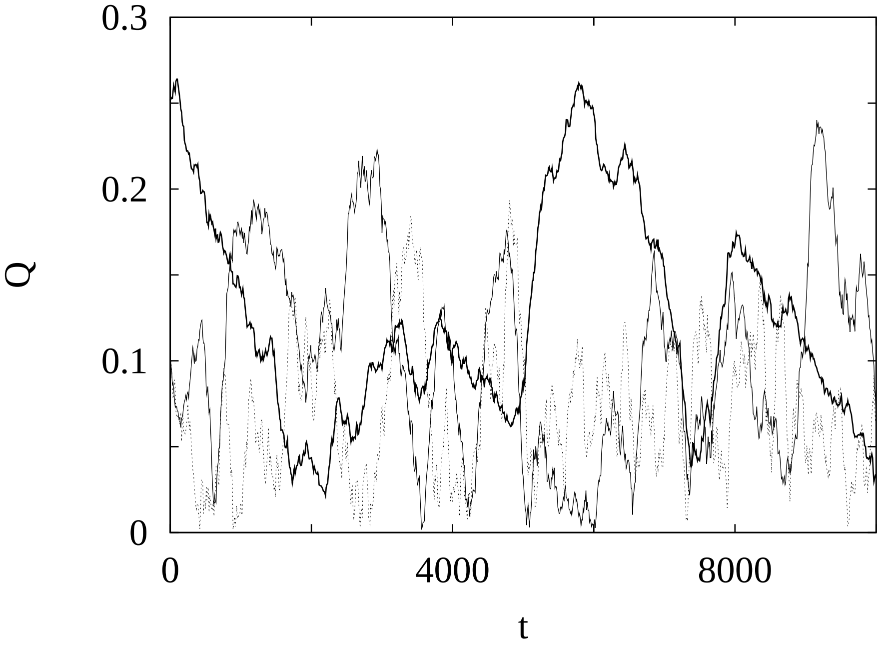

Figure 2.6: *Variations of the first (solid thick line), second (solid thin line) and third (broken line) Fourier component with time. The system size is* $L = 128$. *[Figure taken from Das* et al.*, Phys. Rev. E* **64**, *046126 (2001).]*

2.3 Steady State Dynamics

In this thesis we study the dynamics associated with FDPO. To investigate the dynamical properties of the steady state, we monitor auto-correlation function and space-time correlation function which we describe below in the following two subsections.

2.3.1 Auto-correlation Function in Steady State

We have studied the auto-correlation $A(t, L)$ in sliding particle (SP) model and CD model

$$
\begin{aligned}
A(t, L) &= \frac{1}{L}\sum_{i=1}^{L}\langle\sigma_i(0)\sigma_i(t)\rangle \qquad \text{(SP)} \\
&= \frac{1}{L}\sum_{i=1}^{L}\langle s_i(0)s_i(t)\rangle \qquad \text{(CD)}
\end{aligned} \tag{2.9}
$$

We have mainly considered a half-filled system ($\mathcal{S} = 0$) with periodic boundary conditions. We will see below that in the steady state of a system of size L, the auto-correlation $A(t, L)$ is a scaling function of $\frac{t}{L^z}$, where z is the surface dynamic exponent defined earlier. Since the particles try to settle in the valleys, the time-scale of the decay of the density auto-correlation is expected to be of the order of the lifetime of large valleys. In a system of size L the breadth of the large valleys are $\sim L$ and the corresponding lifetime is $\sim L^z$. This scaling function shows a cusp in the small argument limit, as seen previously in the static correlation scaling function [Eq. (2.7)]:

$$
A(t, L) = h\left(\frac{t}{L^z}\right) \tag{2.10}
$$

$$
= m^2\left[1 - b\left(\frac{t}{L^z}\right)^{\beta'}\right], \quad \frac{t}{L^z} \to 0 \tag{2.11}
$$

m is a measure of the LRO as explained in section 2.2. Note that at a large enough but finite (L-independent) time, the auto-correlation function reaches the same value m^2 as the static correlation $C(r, L)$, like any phase-ordered system.

As shown in Eq. 2.2, the fluctuations of the height field of the underlying surface show a power law behavior and an L-independent scaling form (in fact the L-dependence enters only as a finite size correction which is negligible as L becomes large). On the contrary, the density fluctuations of the passive sliders, although driven by this fluctuating height field, show a completely different scaling form, with a strong L-dependence [see Eq. 2.11] as in phase-ordered systems where typical time-scale is $\sim L^z$. In other words, the particles go into an ordered state, driven by a field that shows critical behavior (power law correlation).

However, the most striking feature of Eq. 2.11 is the cusp exponent β'. For an ordinary phase-ordered system, the scaling function h in Eq. 2.10 always decays linearly for $t \ll L^z$. This is nothing but the dynamical analog of Porod law and can be understood as follows: the auto-correlation function at a site would show a drop only if a domain wall has crossed that site in time t and for $t \ll L^z$ probability that this occurs is proportional to t/L^z. On the contrary, we find that it decays with a cusp with exponent $\beta' < 1$ which points to the existence of an unusual ordered state.

However, for small time, $t \lesssim 1$, which falls outside the scaling regime, the auto-correlation function shows a linear drop with an L-dependent slope:

$$A(t, L) \approx 1 - b' \frac{t}{L^\delta}, \qquad (t \lesssim 1) \tag{2.12}$$

If $m^2 = 1$, as shown below for the CD model, matching Eqs.(2.11) and (2.12) for $t \simeq 1$ yields

$$\delta = z\beta' \tag{2.13}$$

If $m^2 \neq 1$, as happens for the SP model, a relation between the exponents cannot be obtained. Instead, the matching condition determines a time scale t^* for the crossover from the linear decay in Eq.(2.12) to the cuspy decay in Eq.(2.11). In the large L limit, we find to the leading order,

$$t^* = \frac{1 - m^2}{b'} L^\delta \tag{2.14}$$

We have summarized the values of the intercept and the exponents in table 2.1, for the CD model and the SP model on EW and KPZ surfaces.

Small time decay of $A(t, L)$

Let us illustrate these properties, by discussing the auto-correlation in the CD model, defined as $A_{CD}(t, L) = \langle s_i(0)s_i(t)\rangle$. First consider short times $t \lesssim 1$. At $t = 0$ let the initial configuration of the surface be $\{h_i(0)\}$. As time passes, there are stochastic corner flips, as described in section 3. However, only those flips occurring close to the average level can cause a change in the CD variable $s_i(t)$, as any local fluctuation far above or below the average level, would not

	CD Model		SP Model	
	EW	KPZ	EW	KPZ
m^2	1.0	1.0	0.82 ± 0.03	0.75 ± 0.04
α	0.5	0.5	0.4 ± 0.05	0.21 ± 0.04
β'	0.25	0.31 ± 0.02	0.22 ± 0.02	0.18 ± 0.01
δ	0.5	0.5	0.26 ± 0.005	0.15 ± 0.005
γ	0.75	0.84 ± 0.02	0.69 ± 0.02	0.82 ± 0.04

Table 2.1: *The values of relevant exponents and intercepts for dynamical characterization of CD model and SP model with* S= 0.

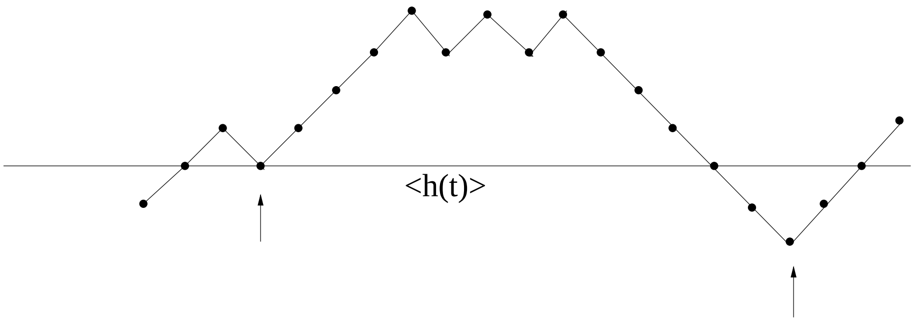

Figure 2.7: *Sites contributing to the small time linear decay of the auto-correlation function shown by arrow.*

change the sign of $s_i(t) = (h_i(t) - \langle h(t) \rangle)$. More precisely, only those sites in $\{h_i(0)\}$ which have at least one neighbor situated exactly on the average level, putatively contribute to the drop in auto-correlation function. In fig 2.7 we show two such sites. Now, for a self-affine surface of length L and roughness exponent χ, the number of such points scales as $L^{1-\chi}$ and the density of such points goes as $L^{-\chi}$ [40]. For small t, the probability that any one of these points will actually take part in a local fluctuation is proportional to t. This immediately implies $A_{CD}(t \lesssim 1, L) \approx 1 - {b_1}' \frac{t}{L^{\chi}}$. Comparison with Eq.(2.12) shows that for the CD model, we have $\delta = \chi = \frac{1}{2}$. Note that although EW and KPZ surfaces have different dynamics, the above argument holds for both of them as their stationary measure is the same in 1-d.

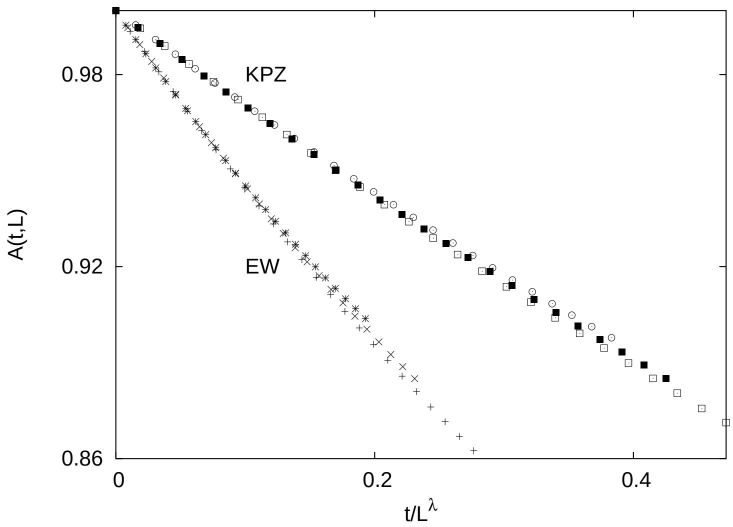

Figure 2.8: *Illustrating the linear drop of $A(t, L)$ for short times $t \lesssim 1$ in the SP model for system size* $L = 128, 256, 512$.

For the particle model, although the initial drop is found to be linear as described in Eq.(2.12), the exponent δ takes the value 0.26 ± 0.005 for particles on an EW surface and 0.15 ± 0.005 for particles on a KPZ surface. The data are shown in fig 2.8.

Analytical Calculation in the Scaling Regime

For $t \geq 1$, we have analytically calculated $A_{CD}(t, L)$ for an EW interface. This exploits the fact that $h_i(t)$ in this case is a Gaussian variable, implying s_i correlations satisfy the following relation [see appendix B]

$$\langle s_i(t)s_i(0)\rangle = \frac{2}{\pi}\sin^{-1}\left(\frac{\langle H_i(t)H_i(0)\rangle}{\sqrt{\langle {H_i}^2(t)\rangle\langle {H_i}^2(0)\rangle}}\right) \tag{2.15}$$

where $H_i(t) = h_i(t) - \langle h(t)\rangle$, which is also a Gaussian variable. If $\tilde{h}_k(t)$ is the Fourier transform of $h_i(t)$, the numerator in the argument of arcsine can be written as $\sum_{k\neq 0}\langle \tilde{h}_k(t)\tilde{h}_{-k}(0)\rangle = \sum_{k\neq 0}\Gamma \exp\left(-c_k t\right)/c_k$, using the discrete version of the EW equation. Here, $c_k = 4\nu_1 \sin^2 \frac{k}{2}$. Moreover, $\langle {H_i}^2(t)\rangle = \langle {H_i}^2(0)\rangle =$

$\Gamma \sum_{k\neq 0} \frac{1}{c_k}$. Thus we have

$$\langle s_i(t)s_i(0)\rangle = \frac{2}{\pi}\sin^{-1}\left[\frac{\sum_{k\neq 0}\frac{\exp(-c_k t)}{c_k}}{\sum_{k\neq 0}\frac{1}{c_k}}\right] \tag{2.16}$$

We have numerically evaluated this discrete sum and plotted it in Fig.(2.9a) against the scaling argument t/L^2 for different L values. The cusp exponent can be read off from the plot in the inset.

In the continuum limit, Eq.(2.16) becomes

$$\langle s(x,t)s(x,0)\rangle = \frac{2}{\pi}\sin^{-1}\left[\frac{\int_{\frac{2\pi}{L}}^{\pi} dk \frac{\exp\left(-k^2 t\right)}{k^2}}{\int_{\frac{2\pi}{L}}^{\pi}\frac{dk}{k^2}}\right] \tag{2.17}$$

Here, the lower limit of the integration is the first Fourier mode which takes the value $2\pi/L$ for periodic boundary condition. The integral in the numerator takes the form $\frac{L\Gamma}{\pi}\left[\frac{L}{2\pi}\exp\left(-\frac{4\pi^2 t}{L^2}\right) + \sqrt{\pi t}\, erf\left(\frac{2\pi\sqrt{t}}{L}\right) - \sqrt{\pi t}\right]$. In the limit $t/L^2 \ll 1$, this becomes, to the leading order, $\frac{L\Gamma}{\pi}\left[\frac{L}{2\pi} - \sqrt{\pi t}\right]$. Noting that the denominator is $\frac{L\Gamma}{\pi}.\frac{L}{2\pi}$ and expanding for small values of $\frac{\sqrt{t}}{L}$, we get

$$\langle s(x,t)s(x,0)\rangle \approx 1 - \frac{4}{\pi^{\frac{1}{4}}}\left(\frac{t}{L^2}\right)^{1/4} \qquad \left(t/L^2 \ll 1\right) \tag{2.18}$$

Comparing with Eq.(2.11) gives $m^2 = 1$, $\beta' = \frac{1}{4}$, $z = 2$.

Numerical Results

For the KPZ surface, the time evolution equation for the height field is not Gaussian and hence such an analytical treatment is not possible. We study $A_{CD}(t)$ using Monte Carlo simulation. No initial equilibration is required as the steady state measure for a KPZ surface with periodic boundary conditions gives equal weight to every configuration. The initial configuration was thus chosen randomly. We followed the update rules discussed in section 2 and averaged over sites as well as over 10^5 histories. The results are shown in Fig.(2.3b). A good scaling collapse is obtained for different L, on rescaling the time to t/L^z with $z = \frac{3}{2}$. The cusp exponent β' was extracted by plotting $m^2 - A_{CD}(t)$ against t/L^z (shown in the inset), using $m^2 = 1$ and this gives β' to be 0.31 ± 0.02. Our best estimate corresponds to the largest system size $L = 2048$. The error-bar is based on the values of β' obtained for smaller system size ($L = 512, 1024$); the statistical error is much smaller.

For the sliding particle (SP) model, the steady state measure is not known analytically. In our simulation, we started from a randomly disordered configuration and allowed a long time $\sim 10L^z$ for the system to reach a steady state. We then measured $\frac{1}{L}\sum_{i=1}^{L}\sigma_i(0)\sigma_i(t)$ for approximately L^z time-steps. We waited several thousand time-steps before taking the next set of measurement, and averaged over 10^4 such histories .

For particles sliding on an EW interface, we obtained a good scaling collapse of $A_{SP}(t, L)$ for different L after rescaling time to t/L^2 [Fig.(2.9a)]. The cusp exponent was extracted by fitting $m^2 - A_{SP}(t, L)$ to a power law. We have estimated m^2 by using the same technique as discussed in [25]. The best estimate of m^2 corresponds to the value for which the structure factor (the Fourier transform of the static correlation function $C(r, L)$) has the largest power law stretch. We found that m^2 shows a systematic dependence on L and the cusp exponent β' is in fact quite sensitive to the value of m^2. We have used $m^2 \simeq 0.82$, our estimate from the largest system size we could access ($L = 4096$). This yields $\beta' \simeq 0.22$. On the other hand, using $m^2_\infty \simeq 0.85$, which we get by extrapolating the dependence of m^2 on L for an infinite system, we find $\beta' \simeq 0.20$.

For the SP model on a KPZ surface, we find $m^2 \simeq 0.75$. Figure (2.3b) shows the scaling collapse for different L after rescaling the time by $L^{3/2}$. The inset shows that $m^2 - A_{SP}(t, L)$ follows a power law and the exponent is found to be $\beta' \simeq 0.18$. The value of β' obtained using m^2_∞ is $\simeq 0.17$.

Apart from the half-filled case, we have also studied the auto-correlation function for filling fractions 1/4 and 1/8 (corresponding to $\mathcal{S} = -1/2$ and $\mathcal{S} = -3/4$, respectively). We found that the same scaling form [Eq.(2.11)] holds. However, the value of the intercept changes while the cusp exponent remains the same.

ρ	m^2	
	EW	KPZ
1/4	0.60	0.59
1/8	0.32	0.34

Table 2.2: *The values of the intercept for filling fractions other than* 1/2*.*

2.3.2 Space-time Correlation Function in Steady State

In this section, we discuss the behavior of space-time correlation $G(r,t,L)$ in steady state defined as follows:

$$\begin{aligned} G(r,t,L) &= \langle \sigma_i(0)\sigma_{i+r}(t)\rangle \qquad \text{(SP)} \\ &= \langle s_i(0)s_{i+r}(t)\rangle \qquad \text{(CD)} \end{aligned} \tag{2.19}$$

$G(r,t,L)$ does not show any $L-$independent scaling between r and t. Rather, it is a function of the scaled variables $\xi = r/L$ and $\tau = t/L^z$

$$G(r,t,L) = g(\xi,\tau). \tag{2.20}$$

Compare this scaling form with Eq. 2.2 which show the $L-$independent scaling between r and t of the the height fluctuations of the underlying surface.

Note that $G(r,t=0,L) \equiv C(r,L)$ and $G(r=0,t,L) \equiv A(t,L)$. Therefore $g(\xi,0)$ reduces to the pair correlation function $f(\xi)$ [see Eq.(2.6)] and for $\tau \gg \xi^z$, $g(\xi,\tau)$ merges with the auto-correlation scaling function $h(\tau)$ [see Eq.(2.10)]. With ξ held fixed, g shows an interesting non-monotonic behavior with τ. As τ increases, $g(\xi,\tau)$ is observed to rise and attain a peak [see fig 2.10a and 2.10b]. From our knowledge of the scaling functions $f(\xi)$ and $h(\tau)$, we have been able to verify that $f(\xi) < h(\tau = \xi^z)$. This implies that $g(\xi,\tau)$ must show an initial rise.

For the CD model on an EW interface,

$$G_{CD}(r,t,L) = \frac{2}{\pi} sin^{-1}\left[\frac{\sum_{k>0}\frac{\exp(-c_k t)2\cos(kr)}{c_k}}{\sum_{k>0}\frac{1}{c_k}}\right]. \tag{2.21}$$

We have evaluated this sum numerically and plotted it against τ, for a fixed value of ξ in the inset of fig 2.10a, which shows the non-monotonic nature of $g(\xi,\tau)$. In the continuum limit, the argument of arcsine takes the form

$$2\cos(2\pi\xi) - 2\pi^2\xi + 2\pi\xi Si(2\pi\xi) - 2\pi\nu_1 N(\xi,\tau) \tag{2.22}$$

where the sine integral function is defined as $Si(x) = \int_0^x \sin(t)/t dt$ and $N(\xi,\tau)$ is given by

$$\int_0^\tau dy\sqrt{\frac{\pi}{\nu_1 y}}\exp\left(-\frac{\xi^2}{4\nu_1 y}\right)\left[erf\left(2\pi\sqrt{\nu_1 y} - \frac{i\xi}{2\sqrt{\nu_1 y}}\right) - 1\right] \tag{2.23}$$

. Eq.s 2.22 and 2.23 show explicitly that $G_{CD}(r,t,L)$ is a function of ξ and τ only.

To measure $G_{SP}(r,t,L)$ for particles on an EW surface we performed Monte Carlo simulations as before. After equilibrating the system, we measure $\frac{1}{L}\sum_{i=1}^{L}\sigma_i(0)\sigma_{i+r}(t)$ for about $L^z/10$ time steps, then after a gap of a few hundred time steps, we take another set of data. We finally average over 10^5 such histories. The results are shown in Fig.(2.10a) where we have also included the scaling function $h(\tau)$ to compare the long time behavior. The corresponding results for KPZ surface are shown in Fig.(2.4b).

2.4 Aging Dynamics during approach towards Steady State

So far we have discussed the steady state properties of the sliding particles. Since the particles phase separate in the steady state, the scaling functions of various steady state correlations show a strong dependence on the system size L. In this section, we consider $L \to \infty$ limit and study the properties of the system while it approaches the steady state.

To investigate the dynamical properties of the system during approach towards steady state, we have monitored the aging auto-correlation function, defined as

$$\begin{aligned} \mathcal{A}(t_1,t_2) &= \langle\sigma_i(t_1)\sigma_i(t_1+t_2)\rangle \qquad \text{(SP)} \\ &= \langle s_i(t_1)s_i(t_1+t_2)\rangle \qquad \text{(CD)} \end{aligned} \tag{2.24}$$

We have investigated primarily the half-filled case, but have checked that no qualitative change takes place for other values of the filling fraction. Since the system has not yet reached steady state, one does not have time translational invariance and hence $\mathcal{A}(t_1, t_2)$ depends on both t_1 and t_2. For $1 \ll t_1, t_2 \ll L^z$, $\mathcal{A}(t_1, t_2)$ is a function of $\frac{t_1}{t_2}$, as expected for phase ordering systems [27]. In the limit when $t_2 \gg t_1$, this scaling function has a power law decay (see table 2.1)

$$\mathcal{A}(t_1, t_2) \sim \left(\frac{t_1}{t_2}\right)^{\gamma} \text{ for } t_2 \gg t_1, \tag{2.25}$$

while in the opposite limit, $t_1 \gg t_2$, the scaling function has the form

$$\mathcal{A}(t_1, t_2) \sim m^2 \left[1 - b_1 \left(\frac{t_2}{t_1}\right)^{\beta'}\right] \text{ for } \frac{t_2}{t_1} \to 0 \tag{2.26}$$

This is similar to the form of the steady-state auto-correlation in Eq.(2.11) with L replaced by $t_1^{1/z}$, meaning that locally the system has reached steady state over a length scale of $t_1^{1/z}$.

We first present our results on the CD model. As in the case of steady-state auto-correlation, we have been able to calculate $\mathcal{A}_{CD}(t_1, t_2)$ for an EW surface analytically. Following similar steps to the last section, we obtain

$$\mathcal{A}_{CD}(t_1, t_2) = \frac{2}{\pi} sin^{-1} \left[\frac{\sum_{k \neq 0} \frac{\exp(-c_k t_2) - \exp[-c_k(2t_1 + t_2)]}{c_k}}{\left\{\sum_{k' \neq 0} \frac{1 - \exp(-2c_{k'} t_1)}{c_{k'}}\right\}^{1/2} \left\{\sum_{k'' \neq 0} \frac{1 - \exp[-2c_{k''}(t_1 + t_2)]}{c_{k''}}\right\}^{1/2}} \right] \tag{2.27}$$

Taking the continuum limit and using $t_1, t_2 \ll L^2$, we obtain

$$\mathcal{A}_{CD}(t_1, t_2) = \frac{2}{\pi} sin^{-1} \left[\frac{\sqrt{2t_1 + t_2} - \sqrt{t_2}}{(2t_1)^{1/4} (2t_1 + 2t_2)^{1/4}} \right] \tag{2.28}$$

In the limit $t_2 \gg t_1$, right hand side becomes $\frac{\sqrt{2}}{\pi} \left(\frac{t_1}{t_2}\right)^{3/4}$. Comparing with Eq.(2.25), we get $\gamma = \frac{3}{4}$. In the opposite limit, when $t_1 \gg t_2$, the right hand side becomes, after simplification,

$$\mathcal{A}_{CD}(t_1, t_2) \approx 1 - \frac{2^{\frac{5}{4}}}{\pi} \left(\frac{t_2}{t_1}\right)^{1/4} \tag{2.29}$$

Comparing with Eq.(2.26), we find $\beta' = 1/4$, as expected.

Figure (2.11a) shows the numerical evaluation of the discrete sum in Eq.(2.27). The power law characterizing the decay has been shown in the inset.

In our Monte Carlo simulations, we have a spatial average as well as an average over 10^4 histories. For the CD model of a KPZ surface, we started with a flat interface as an initial condition and evolved it in time to measure $\mathcal{A}_{CD}(t_1, t_2)$. The results are shown in fig 2.5b. The best estimate of the cusp exponent corresponds to $t_1 = 32000$ and the error bar is based on its values for $t_1 = 2000, 8000$. This finally gives $\beta' = 0.31 \pm 0.01$, which is close to the steady state value. The inset shows the power law decay and the exponent γ takes the value 0.84 ± 0.03. Here, the best estimate is for $t_1 = 500$ and the error-bar is for $t_1 = 2000, 8000$.

For the SP model on an EW interface, we start with randomly distributed particles on a random surface profile. The aging auto-correlation $\mathcal{A}_{SP}(t_1, t_2)$ shows a scaling collapse when plotted against t_2/t_1 [see fig 2.11a]. The value of the cusp exponent β' is 0.20 ± 0.02, which characterises the behavior for $t_2 \ll t_1$ is close to the steady state value. The inset shows the plot in the regime $t_2 \gg t_1$. The power law exponent in this case is $\gamma = 0.69 \pm 0.02$.

The SP model on a KPZ surface is also started with a random initial condition. The data are shown in fig 2.5b. The exponents are $\beta' = 0.17 \pm 0.01$ and $\gamma = 0.82 \pm 0.04$.

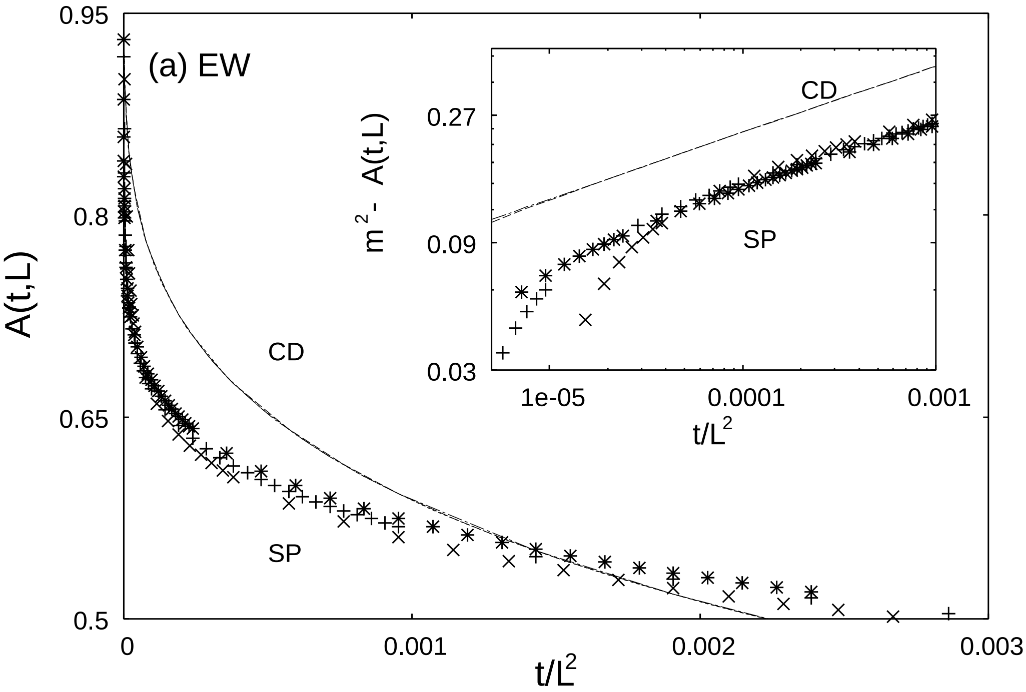

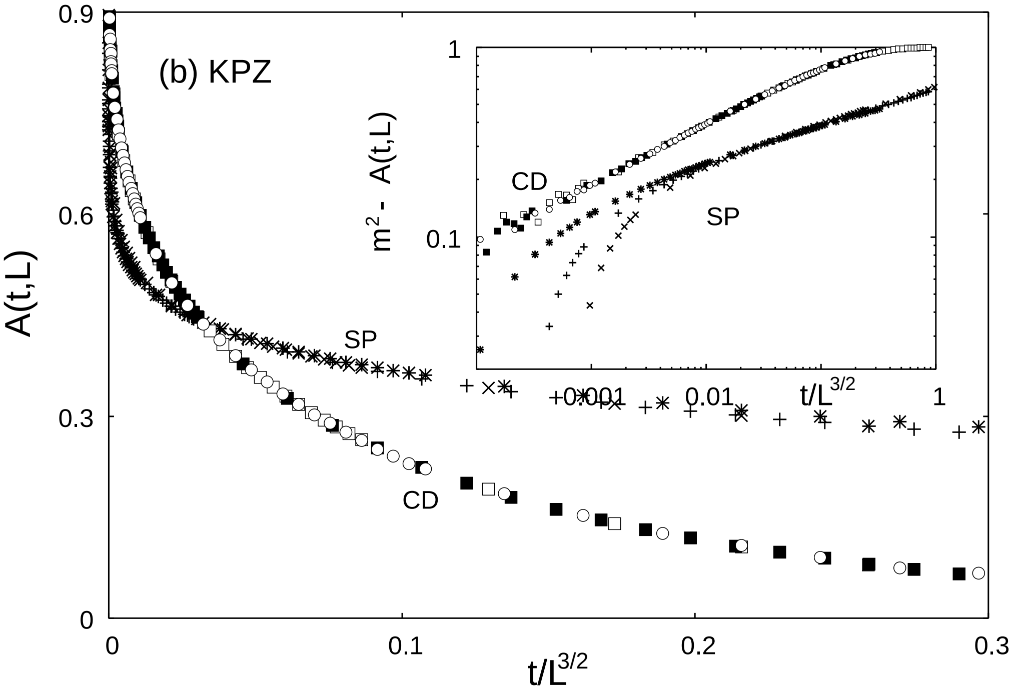

Figure 2.9: *Scaled auto-correlation function in steady state for SP and CD models for (a) EW and (b) KPZ interfaces. In both cases, we used L=512,1024,2048. The cusp exponents were estimated using the plots shown in the inset.*

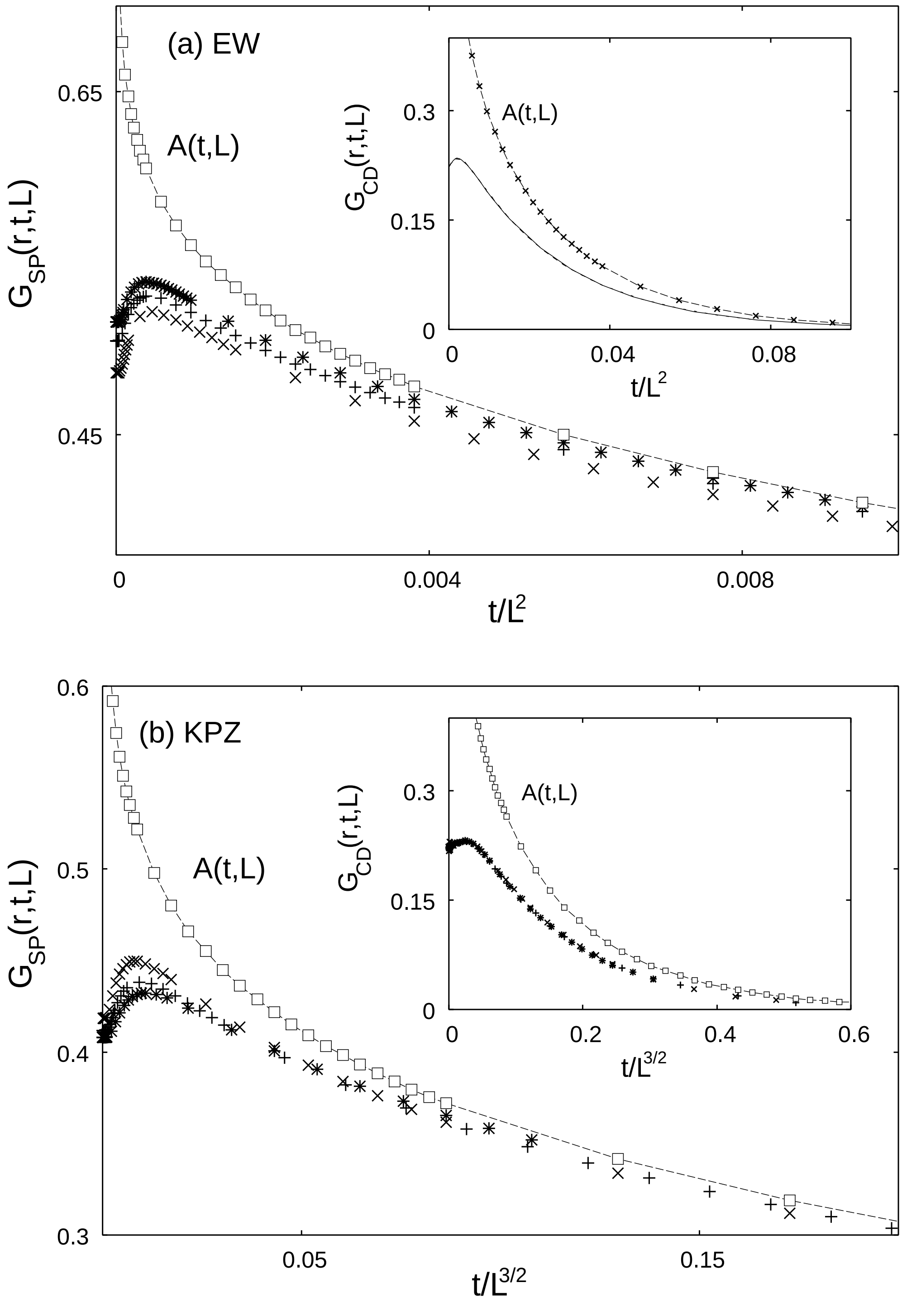

Figure 2.10: *The time dependence of* $G(r,t,L)$ *is shown for particles on an (a)EW and (b) KPZ surface for* $\frac{r}{L} = 0.016$. *The values of* L *are* $256, 512, 1024$ *for (a) and* $512, 1024, 2048$ *for (b). The scaled auto-correlation is also shown, for comparison. The insets show the same quantity calculated for the corresponding CD model with* $\frac{r}{L} = 0.125$ *for both cases.*

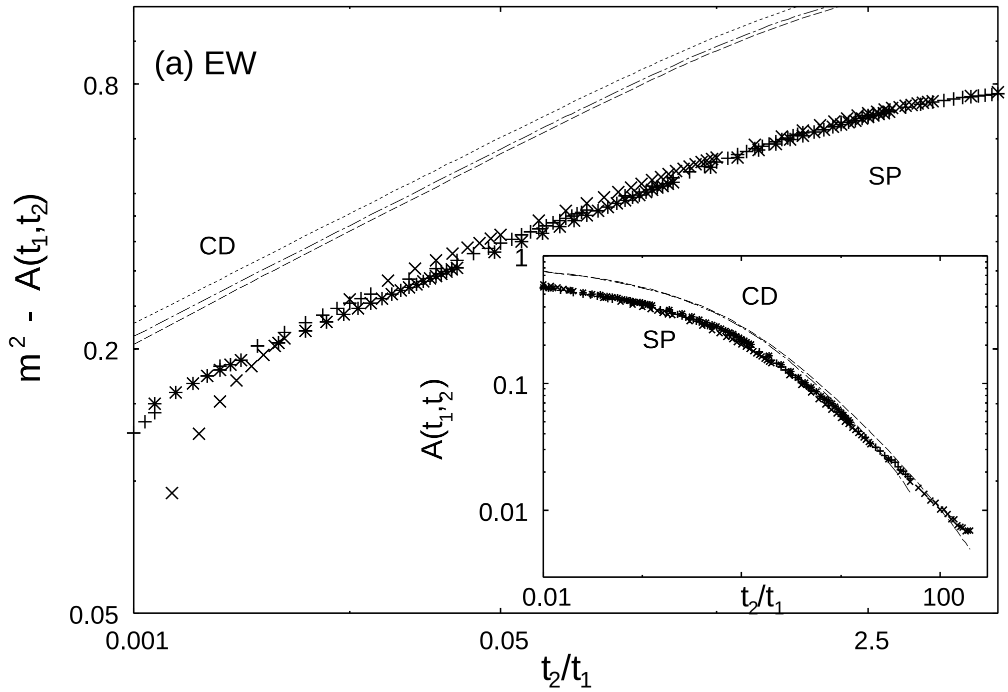

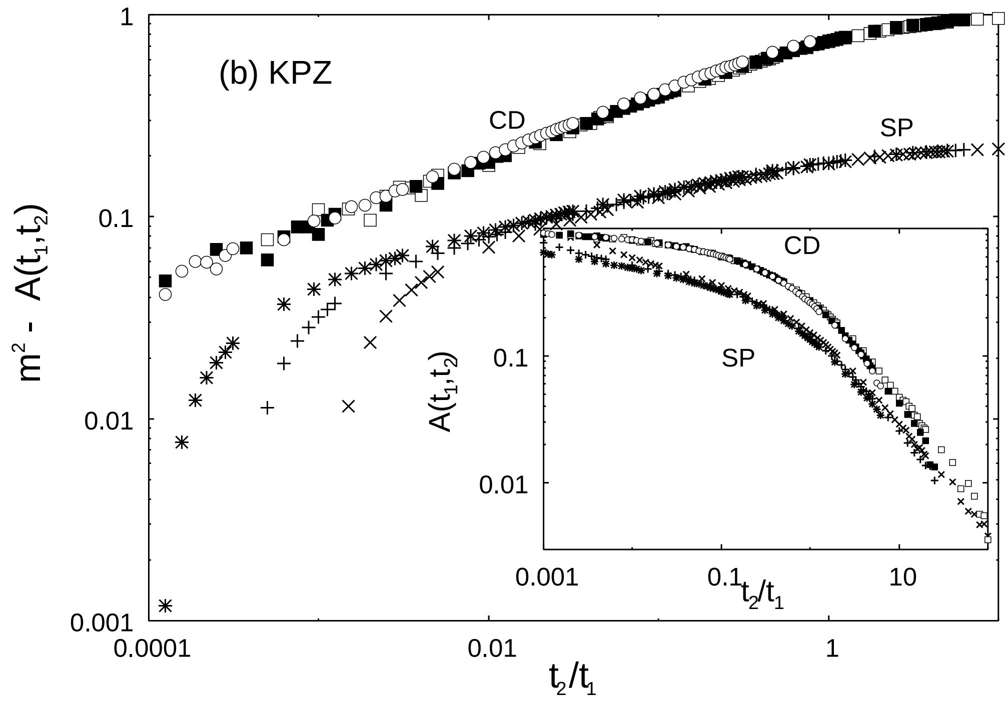

Figure 2.11: *Aging auto-correlation for CD and SP models with (a) EW and (b) KPZ interfaces. The cusp exponent β' was determined for $t_1 \gg t_2$, after subtraction from m^2. The CD model data in (a) has been multiplied by* 1.5 *to distinguish it from the SP model data points. The inset shows the power law behavior in the regime $t_1 \ll t_2$. We used $L = 2048$ in (a) and $L = 8192$ in (b). The Inset shows the data with $t_1 = 500, 2000, 8000$ in both (a) and (b). For extraction of β', we used $t_1 = 2000, 8000, 32000$.*

Chapter 3

More about FDPO

In the previous chapter we have discussed static and dynamical correlation functions of the passive particles on a fluctuating surface. We have seen that the fluctuating height field of the underlying surface gives rise to a clustering tendency among the particles and in the long time limit the particles phase separate. However, the nature of ordering present in the steady state is different from ordinary phase-ordered systems. In this new kind of phase-ordered system, strong fluctuations are present even in the thermodynamic limit. As a result, the correlation functions of the density fluctuation of the particles show some unusual features in the scaling limit which are not found in conventional phase-ordered systems.

In this chapter, we make a more detailed study of these unusual FDPO states. As we have discussed in section 2.2, the order parameter for this system is the first Fourier component of the density profile. In fig 2.6 we show the time-series of this order parameter in steady state; it fluctuates strongly and often becomes zero. But this does not mean that the system becomes disordered. As seen from fig 2.6 a dip in the first Fourier component is almost always accompanied by a simultaneous rise in the second and third Fourier component. This implies that whenever a single large cluster breaks up (causing the first Fourier component to decrease), two or three macroscopic clusters appear (causing the second or third Fourier component to go up).

From the above picture it follows that the first Fourier component alone is not sufficient to characterise the steady state as an ordered state—one should rather specify a large number of Fourier modes. It is however useful to find a single quantity that would correctly describe the nature of ordering present in the system. In the next section we show that the steady state distribution of the largest cluster present in the system serves as an unequivocal signal of ordering.

Another important characteristic of fluctuation is the presence of intermittency which implies that the density fluctuations occur in sudden bursts. The mathematical measure for this intermittent behavior is usually provided by correlation functions; the exponents describing the higher order correlation functions of density fluctuation do not grow linearly with the order; this is also known as multiscaling.

To understand the origin of intermittency, various models have been proposed [49, 50]. In the Kraichnan model of passive scalar advection, a simpler approach was taken where the velocity of the driving fluid was modelled by a random incompressible field which is Gaussian and delta correlated in time. The two point correlator of the velocity was chosen such as to satisfy the condition of incompressibility. Instead of dealing with the complicated Navier-Stokes equation for the velocity field, assuming a simple Gaussian distribution with no time-correlation is a major simplification. But this model still predicts the anomalous scaling of higher order correlation function and thus shows intermittency. Hence it follows that the complex nature of passive scalar flow that gives rise to multiscaling, actually originates from the mixing process, rather than the complexity of the turbulent velocity field of a realistic fluid.

To investigate the existence of multiscaling in our model, we monitor the density fluctuation in a segment of length r. In section 3.2 we numerically obtain the distribution function for the number of particles in a given segment on an EW surface and explain the distribution curve with the help of CD model. In section 3.3 we measure the same distribution on a KPZ surface and find qualitatively different results. We have been able to rationalise some properties of this distribution function with the help of size distributions of particle clusters and hole clusters. Finally, in section 3.4 we explicitly verify the correspondence between CD model and SP model by measuring the correlation between valleys of the surface and clusters of particles.

3.1 Largest Cluster in Steady State

One of the key characteristics of FDPO is the presence of strong fluctuations, even in the thermodynamic limit. In the steady state, large clusters are present in the system and the cluster size distribution follows a power law. As a result of fluctuations, these clusters undergo large changes in their lengths (as follows from fig 2.6), associated with the fact that the macroscopic state of the system keeps changing. For a system of size L, the typical lifetime of a macrostate scales as L^z. The question arises: if the lifetime of a state is so much smaller than exponential, in what sense can we call such a state a 'phase'?

We have addressed this question in the following way. Let $l_{max}(t)$ be the length of the largest cluster present in the system at time t. In a disordered state, when the cluster size distribution falls off exponentially, the largest cluster in the system scales as $\log L$. But starting from a random initial configuration, as the system approaches steady state, $l_{max}(t)$, although a fluctuating quantity, shows an increasing trend. Finally, in steady state, $l_{max}(t)$ is still fluctuating, thereby changing the macroscopic state of the system. But $l_{max}(t)$, despite having a broad distribution in steady state, continues to remain substantially above its disordered state value $\log L$. In other words, the system manages to retain its ordered character despite steady state fluctuations. The system continues to move from one macroscopic state to other over a time-scale of L^z. But each of these states are ordered in the sense that they all correspond to large values of $l_{max}(t)$ which scales with the system size.

We have studied the distribution of l_{max} in steady state as well as in disordered state. After the system has reached steady state, we measure the largest cluster present in that configuration. We let the configuration evolve in time and after waiting for few hundred time steps, we again measure $l_{max}(t)$. We obtain the distribution $P(l_{max}, L)$ after normalizing over 10^6 such data points. As shown in the following figures, $P(l_{max}, L)$ for different values of L undergo a scaling collapse when l_{max} is rescaled by the mean of the distribution $\langle l \rangle$. We have found that $\langle l \rangle \sim L^{\phi}$, where the exponent ϕ depends on the dynamical rules. For particles on an EW surface $\phi \simeq 0.86$, whereas for KPZ advection, $\phi \simeq 0.60$ while for KPZ anti-advection $\phi \simeq 0.91$. We show the data for KPZ advection in fig.(3.1).

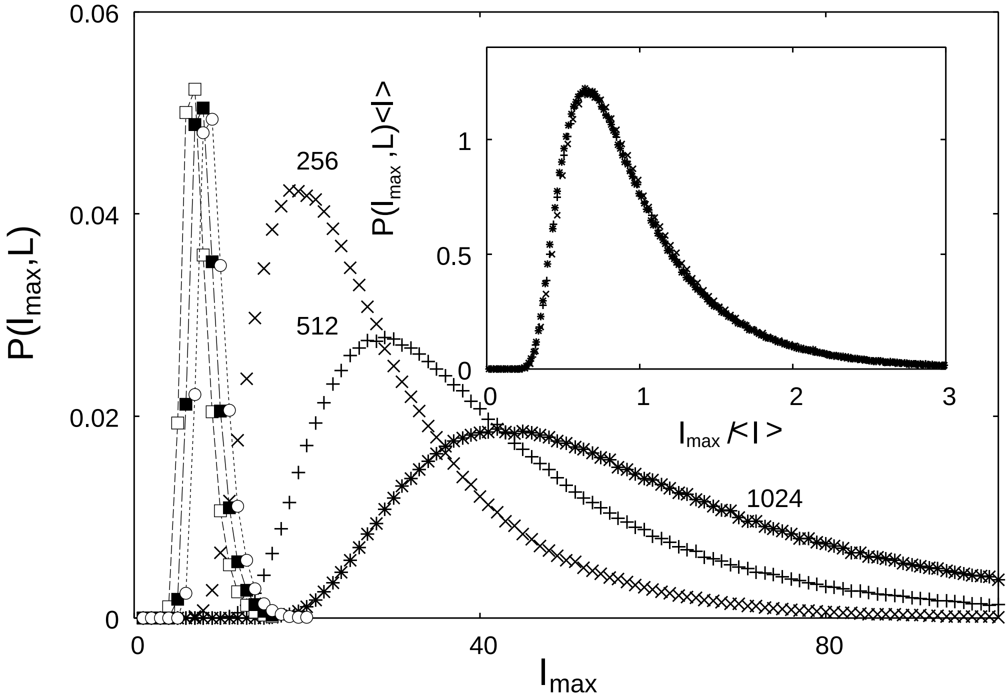

Figure 3.1: *The distribution of the length of the largest cluster* $P(l_{max}, L)$ *for particles advected by KPZ surface is shown for* $L = 256, 512, 1024$, *with the scaling collapse in the inset.The curves to the left show the same distribution in disordered state, after rescaling the y-axis by* 0.2.

For comparison, we show also the disordered state distribution obtained by averaging over 10^8 data points. The mean of this distribution scales as $\log L$ as mentioned earlier.

Our studies show that as system size increases, the overlap between these two distributions falls off. This means that as L grows, it is increasingly unlikely for the steady state l_{max} to come down as low as its value in a disordered state. The time-scale for such unlikely event would in fact be expected to grow exponentially with L. This is consistent with our data for $P(l_{max})$ for small values of l_{max} (the flat portion in fig 3.1).

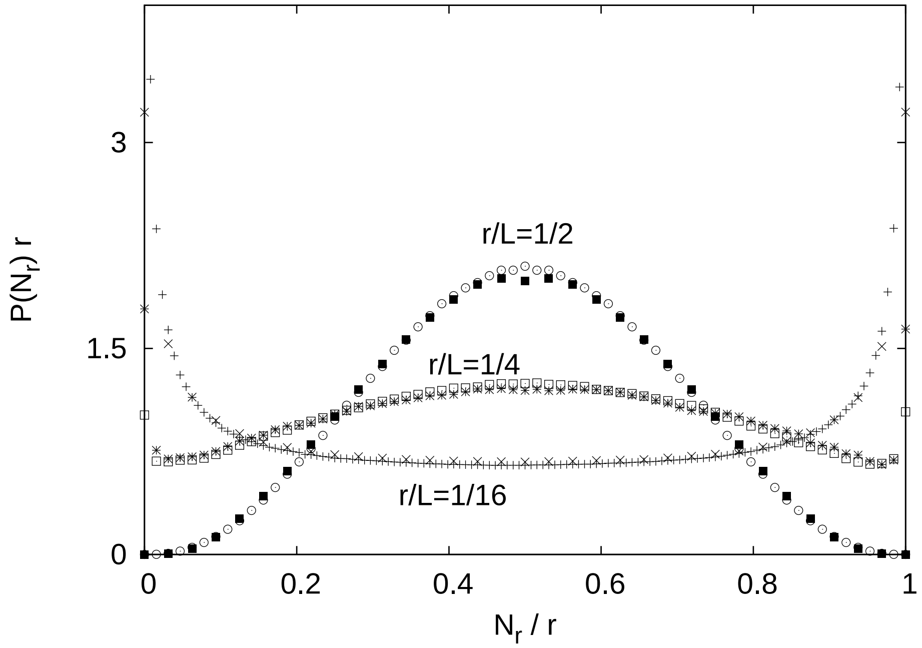

Figure 3.2: *Scaled distribution function for the number of particles in a segment of length r. The system size $L = 512$ and 2048. We have averaged over the system size L and over 10^6 configurations drawn from the steady state ensemble.*

3.2 Density Fluctuation on EW Surface

We measured the steady state fluctuation of the number of particles in a certain given region on an EW surface. Let $N_r(t)$ be the number of particles present in a given segment of length r at time t. As the system evolves in steady state, we measure the distribution function $P(N_r, L)$ for different values of r and L. We find that $P(N_r, L)$ is a scaling function of N_r/r and r/L. In fig 3.2, we show the scaled plot of $P(N_r, L)$ for different values of r/L.

Note that the form of the distribution changes strongly as r/L is changed. For $r/L = 1/2$ the distribution attains a peak at $N_r/r = 1/2$ and falls symmetrically on two sides. This behavior can be explained in the following way. Since the total number of particles in the system is conserved, N_r cannot fluctuate much if $r \sim L$. Hence as r/L becomes large, the distribution $P(N_r, L)$ attains a peak at $N_r/r = \rho$, where ρ is the filling fraction which is 1/2 in our case. The width of the distribution keeps going down as the ratio r/L increases.

However, for smaller values of r/L, the distribution function behaves in a completely different way. $P(N_r, L)$ in this case is a minimum at $N_r/r = 1/2$ and shoots up at the two boundaries $N_r/r = 0, 1$.

It is possible to explain this behavior using CD model, which is a coarse-grained surface model, introduced in section 2.1 of the last chapter. However, for the present case, it would be more convenient to use a slightly different version of the CD model, also known as CD2 model [24, 25]. In the CD2 model, we define the CD variable as

$$s_i(t) = sgn[h_i(t) - h_1(t)]. \tag{3.1}$$

In other words, we define the reference level through the first site and assign a value $s_i = +1$ to all the sites with a positive height and $s_i = -1$ to all those with a negative height. Compare this with the earlier version of the CD model, defined in section 2.1, where $s(i(t) = sgn[h_i(t) - \langle h(t) \rangle]$. Note that the position of the average height level fluctuates in time, whereas in CD2 model, the reference level always passes through the first site. Clearly in this revised CD2 model, translational invariance does not hold. However, we have verified that in the limit of large separation and large time the correlation functions of the s_i variables of this new CD2 model show similar behavior as in the previous CD model and can be described by the same set of exponents as in table 2.1.

According to our interpretation of the CD model [see section 2.1] the particles tend to be present in the 'lowlands'. Hence the study of the static and dynamical properties of the lowlands can be expected to provide some insight into the behavior the the particles. With this in mind, let us now define the following quantity in CD2 model: $S_r = \sum_{i=1}^{r} s_i$. Since in one dimension, any interface configuration can be mapped onto a random walk trajectory (where the height h_i represents the displacement of the walker at the i-th time-step), S_r denotes the excess time the random walker spends on one particular side of the origin. But the distribution $P(S_r)$ is exactly known and has the form

$$P(S_r) = \frac{1}{r} \frac{1}{\pi\sqrt{S_r(1 - S_r)}}, \qquad 0 \ll S_r \ll r. \tag{3.2}$$

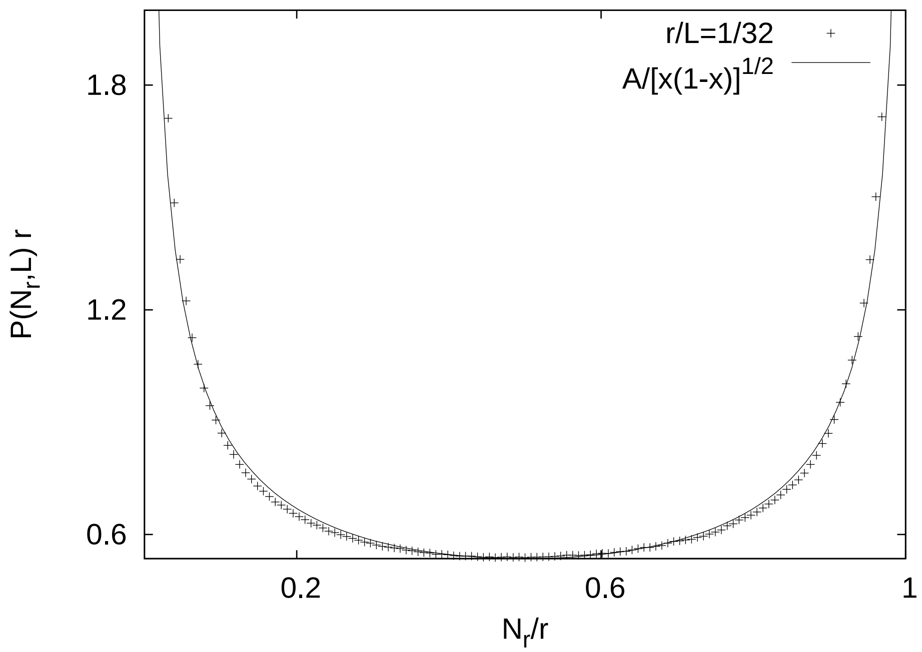

Figure 3.3: *Scaled distribution $P(N_r, L)$ fitted to the form $A/\sqrt{x(1-x)}$ with $A \simeq 0.27$ for $L = 4096$.*

Formula 3.2 is known as discrete arc sine law for sojourn times [43]. In fig 3.2 we fit this functional form to the scaled $P(N_r, L)$ for small r/L.

As r/L increases, because of the conservation of the total number of particles, large fluctuations of N_r become less probable and the distribution starts developing a peak at $N_r/r = 1/2$ as shown in fig 3.2 for $r/L = 1/4$ and $1/2$.

From the distribution function $P(N_r, L)$, we have computed higher order moments of N_r and found that there is no multiscaling, *i.e.* $\langle (N_r - r/2)^p \rangle \sim r^p$.

3.3 Density Fluctuation on KPZ Surface

The distribution function $P(N_r, L)$ for KPZ surface, is found to be a scaling function of N_r/r and r/L, as in the last section. Moreover, for large r/L, due to the conservation of total number of particles the large density fluctuations are suppressed and the distribution function has a peak at $N_r/r = 1/2$, as before.

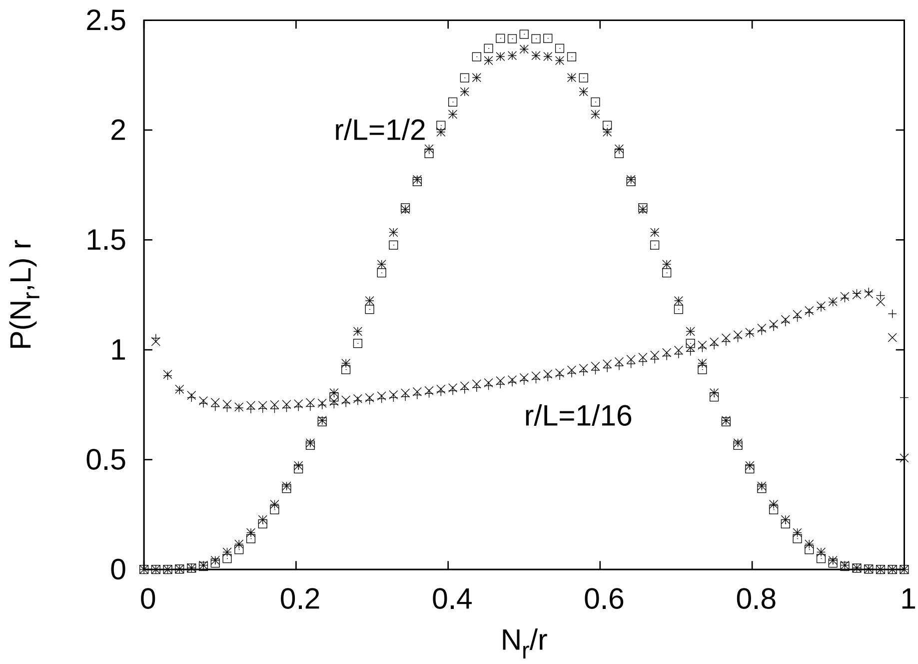

Figure 3.4: *Scaled distribution function for N_r on a KPZ surface. We have used $L = 2048$ and 4096 and averaged over 10^5 configurations in steady state.*

We present the data in fig 3.4

However, for small values of r/L the behaviour is completely different. In fig 3.5 we have shown the unscaled distribution for the number of particles in a small segment of length r. We find that the distribution of particle numbers is maximum at $N_r = 0$ and as N_r increases, the distribution function drops sharply and again slowly increases. We have been able to rationalise this behavior in the following way.

Consider the size distribution of particle clusters ($p(l)$) and hole clusters ($h(l)$) on a KPZ surface. As seen from fig 2.4:

$$\begin{aligned} h(l) &> p(l) \quad \text{for very small } l \\ h(l) &< p(l) \quad \text{for moderate } l \\ h(l) &\gg p(l) \quad \text{for large } l \end{aligned} \tag{3.3}$$

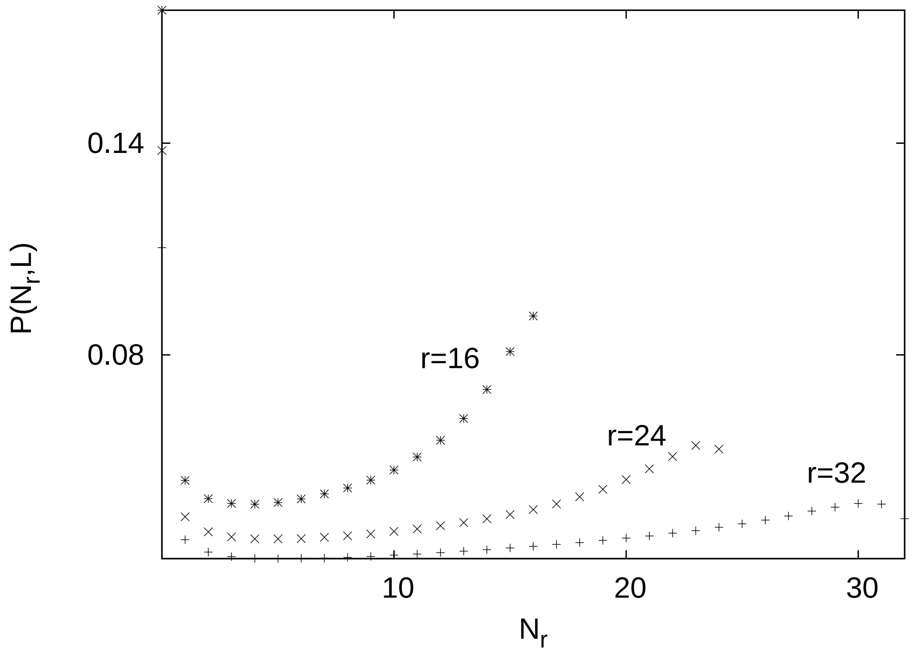

Figure 3.5: *Number fluctuation of particles in a segment of length* $r = 32, 24, 16$ *and* $L = 512$.

Let us now consider the following scenario: the particle clusters are formed in the valleys of the surface but these clusters are not very big as they are interrupted by very small hole clusters (of size 1 or 2). So even if the particles are mostly found in the valleys, they do not form very big clusters because of the small number of holes present. On the other hand, the hole clusters can be quite big. These big hole clusters are naturally found in the hills of the surface. Although it is possible to find one or two particles in the hills, they are too few to cause a serious reduction in the hole cluster length. In fig 3.6 we have schematically shown one such configuration.

Clearly, the scenario described in the last paragraph, is consistent with the behavior of $p(l)$ and $h(l)$ in fig 2.4. Let us now examine whether this picture fits in with our results for $P(N_r, L)$ in fig 3.5. For a fixed r and L, small values of N_r implies that the segment under consideration lies in a hill. Since the hills contain large hole clusters if r is not too big, most of the time the segment is empty

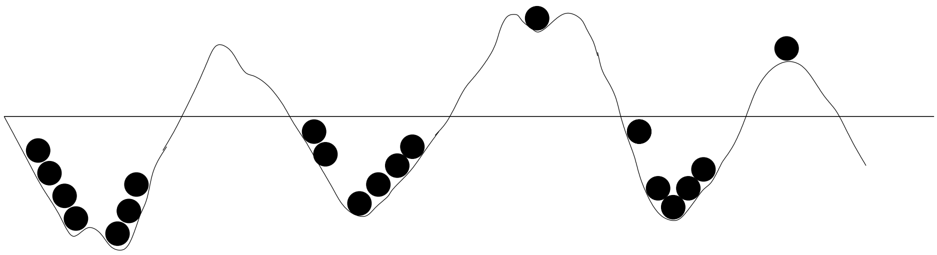

Figure 3.6: *Particle clusters are interrupted by the presence of holes in the valleys.*

which explains the large value of $P(N_r = 0)$. Small non-zero values of N_r mean that the segment still lies in the hill but passes through small and rare particle clusters. The sharp drop in $P(N_r)$ reflects the rare occurrence of these particle clusters in the hills. However, as N_r increases, we get contribution from the valleys which contain particle clusters of moderate lengths. These moderately large particle clusters in the valleys are more probable than the small particle clusters in the hills and hence $P(N_r)$ shows a rise after the initial sharp fall. But it never becomes as large as $P(N_r = 0)$ because even if the segment lies in a valley, it does not contain a large number of particles very often because of the presence of several small hole clusters in the valleys.

Hence we have been able to arrive at a picture of what a typical configuration looks like, and this picture successfully explains our results for cluster size distribution and density fluctuations. However, calculation of higher order moments of N_r shows that no multiscaling exists in this system.

3.4 Correspondence between Particle Densities and Valleys

In the previous chapter and the present chapter, we have seen that CD model often explains many features of the SP model. Since the particles tend to be present in the valleys, by studying the fluctuation of the valleys one can understand many things about the density fluctuation of the particles. In this section, we explicitly examine how often the particle clusters are indeed found in the valleys.

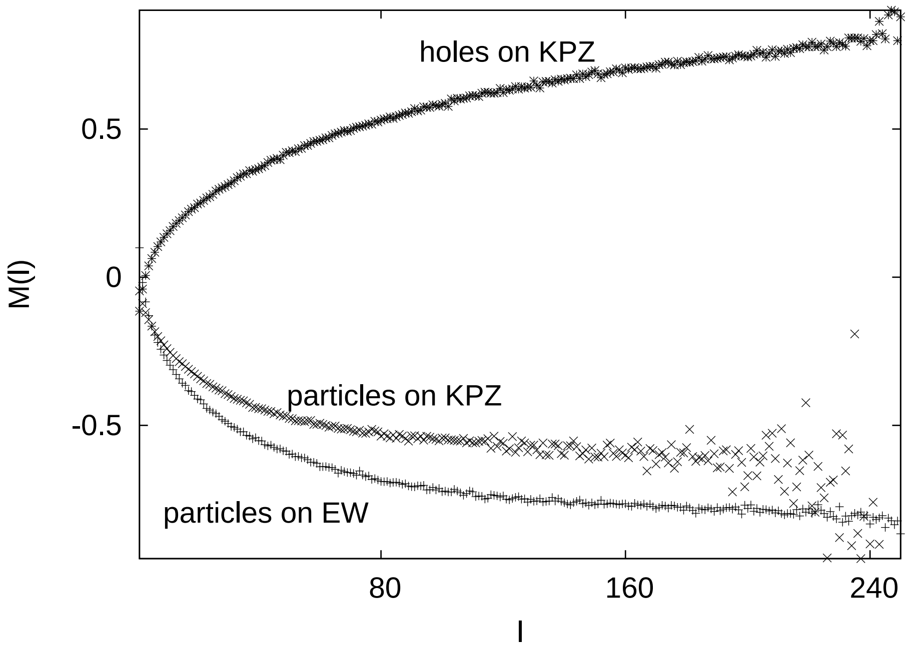

Figure 3.7: *Plot of $M(l)$ vs l for particle clusters and hole clusters on KPZ surface and particle clusters on EW surface. We have used $L = 512$.*

Consider a particle cluster of length l which extends from the i-th site to $(i+l-1)$-th site. Now, define the quantity

$$M(l) = \frac{1}{L}\langle\left(\sum_{j=i}^{i+l-1} s_j(t)\right)\rangle \tag{3.4}$$

where $s_j(t)$ is the CD variable defined as $s_j(t) = sgn[h_j(t) - \langle h(t)\rangle]$, as in section 2.1 of the last chapter. Note that if the particle cluster is in a valley then the values of CD variable at those sites would be negative and hence the average quantity $M(l)$ would also be negative. In fig 3.7 we show our results for $M(l)$ vs l for particle clusters on EW surface and particle and hole clusters on KPZ surface. We find that for particle clusters of length l, $M(l)$ becomes more and more negative as l increases, implying larger clusters are formed in deeper valleys. Similarly, for the hole clusters $M(l)$ increases on the positive side as the large hole clusters are always found in the hills.

Chapter 4

Discussion: Passive Scalars

In chapters 2 and 3, we have discussed the static and dynamical properties of interacting passive scalars driven by a fluctuating Edwards-Wilkinson or Kardar-Parisi-Zhang surface (or, equivalently, a Burgers fluid). Our studies show that the steady state of the system is an unconventional ordered state which supports strong fluctuations.

In this short chapter we compare our results on static and dynamical properties of passive scalars with some relevant earlier work.

Mitra and Pandit had studied the dynamics of passive scalars in [26] where they considered the dynamical properties of a system of non-interacting passive particles, advected by an incompressible fluid, whose velocity field is drawn from the Kraichnan ensemble, and therefore has power law correlations in space, but is delta-correlated in time. In an Eulerian (space-fixed) framework, they find that the space-time correlation function $G(r, t, L)$ satisfies a diffusion equation in r and t, with an L-dependent diffusion constant. In the quasi-Lagrangian framework (with the origin moving on a Lagrangian trajectory), they obtain $r \sim t^{1/z}$ with $z < 2$ and no dependence on L.

By contrast, we have studied passive particles with hard-core interactions, advected (in the Burgers case) by a compressible flow which has power law correlations in time. Particles are driven together in our case, rather than spreading out. $G(r, t, L)$ is a function of the scaling combinations r/L and t/L^z, as in a phase-ordered system. However, there appears to be no indication of non-trivial $r - t$ scaling.

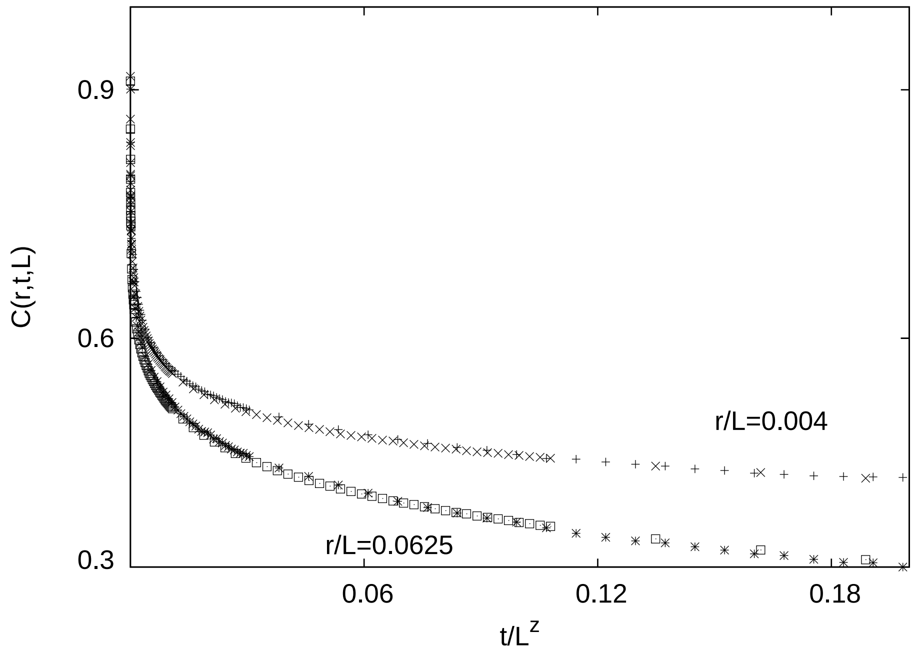

Figure 4.1: *The Lagrangian correlation function $C(r, t, L)$ is plotted against scaled time t/L^z for fixed values of r/L. We have used $L = 1024, 2048$.*

Throughout, we have used Eulerian framework. However, our studies in a Lagrangian framework, where distances are measured from an origin that moves with one of the passive particles, shows that a similar L-dependent scaling form remains valid. In fig 4.1 we present our results on Lagrangian auto-correlation function defined as $C(r, t, L) = \langle\theta(r, 0)\theta(r, t)\rangle$ where $\theta(r, t)$ is the density field at a distance r away from a tagged particle. We find that $C(r, t, L)$ is a scaling function of $\xi \equiv r/L$ and $\tau \equiv t/L^z$. In fig 4.1 we show the scaling collapse as a function of τ for different fixed values of ξ.

This difference of behavior between our results and those in [26] reflects the difference between passive scalars with strong clustering or phase-ordering tendencies, and those which spread out in space. In turn, this clustering tendency is presumably a reflection of the strongly compressible nature of the Burgers fluid.

Even when the driving field is compressible, the degree of clustering of the passive particles depends on the nature of the interaction between them. In the presence of the hard-core interactions, the system reaches a phase-ordered state, albeit one with strong fluctuations. As a consequence, in the limit of small scaling argument, the spatial and temporal correlation functions show a cuspy approach to a finite intercept. However, in the absence of any interaction, the passive particles go into a much more strongly clustered state, where the correlation functions show a power law divergence at the origin [22, 23].

Finally, the study of the largest cluster allows us to arrive at a simple picture of a fluctuation-dominated phase-ordered state. Strong fluctuations often make the order parameter (the first Fourier component of the density profile) zero. But the system does not lose its ordered character. Rather, fluctuations carry the system from one ordered configuration to another macroscopically distinct one, over a time-scale $\sim L^z$. However, the probability for the system to leave this attractor of ordered state vanishes exponentially with the system size.

Chapter 5

Non-equilibrium Probes in Driven Diffusive Systems

In the last few chapters of this thesis, we have discussed advection of passive particles which do not affect the medium. On the other hand, if probe particles are introduced in a medium, then these probe particles may influence the medium properties. However, one would expect that probe particles would produce local effects and therefore for sufficiently low concentration of the probe particles, the effect would not be strong. We find that this assumption may not always hold true and depending on the nature of the probe and the medium, the effect of a probe particle may be short ranged or long ranged or even macroscopic, in the low dilution limit.

In the remaining part of this thesis, we discuss how the dynamical evolution of a medium gets affected by the presence of probe particles and the influence of the medium on the probe dynamics itself. We have considered a medium which can be described by simple one-dimensional lattice models of nonequilibrium (driven) systems and their equilibrium counterparts. We are primarily interested in the simplest such models where no interaction is present among the medium particle, other than hard-core exclusion. Two different kinds of nonequilibrium probe particles is considered—shock tracking probes (STPs) and directed probe particles

(DPPs). The exchange rules are:

$$\begin{aligned}
Medium: \quad & +- \xrightarrow{1} -+ \\
& -+ \xrightarrow{\text{q}} +- \\
\\
Probe: \quad & 0- \xrightarrow{1} -0 \\
& +0 \xrightarrow{\text{w}} 0+
\end{aligned} \tag{5.1}$$

where '+' denotes a particle, '−' denotes a hole and '0' denotes a probe. We will consider equal densities of particles and holes in the medium, *i.e.* $\rho_0 = 1 - 2\rho$ where ρ and ρ_0 denote the densities of the particles and the probes, respectively.

STPs exchange with the particles and holes of the medium in opposite directions but with equal rates, *i.e.* $w = 1$. For a DPP on the other hand, these two rates are different—we consider $w < 1$. Note that these dynamical moves for the probes do not satisfy detailed balance. Hence these probes are intrinsically nonequilibrium. Moreover, as seen from the exchange rules, both STPs and DPPs tend to have an excess of holes to their left and particles to their right. For example, consider this configuration: $+---0++++-$. Here, the probe is locally stable and moves only when the medium around the probe rearranges itself, *e.g.* in this case, the probe can move only when a particle(hole) approaches the probe from left(right).

In other words, around a probe, a strong density variation or 'shock' is developed. However, depending on the exchange rules of the medium and the probe (which is controlled by the parameters q and w, respectively), the density profile around a probe can be qualitatively different. For example, when $q = 1$, the medium is described by a symmetric exclusion process, in absence of any probes. In this initially equilibrium medium, when even a single nonequilibrium probe is added, the shock around the probe extends through macroscopic distance for all values of w.

Consider another limiting case, $q = 0, w = 1$. In this case, the medium is described by a totally asymmetric exclusion process and a single probe gives rise to a shock that decays as a power law [34]. For $q = 0$ and $w = 0$, however, as seen from Eq. 5.1, a single probe behaves as a tagged medium particle and no shock

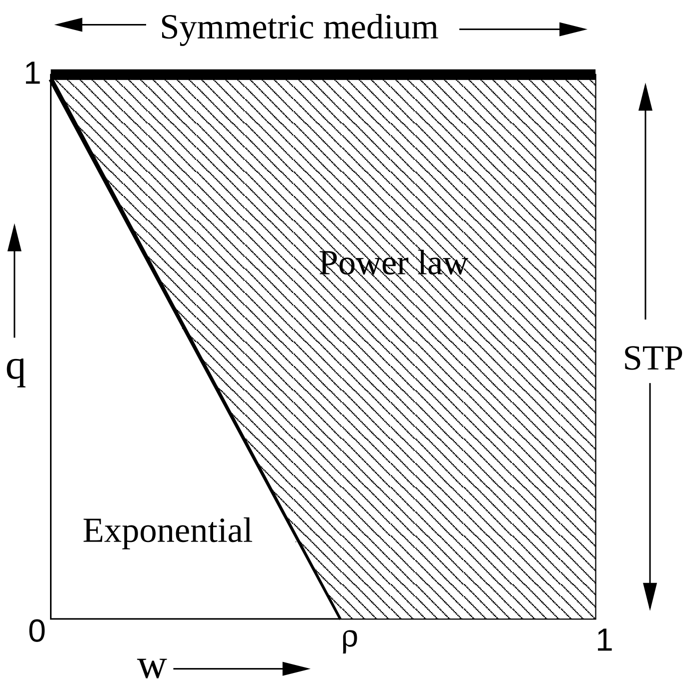

Figure 5.1: *Phase diagram for a single nonequilibrium probe in an ASEP. The x-axis refers to the properties of the probe while the y-axis refers to that of the medium. The top thick line corresponds to the symmetric medium (SEP) where a single probe produces macroscopic effect. The shaded region corresponds to the power law decay of the density profile around a single probe and in the unshaded part the shock across a single probe is short ranged.*

is produced. For intermediate values of q and w an interesting phase diagram is obtained [see fig 5.1].

In chapter 6, 7 and 8 we summarise our results for different lattice models of equilibrium and nonequilibrium medium and describe how the interplay between equilibrium and nonequilibrium characteristics of the medium and the probe particles gives rise to interesting effects.

Chapter 6

Nonequilibrium Probes in an Equilibrium Medium

In this chapter, we discuss the situation when nonequilibrium probes are introduced in a medium that is initially in equilibrium. We primarily consider the case when the medium is described by a symmetric exclusion process (SEP). The dynamical moves are shown below:

$$
\begin{aligned}
Medium: \quad & +- \xrightarrow{1} -+ \\
& -+ \xrightarrow{1} +- \\
\\
Probe: \quad & 0- \xrightarrow{1} -0 \\
& +0 \xrightarrow{\mathrm{w}} 0+
\end{aligned}
\tag{6.1}
$$

These moves are same as in Eq. 5.1 of last chapter, with $q = 1$. When the backward exchange rate of the probe w becomes unity, the model reduces to a special case of the model proposed by Arndt *et al.* (popularly known as AHR model) [45], with the asymmetry parameter set equal to its critical value 1. In section 6.5 we include a discussion on the AHR model.

In the next section, we discuss how the static properties of the medium get strongly affected by the presence of a single probe. In section 6.3 and 6.4 describe our results on the dynamical properties of the medium and the probe, respectively. In section 6.5 we consider the case when a macroscopic number of such probes are present and in section 6.6 we generalise our conclusions for a few other examples of equilibrium media.

6.1 Properties of Symmetric Exclusion Process

In the absence of any probe, the medium is described by a one dimensional symmetric exclusion process (SEP), which is one of the most important lattice gas models for equilibrium systems. In this section, we include a brief discussion on SEP.

SEP being an equilibrium lattice gas model, its steady state obeys detailed balance. It can be shown that the steady state of the system is described by a product measure with uniform density ρ. As a result, the two point and all the higher order static correlation functions of the local density variable factorise in steady state.

Although the steady state density profile is uniform throughout the system, in a typical configuration, density fluctuations are present. It is interesting to study how these density fluctuations dissipate in time. For this purpose one can monitor the mean squared displacement of a tagged particle defined as follows. Let $Y_k(t)$ be the position of the k-th tagged particle at time t. Then its mean squared displacement $C_+(t)$ is defined as

$$C_+(t) = \langle (Y_k(t) - Y_k(0) - \langle Y_k(t) - Y_k(0) \rangle)^2 \rangle. \tag{6.2}$$

Note that for a SEP, since there is no current in the steady state, the average $\langle Y_k(t) - Y_k(0) \rangle = 0$. In one dimension, $C_+(t)$ can be exactly calculated and has the asymptotic form [44]

$$C_+(t) \approx \sqrt{(2/\pi)}(1-\rho)/\rho t^{1/2}. \tag{6.3}$$

Notice the sub-diffusive growth of $C_+(t)$—although an individual particle behaves like an unbiased random walker, because of the hard-core constraint, the trajectory of the k-th particle is bounded from two sides by the trajectories of the $(k-1)$-th and $(k+1)$-th particles. This is known as 'caging effect' and leads to the sub-diffusive growth of $C_+(t)$. This is a special property found only in one dimension. $C_+(t)$ for SEP in higher dimensions does grow diffusively.

6.2 Static Properties of the Medium

As described above, in the absence of any probe, the system obeys detailed balance and its steady state is given by a uniform product measure. With the introduction of a single probe, the condition of detailed balance is violated, since the dynamical rules for the probe do not satisfy detailed balance. As a result, when a single probe is present, there is a small ($\sim 1/L$) current in the system.

Density Profile measured from the single Probe: In this nonequilibrium steady state, there is a system-wide density gradient around the probe. This can be explained as follows. First note that a probe exchanges with particles (holes) to its left (right) with rate w (1). As of now, set $w = 1$. Then a periodic system with a single probe can be alternatively viewed as an open chain SEP where particles (holes) are injected from the left (right) and taken out from the right (left) end with rate unity. The particle density at the left end should then be 1 and at the right end it should be 0. The current in this boundary driven diffusive system would be proportional to the density gradient. The continuity equation then becomes

$$\frac{\partial \rho}{\partial t} = D \frac{\partial^2 \rho}{\partial x^2} \tag{6.4}$$

In steady state, the left hand side vanishes and solving with the boundary condition for ρ, gives

$$\rho(r, L) = 1 - \frac{r}{L} \tag{6.5}$$

Note that since we have interpreted a periodic system with a single probe as an open chain SEP, the latter has a special property that as soon as a particle (hole) leaves the chain from right (left) end, it immediately reappears at the left (right) end. This implies a correlation between the injection and extraction at the two boundaries.

Figure 6.1 shows the density $\rho(r) \equiv \langle n(r) \rangle$ at a distance r away from a single STP, where $n(r)$ is the occupancy at r. We find that

$$\rho(r, L) = A(1 - r/L), \qquad A \simeq 1. \tag{6.6}$$

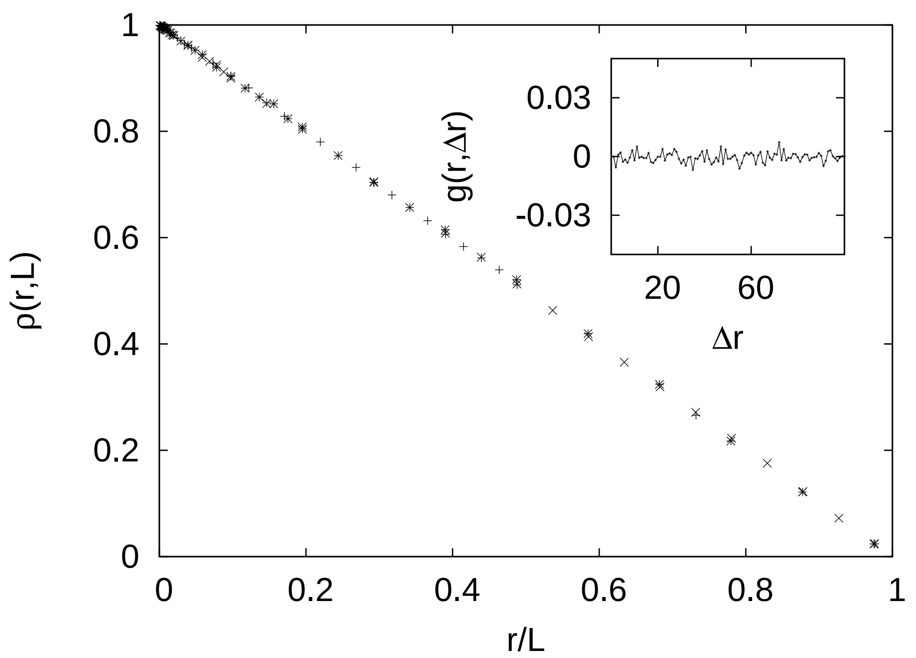

Figure 6.1: *Density profile as a function of the scaled distance away from the probe in the SEP with* $w = 1$ *for* $L = 513, 1025, 2049$. *The data are averaged over* 50000 *histories. The inset shows* $g(r, \Delta r$ *for* $r = 1024$ *(*$L = 2049$*, averaged over* 10^4 *histories) and illustrates that the pair correlation is close to zero.*

Above form of the density profile remains valid as long as the backward exchange rate w for the probe in non-zero. However, when $w = 0$, the form of $\rho(r, L)$ changes. Note that for $w = 0$, the probe can move only in the forward direction by exchanging with the holes in the medium, but it cannot exchange with the particles of the medium. We find that in such a case, $\rho(r, L)$ falls exponentially with length scale proportional to L: $\rho(r, L) = A_0[1 - exp(-r/L)]$ with $A_0 \simeq 1$ [see fig 6.2].

Two point Correlation Function in the Medium: To study the fluctuations present in the medium around the average density profile, we have monitored two point density-density correlation function defined as

$$g(r, \Delta r) = \langle n(r)n(r + \Delta r)\rangle - \rho(r)\rho(r + \Delta r) \tag{6.7}$$

for a fixed value of the distance r measured from the probe. Our data presented

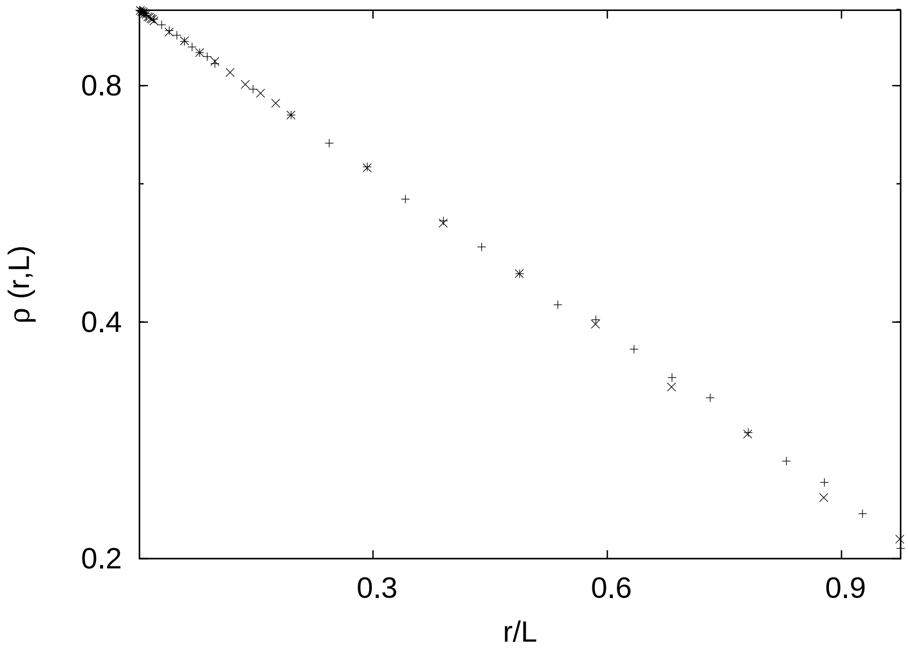

Figure 6.2: *Density profile as a function of the scaled distance away from the probe with* $w = 0$*. Logarithmic scale has been used in the* y *direction. We have used* $L = 513, 1025$ *and averaged over* 50000 *histories.*

in the inset of fig 6.1 shows that $g(r, \Delta r)$ is close to zero for all values of Δr, which points to the existence of product measure.We have verified that this holds for all values of w.

Note that in order to establish the presence of inhomogeneous product measure, one should in principle measure all higher order correlation functions and verify that each of them factorises. We have measured only two-point correlation function and from this study it cannot be said conclusively whether the steady state of the system supports inhomogeneous product measure or not. However, from our interpretation involving an open chain SEP, and from the known result that an open chain SEP shows inhomogeneous product measure [47], it seems plausible that inhomogeneous product measure might actually exist even in this system.

6.3 Dynamical Correlation Function in the Medium

In the last section, we have seen that presence of a single probe takes the system from an equilibrium state to a nonequilibrium current-carrying state. However, at a macroscopic distance away from the probe, the system still behaves as in local equilibrium—local properties of the medium still resembles those of the SEP. We demonstrate this by measuring the mean squared displacement $C_+(r,t)$ of a tagged particle which is initially at a distance r away from the probe.

In absence of any probe when the system is executing a SEP, mean squared displacement of a tagged particle can be exactly calculated and the asymptotic behavior is shown in Eq. 6.6. When a probe is present, $C_+(r,t)$ for large r becomes same as in Eq. 6.6 with ρ replaced by the local density $\rho(r,L)$. In fig 6.3 we present data for $C_+(r,t)$ for different values of local densities.

Note that this agreement is expected to hold as long as the tagged particle remains in the region with local density $\rho(r,L)$. As shown in fig 6.1, density of the medium changes over a length scale $\sim L$ and typical velocity of a tagged particle is $\sim 1/L$ (since there is a current $\sim 1/L$ in the system). This implies that the tagged particle will remain in the region with local density $\rho(r,L)$ for a time-scale $\sim L^2$. In other words, the region of validity in fig 6.3 extends upto a time-scale $\sim$ Ł^2.

6.4 Mean Squared Displacement of the Tagged Probe

The mean squared displacement of the single probe grows diffusively with a diffusion constant $D \sim 1/L$. This can be explained as follows. For equal densities of particles and holes in the medium and for $w = 1$, the probe has an equal probability of moving to the left or right. In order to move to the right (left), the probe must have a hole (particle) to its right (left) [see Eq. 6.1] and according to Eq. 6.6, this probability is $\sim 1/L$ in each Monte Carlo step. The mean squared displacement of the probe therefore scales as $1/Lt$ for large t. We present our data in fig 6.3 for $w = 1$.

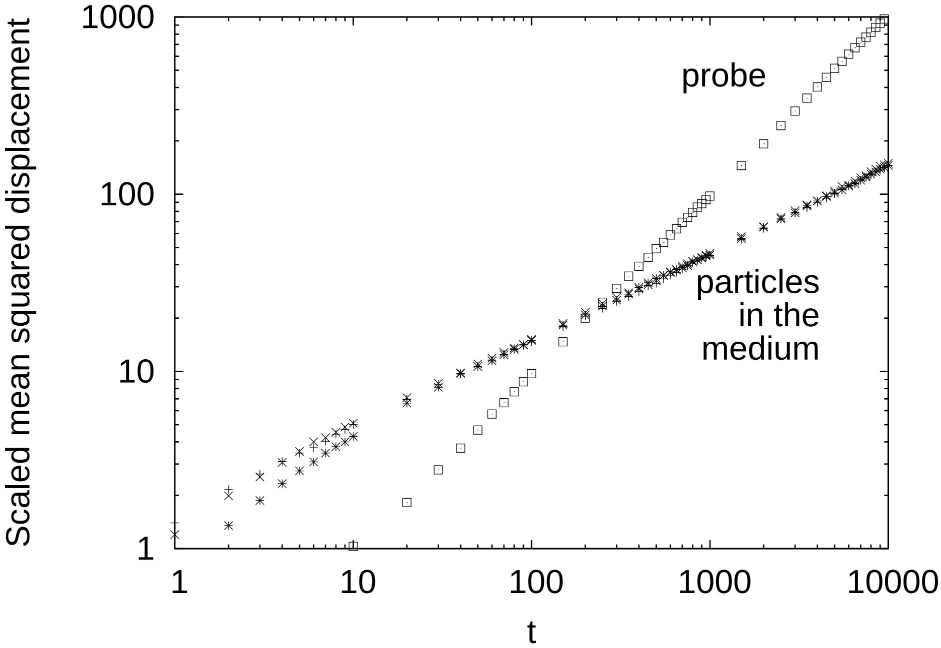

Figure 6.3: *Scaled mean squared displacement of tagged particles at distances* $r = 580, 985, 1390$*, away from the probe, corresponding to* $\rho(r, L) = 0.72, 0.52, 0.32$ *(*$L = 2049$ *and* $w = 1$*, averaged over* 10^4 *histories). The curves are seen to merge when the coefficient* $(2/\pi)^{1/2}(1 - \rho(r, L))/\rho(r, L)$ *is divided out. Also shown is the mean squared displacement of a single probe scaled up by a factor of* 100.

For $0 < w < 1$, the probe has a non-zero velocity. But since the density profile around the probe remains same as in Eq. 6.6, the probability to move to the left is $\sim 1/L$ as before, but the probability for moving to the right now becomes $\sim w/L$. As a result, the diffusion coefficient shows same $1/L$ scaling with the system size.

6.5 Macroscopic Number of Probes

So far we have considered only a single nonequilibrium probe introduced in a system executing SEP. We have found that a single probe gives rise to a macroscopic effect in the system. When a macroscopic number of these probes are introduced, we find that the medium induces a very strong clustering tendency among them. In fact for $w \neq 0$ these probes form essentially a single cluster and are phase separated. The other phase is comprised of the medium, which continues to remain in local equilibrium with a similar density gradient as in the single probe case.

We understand this phenomenon using the following picture. First consider a single probe in the medium which produces a macroscopic density gradient. Now, if another probe is added to the system, it will feel the presence of the density gradient, regardless of its initial separation from the first probe, since the density gradient extends over macroscopic distances. If $w \neq 0$, the second probe will now move along the direction of increasing density (by exchanging with particles and holes of the medium in the opposite directions) until it reaches the neighboring site of the first probe. This explains the strong attraction between a pair of probes. By extending similar reasoning for a macroscopic number of probes, one can explain why the probes form essentially a single cluster.

Note that for $w = 0$, clustering among the probes is not possible, since the number of particles between any two probes is a constant of motion and can not change. However, even in this case the two point density-density correlation function between the probes is a scaling function of r/L with r being the spatial separation and L the system size.

It will be useful to compare our results for many probes with the known results for another model, which is commonly known as the AHR model [45]. This is a two component model defined on a one dimensional periodic lattice. The dynamical moves are as follows:

$$+- \xrightarrow{\text{r}} -+ \tag{6.8}$$

$$-+ \xrightarrow{1} +- \tag{6.9}$$

$$+0 \xrightarrow{1} 0+ \tag{6.10}$$

$$0- \xrightarrow{1} -0 \tag{6.11}$$

As mentioned at the beginning of this chapter, our present model of SEP with STPs ($w = 1$) reduces to AHR model when the asymmetry parameter r is set equal to unity.

Arndt *et al.* had claimed that this model shows spontaneous breaking of translational invariance and phase separation as r is varied. For $r < 1$ the system is in the 'pure phase', where a typical configuration contains three blocks, one each of particles, holes and probes. In the thermodynamic limit, the current vanishes exponentially with the system size.

When r is slightly greater than 1, the system is found in a 'mixed phase', where the two pure blocks of particles and holes that was found for $r < 1$, merge and the rest of the system consists of the probes and occasional presence of particles and holes, distributed in an uniform way.

For still larger values of r, phase containing the probes grows in size and finally when r exceeds a critical value r_c, this phase takes over the entire lattice and the system goes to a 'disordered phase'. In [45] it was therefore claimed that this model shows two phase transitions: one at $r = 1$ and the other at $r = r_c$. However, subsequent studies of Rajewsky *et al.* show that the second phase transition at $r = r_c$ is not real—at this point the correlation length becomes very very large ($\sim 10^{70}$) but remains finite.

The only critical point, therefore, is at $r = 1$. Our studies show that while the pure block of the probes can still be found at $r = 1$, the pure blocks of particles and holes that are present for $r < 1$, disappear. The system at $r = 1$ consists of two phases, one is comprised of the probes and a linear density gradient of the particles is present across the other phase.

6.6 Probes in Other Equilibrium Media

So far we have considered a medium which is described by a SEP, in the absence of any probe. In this section, we briefly describe our results for a few other examples of an equilibrium medium.

Symmetric k-hop Model: We have defined a symmetric variation of k-hop model, first introduced in [48]. In this model, extended range for particle hopping is allowed. The dynamical rules are as follows. If a randomly chosen site contains a particle (hole), then it exchanges with the nearest hole (particle) or probe that lies within a distance k from the chosen site; the range k is chosen on either side of the chosen site with probability 1/2. If the chosen site contains a probe, then

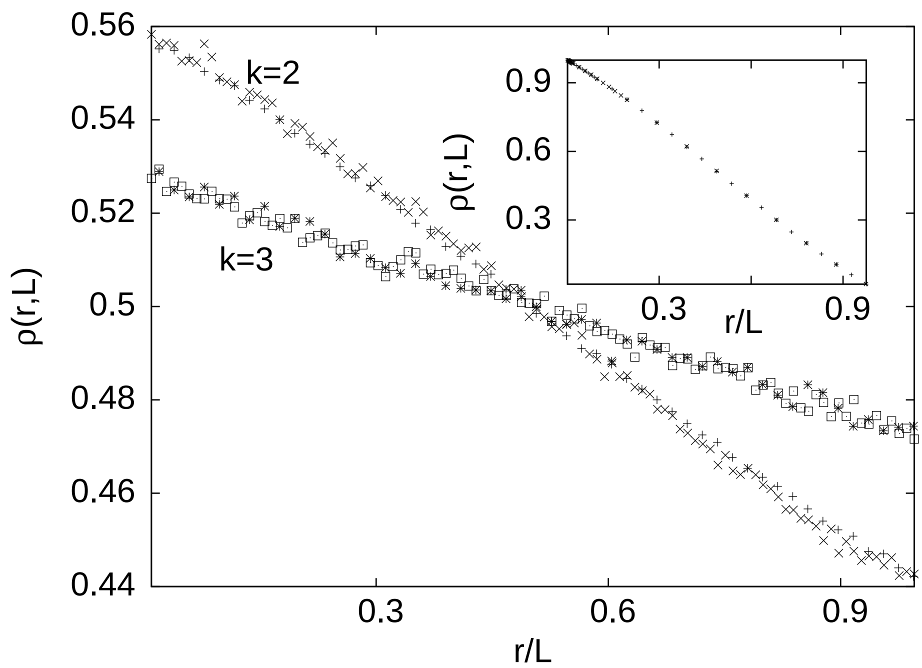

Figure 6.4: *Scaled density profile for symmetric k-hop model for $k = 2$ and $k = 3$. Inset shows the same plot for Kawasaki model with $=$ epsilon $= 0.2$. We have used $L = 513, 1025$ and $w = 1$.*

with equal probability it exchanges with its left or right neighbor if the left or right neighbor is a particle or hole, respectively. For example, the configuration $- - 0 + + + -$ goes to $- - 0 - + + +$ when the $+$ next to the 0 is chosen to move to the right. Note that $k = 1$ corresponds to SEP with STPs present in it.

When no probes are present, the dynamics of the system satisfies detailed balance and its steady state is given by a uniform product measure. We find that a single probe gives rise to macroscopic shock as seen is section 6.2. However, as k value increases, the particles and holes in the medium can hop over a larger and larger range and it becomes increasingly difficult for the probe to sustain a density gradient. As a result, the amplitude of the shock around the probe, *i.e.* the prefactor in Eq. 6.6, falls off as k increases. We present our data for $k = 2$ and $k = 3$ in fig 6.4

Kawasaki Model: In this case, the particles and holes in the medium evolve according to Kawasaki dynamics, *i.e.* there is an Ising interaction $V = -\epsilon[(n(i) - \frac{1}{2})((n(j) - \frac{1}{2})]$ between the neighboring particles $\langle ij \rangle$ in the medium and each of the first two moves in Eq. 6.1 takes place with rate $(1 - \Delta V)$ where ΔV is the change in Ising energy. The exchange rules for the probes remain same as in Eq. 6.1.

We find that even in this case, the medium is strongly affected by the probe. A single probe gives rise to macroscopic density gradient [see fig 6.4] and a small current in the medium and the composite system goes to a nonequilibrium steady state.

Chapter 7

Probes in a Nonequilibrium Medium

In the previous chapter, we have discussed the effect of nonequilibrium probes in an initially equilibrium medium. We have seen that their effect is quite strong and even a single nonequilibrium probe produces a macroscopic effect on the medium. However, the effect is less drastic for a medium which is initially in a current-carrying nonequilibrium state. The effect of a single probe is not macroscopic in this case but it decreases as a function of the distance away from the probe. In this chapter, we will consider the case when the probes are introduced in a medium described by asymmetric simple exclusion process (ASEP). The dynamical rules discussed in chapter 5 were

$$
\begin{array}{lccc}
Medium: & +- & \xrightarrow{1} & -+ \\
 & -+ & \xrightarrow{\mathrm{q}} & +- \\
 & & & \\
Probe: & 0- & \xrightarrow{1} & -0 \\
 & +0 & \xrightarrow{\mathrm{w}} & 0+
\end{array}
\tag{7.1}
$$

with $0 \leq q < 1$ and $0 \leq w \leq 1$. Depending on the values of q and w the density perturbation created by a single probe may show a long-ranged decay (power law) or a short-ranged decay (exponential) as a function of the distance away from the probe. A phase transition takes place between this power law phase and exponential phase which gives rise to an interesting phase diagram in the $q-w$ plane.

In the next section, we summarise a few known results on ASEP and in section 7.2 we discuss properties of macroscopic number of shock-tracking probes or STPs ($w=1$) in a medium described by totally asymmetric exclusion process or TASEP ($q=0$). In section 7.3 discuss the single-probe phase diagram for general values of q and w and the consequence of this phase diagram on the static and dynamic properties of a macroscopic number of probes.

7.1 Properties of ASEP

In one dimension, the dynamical rules for an ASEP can be described by the first pair of exchanges shown in Eq. 7.1 with $0 \leq q < 1$. In steady state, in the thermodynamic limit, the system is known to have uniform product measure (uncorrelated occupancy of the sites) with density ρ [51]. There is a current through the system in steady state and is given by $J = (1-q)\rho(1-\rho)$. The average speed of any particular tagged particle is therefore $J/\rho = (1-q)(1-\rho)$.

The variance $C_+(t)$ of the displacement of a tagged particle, as defined in Eq. 6.2, is known to grow linearly in time for an infinite system with a diffusivity $D = (1-\rho)(1-q)$ [52]. In a finite system $C_+(t)$ is non-monotonic due to the existence of a kinematic wave which carries the density fluctuations through the system with speed $dJ/d\rho = (1-q)(1-2\rho)$ [53, 54]. Since the average speed of the tagged particle is $(1-q)(1-\rho)$, it moves from one density patch to the other with relative speed $\Delta v = (1-q)\rho$; the variance of its displacement increases linearly, since each patch contributes a random excess to the relative velocity of the tagged particle.

Now for a finite periodic system, the tagged particle returns to its initial environment (density patch) after a time $L/\Delta v$. The variance of the tagged particle displacement at this time, measures the dissipation of this density patch. $C_+(t)$ is then expected to show a dip each time the tagged particle comes back to its initial environment which occurs at times $L/\Delta v$ or integral multiple of that [see fig 7.1].

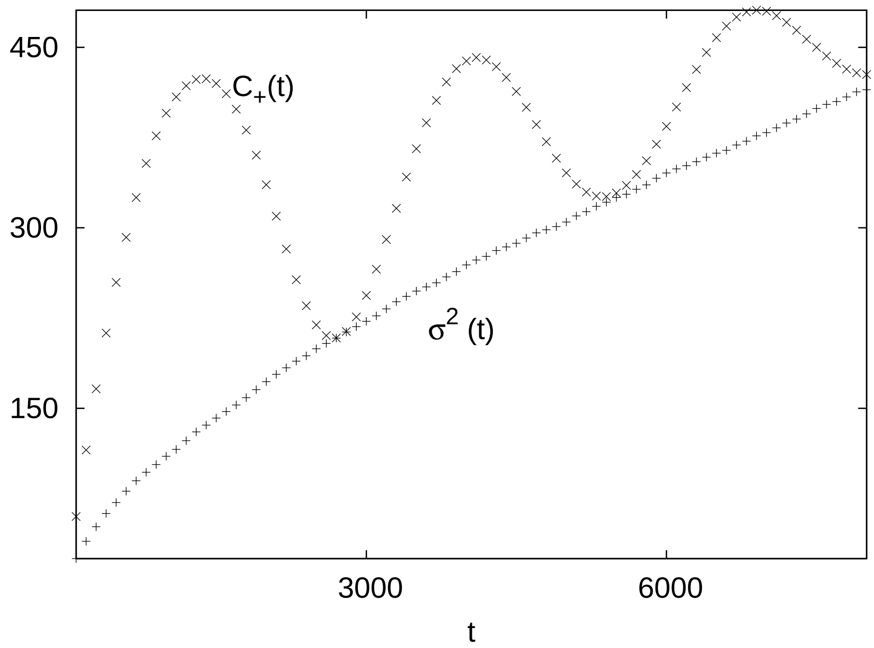

Figure 7.1: *$C_+(t)$ and $\sigma^2(t)$ for tagged particles in an ASEP. We have used $L = 1024$ and $\rho = 0.375$ and averaged over 10000 iterations.*

The quantity $C_+(t)$ does not directly capture the dissipation of the density pattern, except when it becomes minimum. In order to study the dissipation of the density fluctuations at all times, one has to apply a Galilean shift to keep up with one particular density patch. The effect of this Galilean shift is to keep track of which particle is present at that density patch at time t; it is given by $k' = k - \Delta v t$. This leads to the following definition of the sliding tag correlation function [55, 56]:

$$\sigma^2(t) = \langle (Y_{k'}(t) - Y_k(0) - \langle Y_{k'}(t) - Y_k(0) \rangle)^2 \rangle \tag{7.2}$$

Note that the above correlation function involves different tags at different times, thus monitoring the evolution of the same density patch at all times. This correlation function therefore measures the dissipation of the density fluctuations and forms the lower envelope of $C_+(t)$, as shown in fig 7.1. In the long time limit, $\sigma^2(t) \sim t^{2/3}$.

There is an alternative way to track the dissipation of density fluctuations in the system. In this method, introduced by van Beijeren [62], one monitors the quantity

$$B(t) = \overline{\left(Y_k(t) - Y_k(0) - \overline{(Y_k(t) - Y_k(0))}\right)^2} \tag{7.3}$$

where the overhead bar denotes averaging over different evolution histories, starting from a *fixed* initial configuration drawn from the steady state ensemble [62]. Note that in this averaging process, the initial pattern of density fluctuations around a particular tagged probe is identical for all evolution histories. The mean $\overline{(Y_k(t) - Y_k(0))}$ shows fluctuations superposed on a linear growth law as shown in fig 7.2. These fluctuations are determined by the density pattern in the initial configuration [63]. $B(t)$ therefore gives the spread of this pattern with time and for large time $B(t) \sim t^{2/3}$.

7.2 Properties of Shock Tracking Probes in a TASEP

In this section, we discuss the dynamical properties of the tagged STPs ($w = 1$) in a medium described by TASEP ($q = 0$). Since a probe exchanges with the particles and holes of the medium in opposite directions and with equal rate, it tends to migrate to places where there is an excess of holes to its left and particles to its right, *i.e.* a shock. For example, consider the configuration: $++----0++++-$. Here, the probe is stable in its position—until any local fluctuation in the medium brings the particle (hole) at the left (right) end close to the probe, the latter cannot move.

Note that in this case, a particle (hole) exchanges with a hole (particle) and a probe in exactly the same way. The STPs in this case reduce to second class particles [57, 34], *i.e.* they behave as holes for the particles and as particles for the holes. If ρ and ρ_0 are densities of particles and probes, respectively, then a particle behaves as if in a TASEP with an effective hole density $(1-\rho)$, while a hole finds itself in a TASEP with an effective particle density $(\rho + \rho_0)$.

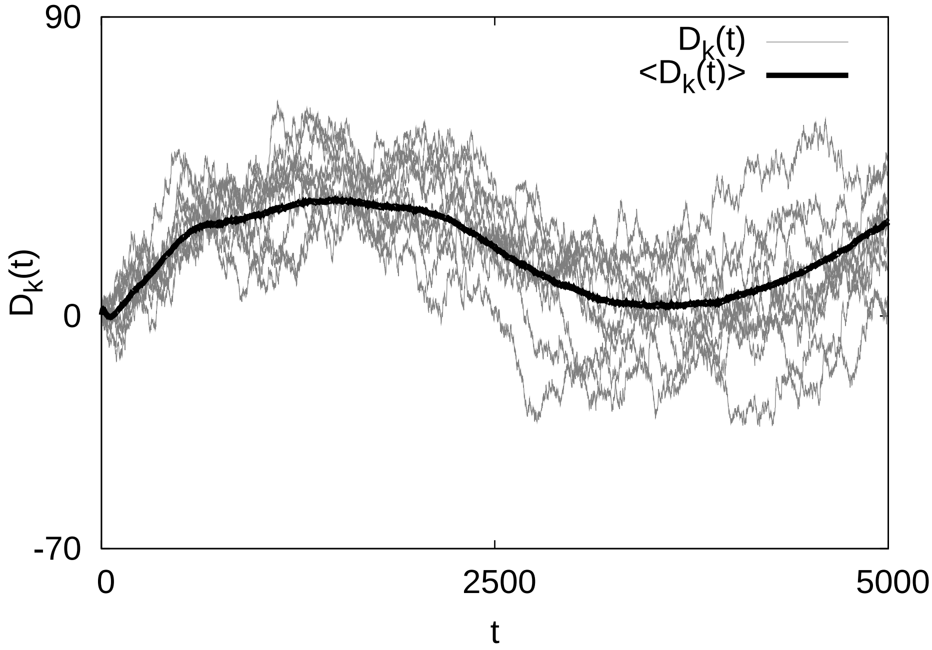

Figure 7.2: *The gray curves show the distance covered, $D_k(t) = Y_k(t) - Y_k(0) - (1-q)(1-\rho)t$, in time t about the mean $(1-q)(1-\rho)t$ by the k-th tagged particle for* 10 *Monte Carlo runs for a single fixed initial configuration, drawn from the steady state ensemble. The black curve shows the mean displacement, $\langle D_k(t)\rangle$ obtained by averaging over* 500 *dynamical evolutions for the same initial configuration. Here, $L = 10^4$ and $\rho = 0.25$. [Figure taken from S. Gupta* et al.*, cond-mat/070346.]*

Static Properties of Second Class Particles

Derrida *et al.* have found the exact steady measure of this system using the matrix method [34]. The steady state factorises about any second class particle, which implies factorisation in the one-component system about the shock position. When there is a single second class particle present in the system, the shock around it decays as a power law with an exponent 1/2. In presence of two (or a finite number of) second class particles the medium induces an attraction between them and they form a weakly bound state and the distance r between two successive second class particles follows a power law distribution $P(r) \sim r^{-3/2}$.

When the number of second class particles becomes macroscopic, the density profile at a distance r away from the probe has the form [see appendix C for details]

$$\rho(r) = \frac{1}{\sqrt{r}} \exp(-r/\xi) \tag{7.4}$$

where the correlation length ξ diverges in the low concentration limit of the second class particles:

$$\xi \approx 4\rho(1-\rho)/\rho_0^2, \qquad \text{as } \rho_0 \to 0. \tag{7.5}$$

We are interested in the dynamical properties of the STPs when a macroscopic number of these probes are present in the system. We find that the dynamics of these STPs is governed by a crossover time-scale that diverges as the STP concentration goes to zero. We show that various dynamical correlation functions of the STPs allow for a scaling description that involves this crossover time-scale. In the remaining part of this section, we present our results for the different dynamical quantities we have monitored.

Variance of the Displacement of the Tagged Probes

For tagged probe particles, the variance of STP displacement $C_0(t)$ shows a crossover from an initial passive scalar advection regime to a long time diffusive regime. The associated crossover occurs on a time-scale that diverges strongly as the probe density approaches zero.

Ferrari and Fontes in [58] have calculated the asymptotic ($t \to \infty$) behavior of $C_0(t)$ for STPs using a graphical construction of the two coupled ASEPs with densities ρ and $(\rho + \rho_0)$. Their calculation shows that $C_0(t) \approx Dt$ with diffusion constant

$$D = \frac{\rho(1-\rho) + (\rho+\rho_0)(1-\rho-\rho_0)}{\rho_0}. \tag{7.6}$$

However, the above diffusive behavior of $C_0(t)$ can be seen only for asymptotically large time. For small time, one actually finds a super-diffusive behavior. Note that in the limit of low concentration of the probe particles, one would expect that for small times, each STP would behave as an individual non-interacting particle, subject only to the fluctuations of the medium. The variance of the displacement of a single probe has been shown analytically to grow as $t^{4/3}$ using the matrix product method [59].

This result can be alternatively understood from passive scalar advection. A single STP moving in a TASEP can be alternatively viewed as a passive particle sliding down along the local slope of a surface which evolves through Kardar-Parisi-Zhang dynamics. The particle would tend to stay in the local valleys of the surface. Note that an STP is not really passive—when it is present in a valley, it tends to block the local fluctuations of the valley, unlike the passive slider advection case discussed in chapter 2 and 3. However, this does not affect the scaling properties of the surface when a single STP is present in the system. The variance of STP displacement in such a case would be expected to grow as $t^{2/z}$. Recalling that $z = 3/2$ for a KPZ surface [23], we recover the $t^{4/3}$ behavior discussed above.

Hence in the case of a small but finite concentration of STPs, $C_0(t)$ shows single particle (super-diffusive) behavior at small times and diffusive behavior for asymptotically large times. One would therefore expect a crossover between these two regimes that would occur at a time-scale τ which is a function of ρ_0. The natural expectation is $\tau \sim \xi^z$ where ξ is the correlation length, defined in Eq. 7.4. Substituting the value of the dynamical exponent $z = 3/2$ and from Eq. 7.5 one obtains

$$\tau \sim \rho_0^{-3} \tag{7.7}$$

in the limit of small ρ_0.

This leads us to propose the following scaling form for $C_0(t)$

$$C_0(t) \sim t^{4/3} F\left(\frac{t}{\tau}\right). \tag{7.8}$$

This form is valid in the scaling limit of large t and large crossover time-scale τ (*i.e.* $\rho_0 \to 0$). Here $F(y)$ is a scaling function which approaches a constant as $y \to 0$. For $y \gg 1$, we must have $F(y) \sim y^{-1/3}$, in order to reproduce $C(t) \approx Dt$.

We verify the scaling form by Monte Carlo simulation. In fig 7.3, we plot $C_0(t)/t^{4/3}$ versus t/τ for various values of ρ_0 and obtain good scaling collapse, except for very small values of t which fall outside the scaling regime.

One important issue in this numerical simulation is the equilibration. To verify the scaling form in Eq. 7.8, one has to consider large values of L to avoid the oscillations in $C_0(t)$ due to the presence of the kinematic waves in the

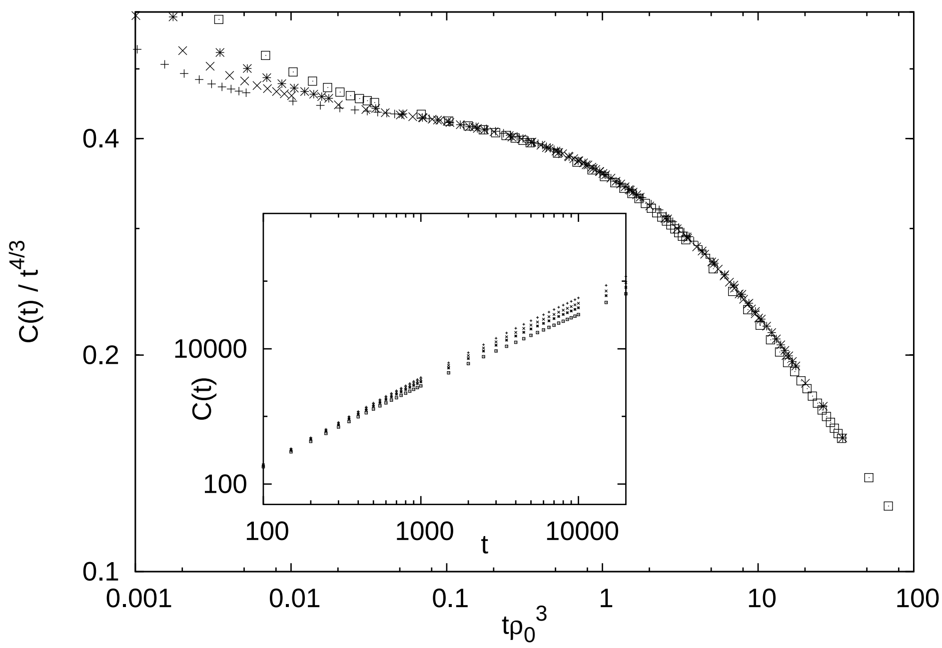

Figure 7.3: *Scaling collapse for mean squared displacement of tagged STPs with densities* 0.08, 0.1, 0.12, 0.15 *(moving upwards). We have used* $L = 131072$ *and averaged over* 100 *histories.*

system (see below). Fortunately, it is possible to save the equilibration time by directly generating steady state initial configurations, following the prescription by Angel [60], which uses a combinatorial description of TASEP with second class particles [see appendix E].

A nontrivial check of the scaling form comes from examining the dependence of τ on ρ_0. Matching the early and late time form for $C_0(t)$ at $\tau \sim \rho_0^{-3}$ then yields $D \sim \rho_0^{-1}$, in agreement with Eq. 7.6. Yet another check comes from considering the implication for a system with a finite size L. Finite size scaling would suggest that once L is smaller than ρ_0^{-2}, the behavior $D \sim \xi^{1/2}$ found above should give way to $D \sim L^{1/2}$. This is in conformity with the calculation of [61] where the diffusion of a single second class particle in a finite system has been solved using Bethe ansatz.

In a finite periodic system of size L, the quantity $C_0(t)$ shows an oscillatory

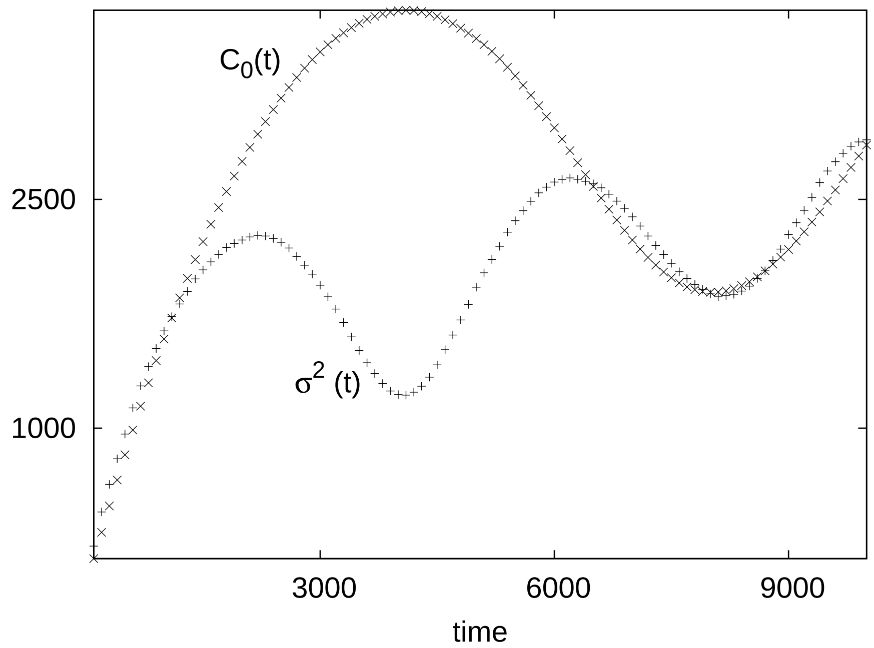

Figure 7.4: *Mean squared displacement $C_0(t)$ of tagged probes shows oscillation with a period $L/(1-2\rho)$. Sliding tag correlation $\sigma^2(t)$ with the Galilean shift of tags $k' = k-(1-2\rho)t$ gives rise to another oscillatory pattern with period halved. We have used $L = 2048$ and $\rho = 0.375$.*

behavior due to the presence of the two kinematic waves present in the system. The two waves carrying the density fluctuations of the particles and holes in the medium move through the system with speeds $\pm(1-2\rho)$, corresponding to the two TASEPs with densities ρ and $(1-\rho)$. The density fluctuations of the probes get affected by both these waves and at the end of one complete cycle when a tagged probe comes back to its initial density patch, $C_0(t)$ shows a dip which occur at times that are integral multiples of $L/(1-2\rho)$ [shown in fig 7.4].

Because of the presence of two kinematic waves with different velocities, it is not possible to keep up with both of them simultaneously by applying Galilean shift, as described in Eq. 7.2. In fig 7.4 we show that when the Galilean shift is applied so as to keep up with one of the waves, the oscillation in $C_0(t)$ do not go away but the period is halved, due to the effect of the other wave. To track the dissipation of the density fluctuations of the probes, we thus use the method of van Beijeren [62] and we describe our results below.

Dissipation of Density Fluctuations

We monitor the correlation function $B_0(t)$ defined in Eq. 7.3. We find that $B_0(t)$ increases as $t^{2/3}$ for large t, and would expect a scaling function to connect this regime to the small time regime $B_0(t) \sim t^{4/3}$, characteristic of single particle behavior. In the limit of large t and small ρ_0, we expect

$$B_0(t) \sim t^{4/3} G\left(\frac{t}{\tau}\right). \tag{7.9}$$

The scaling function $G(y)$ should approach a constant as $y \to 0$ while for $y \gg 1$, one expects $G(y) \sim y^{-2/3}$ [shown as a reference line in fig 7.5]. Our simulation results [fig 7.5] are consistent with this scaling form.

Fluctuation of the Separation between a pair of STPs

In this section, we study how the distance between a pair of STPs (*e.g.* the k-th and $(k+1)$-th) fluctuates in time. Consider the following quantity

$$\Delta(t) \equiv \langle (R(t) - R(0))^2 \rangle \tag{7.10}$$

where $R(t)$ is the separation between the pair at time t. Note that for small time and small ρ_0, the STPs do not interact with each other. Hence for any particular pair, the fluctuations of the position of the two STPs (which result in the fluctuation of the separation between them) are uncorrelated. The quantity $\Delta(t)$ therefore grows diffusively in time. However, since ρ_0 is finite, for large time, $\Delta(t)$ is expected to saturate at a value that depends on ρ_0. The crossover time-scale between the initial diffusive growth and the late-time saturation should be the same τ as found in Eq. 7.8 and 7.9. This leads to the scaling form:

$$\Delta(t) \sim t\, H\left(\frac{t}{\tau}\right) \tag{7.11}$$

where the scaling function $H(y)$ approaches a constant as $y \to 0$ and for $y \gg 1$ one must have $H(y) \sim 1/y$. We verify this scaling form using Monte Carlo simulation and our results are presented in fig 7.6.

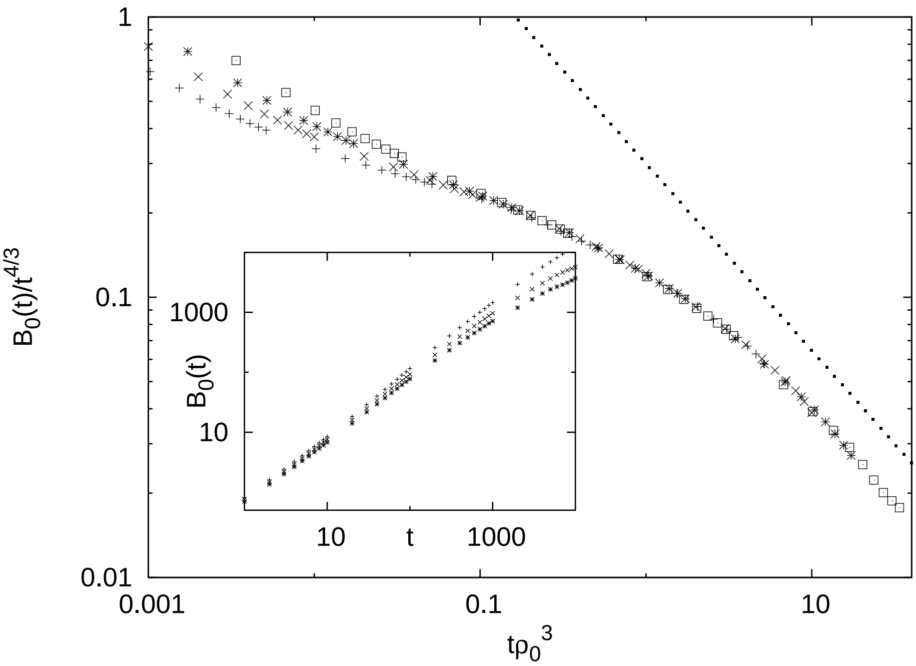

Figure 7.5: *Scaling collapse for* $B_0(t)$ *with probe densities* $0.08, 0.1, 0.12, 0.15$ *(moving upwards). We have used* $L = 16384$ *and averaged over* 25 *initial configurations and* 40 *evolution histories for each. The dashed line shows a power law decay with exponent* $2/3$.

7.3 Directed Probe Particles in an ASEP

In this section, we consider general values of w and q. For $q < 1$ the medium is described by an ordinary ASEP. For $w < 1$ the probe particles have a non-zero drift velocity towards the right and we call them directed probe particles (DPP).

Single Probe

In [64, 59, 65] this model was considered in presence of a single DPP. The exact steady state measure was obtained using matrix method. In [64] $q = 0$ and $w < 1$ was studied and the density fluctuation of the medium at a distance r away from the DPP was found to decay as

$$r^{-1/2} exp(-r/\xi) \tag{7.12}$$

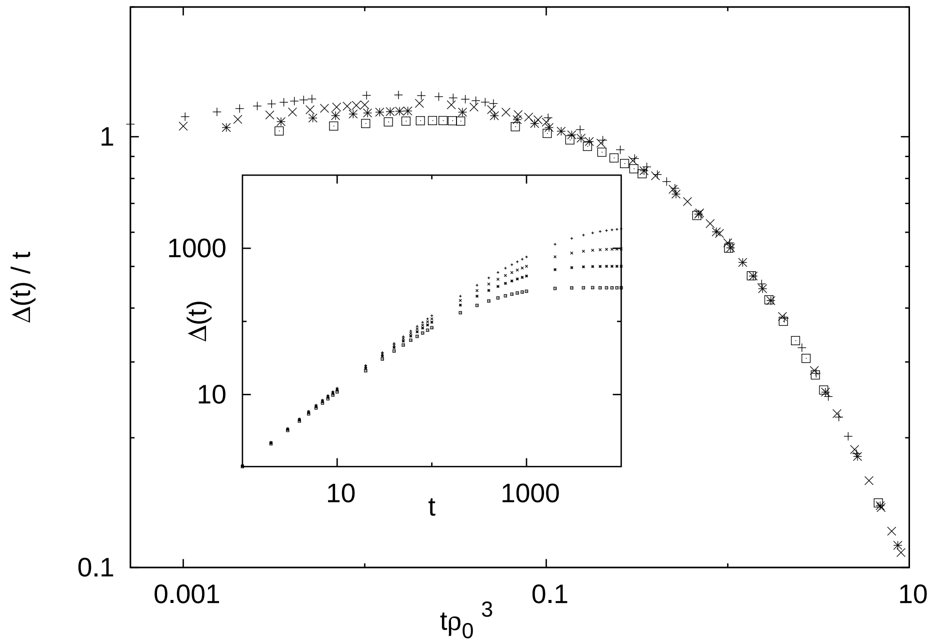

Figure 7.6: *Scaling collapse for the fluctuation of the distance between two successive probe particles with* $\rho_0 = 0.08, 0.1, 0.12, 0.15$ *(moving downwards). Inset shows the unscaled plot of the same quantity. We have used* $L = 16384$ *and averaged over* 1000 *histories.*

where ξ diverges as

$$\xi \approx 4w(1-w)/(\rho-w)^2, \qquad \text{as } w \to \rho. \tag{7.13}$$

For $w \geq \rho$, the shock around a probe decays as a power law with exponent $1/2$. $w = \rho$ marks the critical point between the exponential and the power law phase where ξ shows a divergence. In [65] $q < 1$ was considered and the power law decay was retrieved for $w/(1-q) \geq \rho$, while for $w/(1-q) < \rho$ the decay was exponential. This gives rise to the phase-diagram shown in fig 7.7 for a single DPP.

The above phase diagram was derived using the matrix product method. Below we provide a simple explanation of the phase diagram. In the exponential phase, shown in fig 7.7, far away from the probe the density is equal to ρ. The

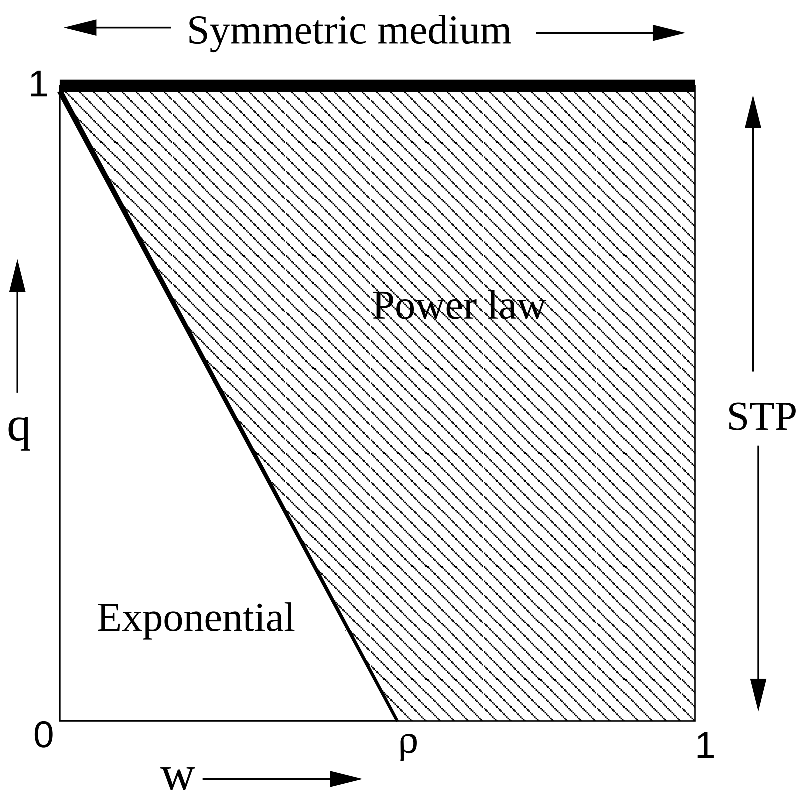

Figure 7.7: *Phase diagram for a single nonequilibrium probe in an ASEP. The x-axis refers to properties of the probe while the y-axis refers to that of the medium. Depending on w and q, the density perturbation created by the probe decays exponentially or as a power law. As w and q are varied, a phase transition is observed. The top thick line corresponds to the symmetric medium (SEP) where a single probe produces macroscopic effect.*

bulk current is therefore $(1-q)\rho(1-\rho)$. Let V be the velocity of the probe. Then the current in the bulk measured from the moving frame of the probe would be $(1-q)\rho(1-\rho)-\rho V$. Again, the current seen by the probe at the bond to its left is $w\rho$. Since the current in every bond should be the same in steady state, we get

$$V = (1-q)(1-\rho) - w \tag{7.14}$$

In the power law phase, on the other hand, the probe essentially behaves as a second class particle [64, 59], which is carried along by local shocks. The velocity of the probe in the power law phase would then be given by the kinematic wave speed $V = (1-q)(1-2\rho)$. Along the critical line, the probe velocity in the two phases must match. This gives

$$\begin{aligned}(1-q_c)(1-\rho) - w_c &= (1-q_c)(1-2\rho) \\ q_c &= 1 - \frac{w_c}{\rho}\end{aligned} \tag{7.15}$$

which is the equation of the critical line.

In [59] the mean squared displacement for a single probe was calculated for $q = 0$. It was found that in the exponential phase $C_0(t)$ grows diffusively with time, while in the power law phase $C_0(t) \sim t^{4/3}$.

Finite Density of Probes

The above phase diagram for a single probe has important consequences for the dynamical properties of macroscopic number of probes. We find that for finite ρ_0 and q, in the power law phase, as well as on the critical line, the dynamical properties of the probes are governed by a crossover time-scale that diverges as ρ_0 becomes small. This diverging time-scale is again related to a diverging correlation length present in the system. Note that the power law decay of shock around a single probe points to the existence of a diverging correlation length in the system. On the other hand, in the exponential phase, the density profile around a single probe decays over a finite length scale, *i.e.* as ρ_0 becomes small, the correlation length remains finite in this case. Accordingly, no diverging time-scale exists in this phase.

Our numerical simulations show that in the power law phase and also on the critical line, the mean squared displacement of the tagged DPPs follows a scaling description as shown in Eq. 7.8. However, to obtain the best collapse we have to rescale the time-axis by τ which diverges for small ρ_0 with an exponent that depends on q and w. Our data in fig 7.8 indicates that for a fixed q as w is decreased, the exponent also decreases. We do not have any simple explanation for this phenomenon.

No scaling description has been found in the exponential phase, since there is no diverging time-scale.

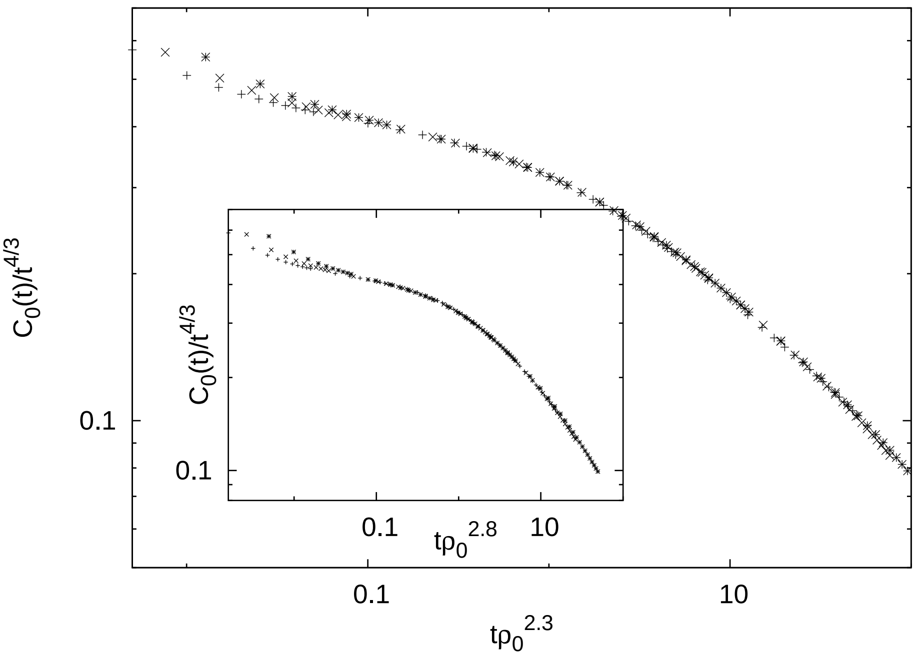

Figure 7.8: *Scaling collapse for $C_0(t)$ for $q = 0$, $w = 0.5$ and $q = 0$, $w = 0.7$ (inset) is shown for $\rho_0 = 0.1, 0.12, 0.15$. We have used $L = 16384$ and averaged over* 2000 *histories.*

Chapter 8

Probes in the 1-d Katz-Lebowitz-Spohn Model

In the previous chapter, we have considered nonequilibrium probes in a non-equilibrium medium, in which no interaction is present except hard-core exclusion between the particles. We have seen that depending on the kinematics of the probe and the medium, the system may have a finite or a diverging correlation length and this gives rise to an interesting phase diagram. In this chapter, we consider a nonequilibrium medium with interaction. The dynamical moves are shown below:

$$\begin{array}{ccc} +\,- & \xrightarrow{1-\Delta V} & -\,+ \\ +0 & \xrightarrow{1} & 0\,+ \\ 0- & \xrightarrow{1} & -0 \end{array} \tag{8.1}$$

Here ΔV is the change in the nearest neighbour Ising interaction potential

$$V = -\frac{\epsilon}{4}\sum_i s_i s_{i+1} \tag{8.2}$$

where $s_i = 0, \pm 1$, according to the occupation of the site i and $-1 \le \epsilon \le 1$. For $\epsilon = 0$ the model reduces to second class particles in a TASEP, as in chapter 7. In this chapter we will only consider $\epsilon > 0$.

In the absence of any probe, the system reduces to the one dimensional version of Katz-Lebowitz-Spohn (KLS) model [66] which is a simple lattice gas model of driven diffusive systems, with nearest neighbor Ising interaction between the particles. The steady state of the KLS model is known to have an Ising measure [66, 67] [for a proof see appendix D]. In presence of probes the system shows an interesting phase transition as the coupling parameter ϵ is varied. Kafri *et al.* [69] have attempted to characterise this phase transition by mapping the model onto a zero-range process. In the next section, we give a detailed account of this mapping and the static properties of the system. In section 8.2 we discuss the dynamical properties.

8.1 Static Properties of Katz-Lebowitz-Spohn Model with Probes

In [69] Kafri *et al.* reported that the KLS model with macroscopic number of probes shows a phase separation transition for $\epsilon > 0.8$ as the density ρ is increased above a critical value ρ_c. In the phase separated state, a macroscopic domain, composed of particles and holes of the medium, coexists with another phase which consists of small domains of particles and holes, separated by the probes. They explained this phase transition by attempting to approximately map the system onto a zero-range process.

To describe the mapping, we first define a domain as an uninterrupted sequence of particles and holes, bounded by probes from both ends. The current J_n out of a domain of length n can then be determined by studying a KLS model in an open chain with boundary rates of injection and extraction equal to the rate at which the particles and holes of the domain would exchange with the probes at the domain boundaries. According to Eq. 8.1 this rate is unity. The current J_n can be calculated exactly for an open KLS chain and for large n it has the form

$$J_n = J_\infty \left(1 + \frac{b(\epsilon)}{n}\right) \tag{8.3}$$

where the coefficient b has the following dependence on ϵ

$$b(\epsilon) = \frac{3}{2}\frac{(2+\epsilon)v + 2\epsilon}{2(v+\epsilon)}, \qquad v = \sqrt{\frac{1+\epsilon}{1-\epsilon}} + 1. \tag{8.4}$$

The study of Kafri *et al.* indicates that b plays an important role in characterising the phase separation transition in the model.

The present system is mapped onto a zero-range process (ZRP) as follows: the i-th probe is defined as the i-th site of ZRP and the length of the domain to the left of the i-th probe is taken to be the occupancy $n(i)$ of the i-th site of ZRP. We illustrate this in fig 8.1.

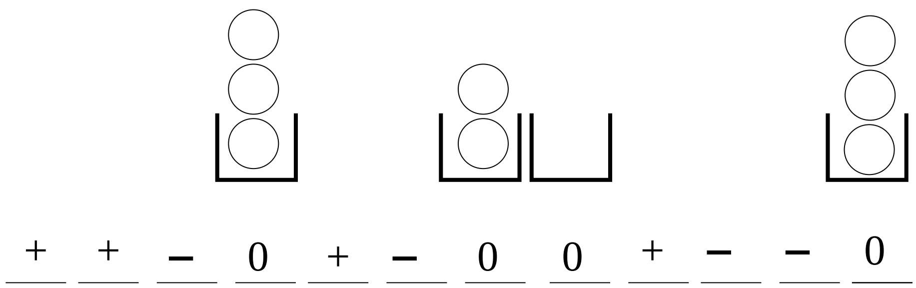

Figure 8.1: *A typical configuration of the KLS model with probes and its corresponding configuration in ZRP.*

The hopping rate out of the i-th site in ZRP is taken to be the domain current $J_{n(i)}$ given in Eq. 8.3. For such a ZRP, therefore condensation transition is expected to take place for $b > 2$ and $\rho > \rho_c$, when the occupancy at a single site becomes macroscopically large, while the remaining sites have an average occupancy ρ_c [70]. The number of particles present on a site follows the distribution function

$$P(n) \sim \frac{1}{n^b}\, exp(-n/\xi) \tag{8.5}$$

where the correlation length ξ diverges at the critical density [70].

The above results for the ZRP imply that in the present model of KLS chain with probes, for large enough ρ and for $\epsilon > 0.8$ [as follows from Eq. 8.4], there should be a macroscopic domain present in the system which is composed of particles and holes (no probes). The rest of the system should consist of small probe clusters, interrupted by the domains (of particles and hole) with size distribution given by Eq. 8.5. The ZRP correlation length ξ, introduced in Eq. 8.5, is related to the particle density by

$$\frac{2\rho}{(1-2\rho)} = \frac{\sum P(n)n}{\sum P(n)}. \tag{8.6}$$

Note that $(1-2\rho)$ is the number of sites in the ZRP and LHS therefore gives the particle density in ZRP in terms of the density in KLS chain (equal densities of particles and holes have been considered here; in [71] the case of unequal particle and hole densities was considered.). The critical density ρ_c is obtained from the above expression with $\xi \to \infty$.

In our numerical simulations, however, it is found that even when $\epsilon < 0.8$ a macroscopic domain may exist for large ρ. Similar observations are reported in [69]. In [69, 72] it has been argued that this is not a true phase separation. The correlation length in this case is not really macroscopic but has a finite (and large) value.

According to the above correspondence with the ZRP, it is expected that close to the critical point, the domain size distribution for $n \ll \xi$ should follow a power law with exponent $b(\epsilon)$. However, our numerical simulations for various values of ϵ and ρ [see fig 8.2] show that the power law exponent seems to be much closer to $3/2$ (which is the value of b at $\epsilon = 0$), independent of the value of ϵ.

This result shows a contradiction. If the correspondence with ZRP has to be believed, then the power law exponent b should be given by Eq. 8.4. On the contrary, we find $b = 3/2$ for all ϵ. This leads us to examine the assumptions that go into this KLS-ZRP mapping.

Independence of Domains: A crucial property of the ZRP is that the occupancies at the sites are uncorrelated. In our present model of KLS chain with probes, this would imply that the domains between the probes should be independently distributed. We have verified this assumption by measuring the conditional probability $P(n|n')$ that the size of a particular domain is of length n given that its neighboring domain is of length n'. We find that $P(n|n')$ does not depend on n' and is same as $P(n)$ which shows that the neighboring domains are distributed independently. Our data is presented in fig 8.3.

Finite Size Correction of Domain Current: Apart of independence of the domains, another requirement for the ZRP mapping to hold is that the current out of a domain of size n is same as the current in an isolated open KLS chain and is given by Eq. 8.3. Evans *et al.* have shown in [71] that this holds true. They have numerically measured actual current out of a domain and compared

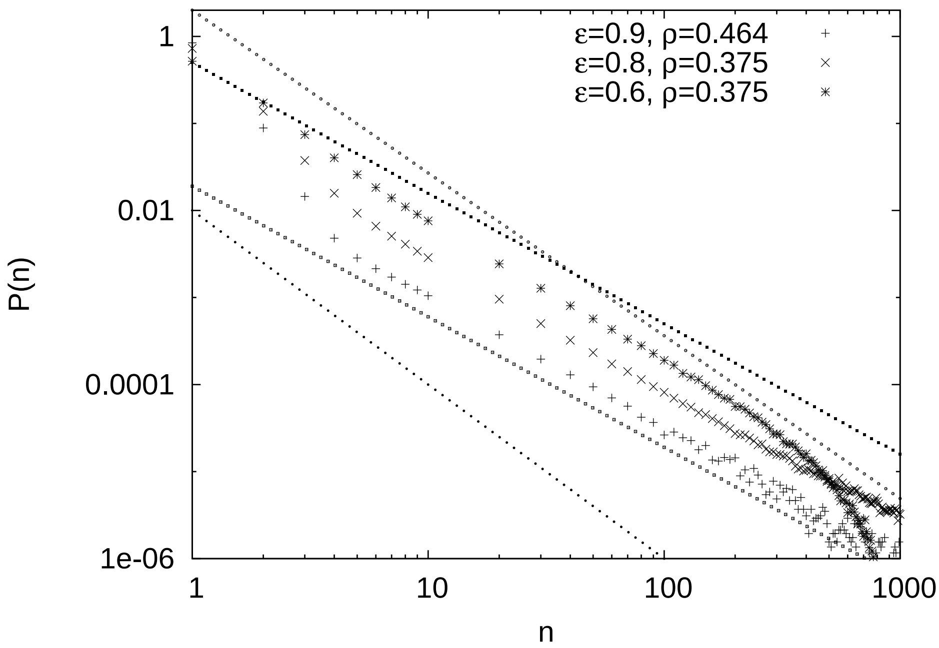

Figure 8.2: *Domain size distribution for different values of ϵ and ρ. From the ZRP correspondence, the expected values of the power law exponents are* 1.87 *for* $\epsilon = 0.6$ *and* 2 *for* $\epsilon = 0.8, 0.9$ *which are shown by dashed lines. On the contrary, the power law exponent is observed to be* 1.5 *(also depicted by dashed line) for the range of ϵ considered.*

this with the exact calculation for an open chain KLS model. Good agreement was found for large n.

To take into account the finite size corrections for moderate n values, we simulate a ZRP where the hopping rate out of a site is read off directly from the actual J_n vs n data, obtained from numerical simulation. The mass distribution for this ZRP is found to have the same form as in Eq. 8.5 with the exponent b given by Eq. 8.4, as expected. Hence the finite size correction to J_n is not the reason for the discrepancy shown in fig 8.2.

Non-Markovian Movement of the Probes: There is however, one aspect of the KLS model with probes that is not captured in the corresponding ZRP. Since a probe exchanges with the particles and holes of the medium in

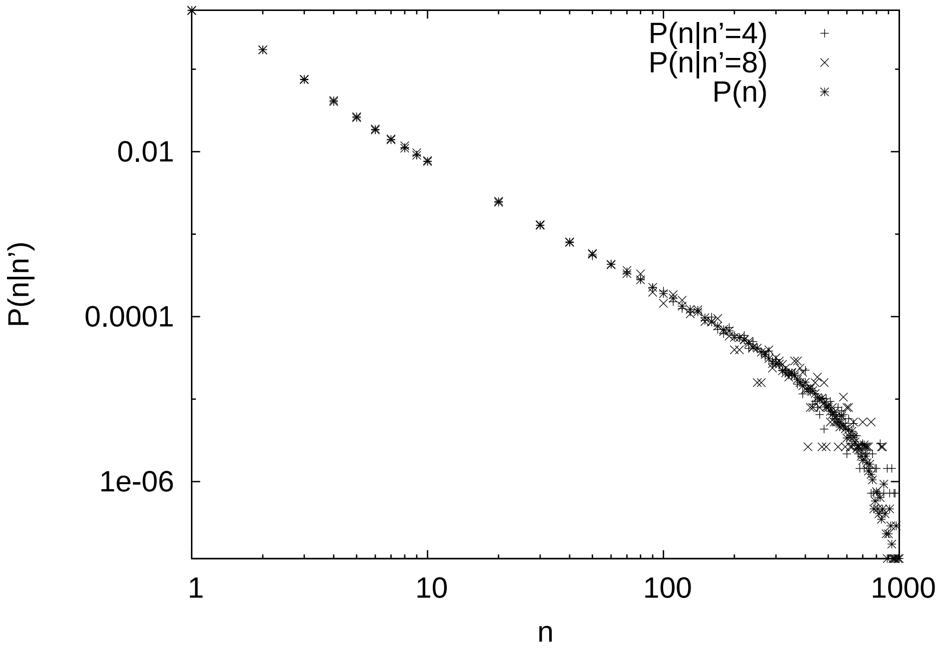

Figure 8.3: *The conditional distribution of domain size $P(n|n')$ as a function of n for $n' = 4, 8$. For comparison $P(n)$ is also shown. $P(n|n')$ is seen to match with $P(n)$ which shows the domains are independently distributed. We have used $L = 2048$, $\epsilon = 0.6$ and $\rho = 0.375$.*

opposite directions, as shown in Eq. 8.1, once a probe moves in one particular direction, it cannot immediately move in the opposite direction at the next time-step. For example, a probe moves to the left by exchanging with a particle in the medium. Right after this exchange the probe has the particle as its right neighbor. Clearly, the probe cannot take a step to the right as long as that particle stays there. In other words, the probes have a finite memory which makes their movement non-Markovian. In terms of the ZRP this would mean that once a site has emitted a particle to its right neighbor, it has to wait for some time till it can receive a particle from its right neighbor. This waiting time should depend on the form of the density profile in a domain. Note that in this non-Markovian ZRP, apart from J_∞ and $b(\epsilon)$, there are other parameters that are associated with the exact form of the waiting time. As a result, the phase-diagram becomes complicated and to specify the criterion of a phase transition a much more detailed analysis is required which might shed some light on the observed discrepancy about domain size distribution.

8.2 Dynamics of Probes in a Katz-Lebowitz-Spohn Model

Two Probes

Levine *et al.* have considered a KLS chain with two STPs in [35]. They have argued that the time-evolution of the separation between the probe pair is governed by a Master equation. Their analysis indicates that the medium induces an attraction among the probe particles and they form a bound state. The steady state distribution of the distance between two probes takes the form $P(r) \sim r^{-b}$ where b is a function of ϵ given by Eq. 8.4. For $\epsilon = 0$ one retrieves $P(r) \sim r^{-3/2}$ as found in [34].

Rakos *et al.* have shown in [73] that the random force between the probe pair is sensitive to the noise correlations present in the medium. When the probe particles are embedded in a KLS ring, such that the random force that drives the probe particles is fully generated by the current fluctuations of the driven medium, the probes inherit the dynamical exponent of the medium, which is 3/2. On the other hand, if the random force has a part that is temporally uncorrelated, the resulting motion can be described by a dynamical exponent $z = 2$.

To study the dynamics of the system, Rakos *et al.* monitored the average distance between the two probes starting from the initial configuration in which the two probes were side by side. The approach to the steady state was modelled by the scaling ansatz

$$P(r,t) \sim r^{-b} f(r/t^{1/z}) \tag{8.7}$$

where $P(r,t)$ is the probability that starting as nearest neighbors, the two probes are at a distance r apart at time t. In the range $1 < b < 2$ this implies that the average distance between the two probes grows as

$$\langle r(t) \rangle \sim t^{(2-b)/z}. \tag{8.8}$$

In [35, 73] time evolution of the average distance between the two probes was monitored numerically. Starting from a randomly disordered configuration, with the restriction that the two probes are placed on nearest neighbor sites, the system was evolved for a time t_{equil} in an attempt to let it reach an equilibrium state. The time evolution followed the exchange rules shown in Eq. 8.1 with the important modification that the two probes were constrained to remain nearest neighbors *i.e.* they hop together as if they occupy only a single site. At the end of this equilibration, the medium is assumed to be locally in steady state, in the vicinity of the probes, up to a distance of the order $t_{equil}^{2/3}$. At this point, defined as $t = 0$, the restriction for the relative position of the probes was released and the distance between them monitored. Even with such partially equilibrated initial condition, the distance between the probes is assumed to follow the scaling form in Eq. 8.7 for $t \ll t_{equil}$ when the two probes move within an equilibrated region. In this time regime, it is numerically verified that $\langle r(t) \rangle$ follows Eq. 8.8 [35, 73].

Note that the scaling form in Eq. 8.7 is expected to be valid in steady state. Therefore, to verify this scaling form, a different and more natural choice of initial condition would be to bring the system first in steady state (without any restriction on the movement of the probes). Then wait till the probes come to a nearest neighbor position with respect to each other and define $t = 0$ at this point. Then one would expect Eq.s 8.7 and 8.8 to remain valid for all t. But our data shows that $\langle r(t) \rangle$ follows Eq. 8.8 only for an initial time-regime, after which the growth exponent changes to 0.33 which is close to the value of the growth exponent at $\epsilon = 0$. We present our data in fig 8.4.

We have also measured $\langle r(t) \rangle$ following the procedure of Rakos *et al.* [35, 73]. We have investigated the effect of different values of t_{equil} and find the same behavior as described in the last paragraph. Moreover, fig 8.4 shows that the curves for this partially equilibrated initial condition, coincide with that of the steady state initial condition (as explained in the last paragraph), for large time. This is in direct contradiction with [73] since the equilibration technique with two probes hopping together is claimed to give rise to an equilibrated medium within $t_{equil}^{2/3}$ distance of the probes which would mean that for small time partially equilibrated data and steady state data should match and differ only at large t.

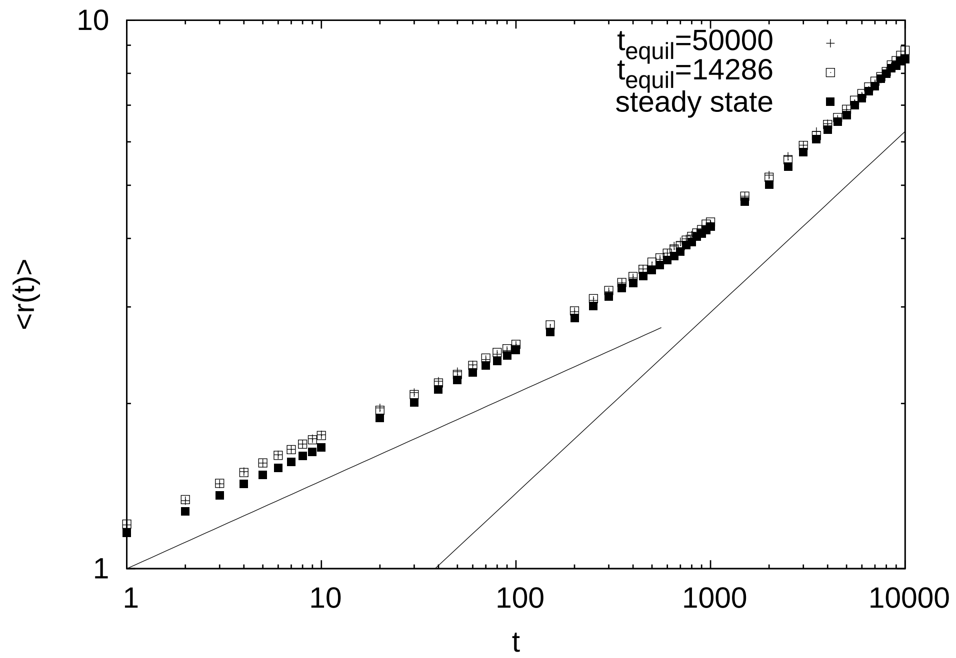

Figure 8.4: *Average distance $\langle r(t)\rangle$ between the probe pair as a function of time. $\langle r(t)\rangle$ shows two different power law growths as time changes. The reference lines show that the growth exponent is $(2-b)/z$ at short times and changes to $1/3$ at large times. The curves for partially equilibrated initial conditions (using the method of Rakos* et al.*) with different values of t_{equil} coincide for small t. We have also measured $\langle r(t)\rangle$ starting from steady state initial condition. The partially equilibrated data and steady state data coincide for large t. We have used $\epsilon = 0.4$ and $L = 1000$.*

We rationalise this in the following way. For a single probe, the density perturbation in the medium asymptotically decays as $\rho(r) \sim r^{-1/2}$ where r is the distance measured from the probe. Above form of the density profile should remain valid for two (or any finite number of) probes. Far away from the probes, therefore the medium behaves as if there is a single probe present in the system. Close to the probe-pair however, the medium would behave differently. In other words, when two probes are hopping together like a single probe then the density profile of the medium close to the probes, is different from the steady state density profile close to a pair of probes that are nearest neighbors, in contrast to what has been remarked in [73]. For small time, the probes in [35, 73] would therefore explore a medium which is not in steady state and hence $\langle r(t)\rangle$ would behave differently than steady state $\langle r(t)\rangle$.

However, the most intriguing fact is that even in steady state, $\langle r(t)\rangle$ does not follow Eq. 8.8 all the way but shows a crossover at large time to the behavior $t^{2/3}$, which is the behavior obtained for $\epsilon = 0$. At this stage, we do not have complete understanding of this phenomenon. One possible explanation could be given from the Ising measure of a KLS model (without probes) which induces a finite ϵ-dependent correlation length in the medium. As long as the displacement of the probes is less than a separation whose scale is set by this correlation length, the effect of ϵ variation can be felt. But for large time, when the probes cover a distance larger than the Ising correlation length, then they behave as if in a medium with no correlation or $\epsilon = 0$. But to arrive at a conclusion in this regard, more detailed studies for various ϵ values are required. Note that since we study finite systems in numerical simulations, even for two probes, $\langle r(t)\rangle$ cannot grow without bound and for very large time, it does saturate. In order to verify whether $\epsilon = 0$ behavior is recovered at large times, one has to consider fairly large systems, especially for larger values of ϵ.

Macroscopic Number of Probes

The study of dynamical properties of the probe and the medium when the number of STPs present in the system is macroscopic shows that the dynamics of the STPs is governed by a diverging time-scale, as in the non-interacting case $\epsilon = 0$. At small time, an STP senses the fluctuations solely due the KLS chain. But a KLS chain is known to have an Ising measure which means that if ϵ is not too large, only short-ranged correlations are present in the medium. This implies that the small time dynamics of the probes in a KLS chain would be similar to those in an ASEP (where no correlation is present in the medium). In other words, the small time behavior of the dynamical correlation functions of the probes are expected to be same as that of the second class particles discussed in the last chapter. However, the dependence of the crossover time on the probe density would in general be different and we discuss this below.

Let r_i be the separation between the i-th and $(i+1)$-th probe and R_m be the distance between the first and the $(m+1)$-th probe, *i.e.* $R_m = \sum_{i=1}^{m} r_i$. Let r_i follow the distribution $P(r_i) \sim r_i^{-\lambda}$. According to [35] $\lambda = b(\epsilon)$. The quantity R_m which is the sum of m such random variables should follow a Lévy distribution with a norming constant $\sim m^{1/(\lambda-1)}$, so long as R_m is less than the correlation length ξ. In other words, the length R_m of a segment which contains m probes scales as $m^{1/(\lambda-1)}$. This scaling relation is valid all the way up to $R_m = \xi$ but fails as R_m increases beyond that. Let $m_>$ be the number of STPs in a segment of length ξ. Then $m_> \sim \xi^{\lambda-1}$. Hence in a system of length L, the total number of probes N_0 can be written as $N_0 = (L/\xi)\,\xi^{\lambda-1}$, which implies that the correlation length $\xi \sim \rho_0^{-1/(2-\lambda)}$ and hence $\tau \sim \xi^{z_0} \sim \rho_0^{-z_0/(2-\lambda)}$, where z_0 is the dynamical critical exponent of the system.

We have monitored the dynamical correlation functions $C_0(t)$, $B(t)$ and $\Delta(t)$, as defined in Eq. 6.2, 7.3 and 7.10, respectively. Our numerical simulations indicate that these quantities follow the same scaling form as in the non-interacting case $\epsilon = 0$. More over they continue to show crossover at a time-scale $\tau \sim \rho_0^{-3}$, very similar to the $\epsilon = 0$ case. In fig 8.5 we show the scaling collapse for $C_0(t)$ and $B(t)$. We present our data for $\Delta(t)$ in fig 8.6.

In case of two probes one might expect $\Delta(t)$ would show the same scaling behavior as the second moment of the distribution $P(r,t)$ in Eq. 8.7, *i.e.* $\Delta(t)$ should grow with time as $t^{(3-b)/z}$. But our numerical simulations show that irrespective of the value of ϵ, $\Delta(t)$ always grows linearly with time (as in $\epsilon = 0$). We have shown our results for $\epsilon = 0.5$ in fig 8.6 inset.

Note that above scaling analysis and our numerical simulation presented in fig 8.5 and 8.6 point towards $z_0/(2-\lambda) = 3$. If $\lambda = b(\epsilon)$ as reported in [35], then for larger values of ϵ this leads to z_0 smaller than unity! For example, for $\epsilon = 0.5$, z_0 turns out to be 0.54 and we have verified that even at this value of ϵ the above scaling form remains valid [see fig 8.6].

The other (simpler) alternative is that $z_0 = z = 3/2$ and $\lambda = 3/2$ as in $\epsilon = 0$ case. This scenario would explain the observed ρ_0 dependence of crossover time τ. In case of two probes, the above value of λ is consistent with the large time growth exponent of the average separation $\langle r(t)\rangle$ between the probe pair (shown in fig 8.4) and also with the linear growth of $\Delta(t)$ shown in the inset of fig 8.6.

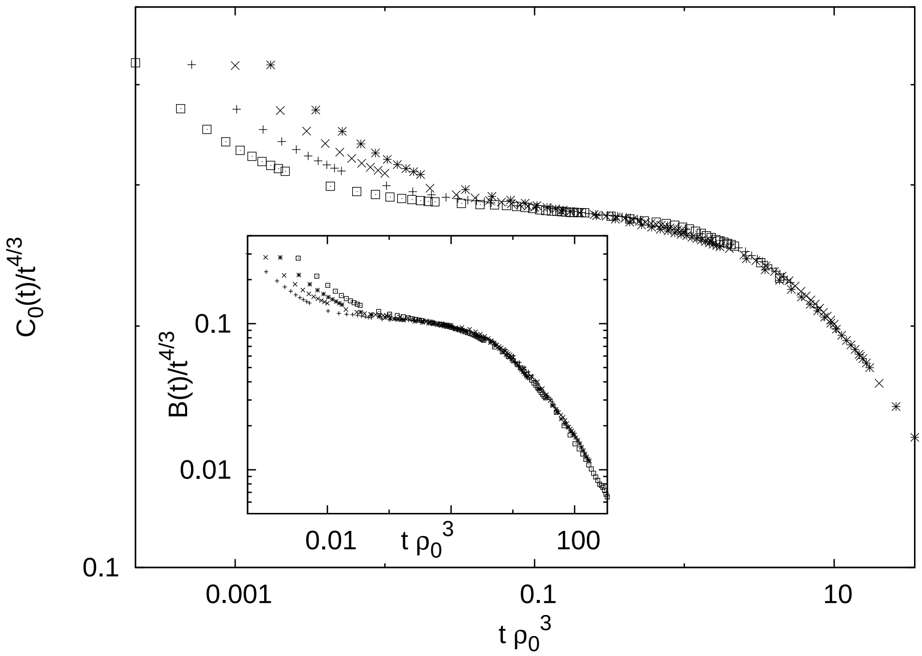

Figure 8.5: *Scaling collapse for $C_0(t)$ for $\epsilon = 0.2$ and $\rho_0 = 0.06, 0.08, 0.1, 0.12$. Inset shows scaling collapse for $B(t)$ with $\epsilon = 0.2$ and $\rho_0 = 0.08, 0.1, 0.12, 0.15$. We have used $L = 16384$.*

The dynamics of the medium was studied by measuring $C_+(t)$, defined in Eq. 6.2. We find that the there are two kinematic waves moving across the system, with equal and opposite velocities. One of them carries the density fluctuations of the medium particles and the other that of the holes of the medium, as in the $\epsilon = 0$ case. As discussed in section 7.1, the dissipation of these density fluctuations can be studied by monitoring the sliding tag correlation function $\sigma^2(t)$. We find that if ϵ is not too large, $\sigma^2(t) \sim t^{2/3}$.

Summary

In this chapter we have considered probe particles in a KLS chain. Earlier studies for finite ρ_0 had reported that for large ϵ, the system shows a phase separation transition to a state where a macroscopic domain consisting of particles and holes (no probes) is formed while the rest of the system comprises of small probe

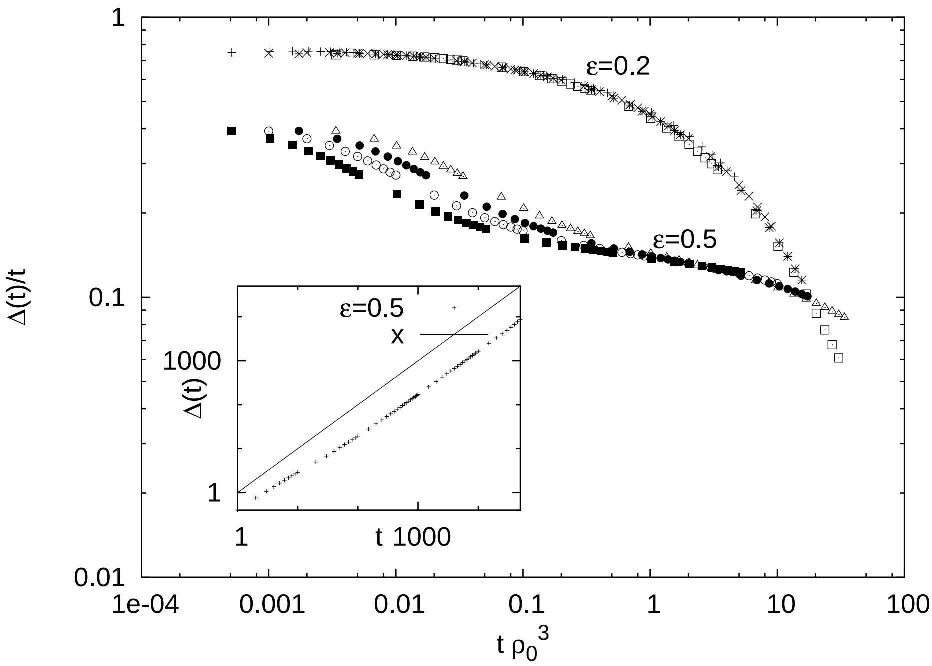

Figure 8.6: *Scaling collapse for* $\Delta(t)$ *for finite* ϵ *values. We have used* $\rho_0 = 0.08, 0.1, 0.12, 0.15$ *and* $L = 16384$*. The inset shows the linear growth of* $\Delta(t)$ *for* $L = 16384$ *in presence of two probes.*

clusters interrupted by small domains of particles and holes. In [69] a description of this phase transition was attempted using an approximate mapping onto zero-range process. However, this mapping fails to explain the observed domain size distribution $P(n)$ in the system. While ZRP predicts a $P(n)$ as in Eq. 8.5 where the exponent b is a function of ϵ given by Eq. 8.4, we find numerically that $P(n)$ shows the same power law exponent $3/2$ irrespective of the values of ϵ.

In order to examine the cause of this discrepancy, we examined the assumptions that are used for the KLS-ZRP mapping. We verified that (i) the domains are independently distributed and (ii) even taking into account the higher order finite size corrections in the domain current (where the hopping rates of ZRP are directly read off from the numerically measured domain currents) does not affect the value of the power law exponent of $P(n)$. However, the probes in a KLS medium have a non-Markovian movement which is not captured in the ZRP mapping. It would be useful to construct an appropriate non-Markovian ZRP and examine whether it can explain the observed $P(n)$.

In [35, 73] the dynamics of the system was studied in presence of two probes. Starting with the initial condition that the two probes are nearest neighbors, the time-evolution of the separation between them was monitored and it was claimed that the average separation $\langle r(t)\rangle$ grows with time as shown in Eq. 8.8. On the contrary, we find that although the short time growth of $\langle r(t)\rangle$ is as predicted by Eq. 8.8, at large times $\langle r(t)\rangle$ shows a crossover to an asymptotic regime where it grows with an exponent 1/3, as in $\epsilon = 0$ case. One plausible explanation of this phenomenon could be that the correlation length in the KLS medium being finite (since a KLS chain has an Ising measure), at large times, when the typical displacement of a probe becomes larger than the correlation length of the medium, the probes behave as in $\epsilon = 0$ case.

For a macroscopic number of the probes, the dynamical correlation functions show a scaling form in terms of a crossover time-scale τ, as in $\epsilon = 0$. Surprisingly, τ shows the same divergence as $\epsilon = 0$, in the limit $\rho_0 \to 0$. This in turn implies that $z_0/(2-b) = 3$. If b is substituted from Eq. 8.4 then for larger ϵ this leads to a dynamical exponent $z_0 < 1$. Instead if one replaces b by 3/2, for all ϵ then z_0 turns out to be 3/2, as in $\epsilon = 0$ case. This also explains the large time crossover of $\langle r(t)\rangle$.

In this chapter, we have discussed STPs in a KLS chain. It is possible to generalise the model by considering DPPs and a partially asymmetric variation of KLS model. Our preliminary numerical studies indicate that as in the non-interacting case one has an 'exponential' phase and a 'power law' phase, separated by a critical line. However, mapping out the complete phase diagram needs further studies.

Chapter 9

Discussion: Nonequilibrium Probe Particles

Probe particles are routinely used to characterise complex systems. The statics and dynamics of a probe particle which comes to a steady state with the medium, often reflect important properties of the medium. In all these studies it is generally assumed that dilute presence of the probe particles do not affect the properties of the medium in a significant way. We have shown in this thesis that this assumption may not hold true in all situations.

We have considered probes whose dynamical rules violate detailed balance. These probes exchange with particles and holes of the medium in opposite directions with possibly different rate. Such probes tend to be present in the region of strong density variations or shocks present in the system. We consider both equilibrium and nonequilibrium medium. We are primarily interested in the case when the medium can be described by symmetric or asymmetric exclusion process. The probes can then be alternatively described as particles sliding down along the local slope of a fluctuating surface (EW or KPZ type). The probes tend to be present in the valleys of the interface but unlike the situation considered in chapter 2 and 3, these probes are not passive anymore as they occupy space in the lattice and block the evolution of the valleys. We find that this deviation from passivity brings about a large effect on the surrounding medium.

For a medium which is initially in equilibrium, the effect of introducing even a single nonequilibrium probe is very strong. There is a density gradient in the medium across the entire system. This follows from the fact that even in the presence of a single nonequilibrium probe the resulting system is a nonequilibrium current-carrying system. To support a current through a medium with diffusive dynamics one has to have a system-wide density gradient. In presence of several probes, the medium induces a strong attraction between them and the probes phase separate.

For an initially nonequilibrium medium however, the effect of a single probe is not macroscopic. The shock around the probe decreases exponentially or as a power law, depending on the kinematics of the probe and the medium. This yields an interesting phase diagram which in turn plays an important role on the dynamics of macroscopic number of probes. The power law regime corresponds to a diverging (as the probe density goes to zero) crossover time-scale in the probe dynamics. It has been possible to give a scaling description of various dynamical correlation functions in terms of this diverging time-scale.

Presence of nonequilibrium probes in a Katz-Lebowitz-Spohn model (a nonequilibrium medium with nearest neighbor Ising interaction) is also considered. However, some of our results are in contradiction with earlier work [69, 35, 73]. In [69] it was reported that KLS model with macroscopic number of probes shows a phase separation transition for large values of the coupling constant. As the Ising interaction strength $\epsilon > 0.8$ and the density exceeds a critical value ρ_c, a macroscopic domain consisting of particles and holes of the medium is formed which coexists with another phase where small domains of particles and holes are found, separated by probes.

Kafri *et al.* have attempted to explain this phase transition by approximately mapping the system onto a zero-range-process [69]. However, this mapping fails to explain the observed power law exponent of the size distribution of the domains—while for a zero-range process the mass distribution decays as a power law with exponent $b(\epsilon)$, the size distribution of the particle-hole domain close to the critical point shows a power law decay with exponent $3/2$, irrespective of the value of ϵ.

To find the root of this discrepancy, we have examined the assumptions that go into the KLS-ZRP mapping. We have numerically verified that the domains in the KLS model with probes are indeed independently distributed, in agreement with [71]. Another assumption used in this mapping is that the current in a domain of length n is same as the current in an open KLS chain. In [71] this was shown to be true.

However, this mapping ignores one important aspect of the probe dynamics. The movement of probe particles in a KLS chain is non-Markovian, whereas the corresponding ZRP is taken to be an ordinary Markov process. It would be interesting to consider an appropriate non-Markovian ZRP and a detailed study might provide some insight into the observed discrepancy about domain size distribution.

In [35, 73] dynamics of two probes in a KLS chain was considered. It was claimed that the medium induces an attraction between the probe pair and in steady state, the probability that they are at a distance r from each other decays as a power law with an exponent $b(\epsilon)$. Levine *et al.* have monitored the time evolution of the average distance $\langle r(t)\rangle$ between the probes starting with an initial condition that the two probes are nearest neighbors and according to [35] the average distance grows with time as a power law with an exponent $(2-b)/z$. On the contrary, we find that although the small time behavior of $\langle r(t)\rangle$ is consistent with the above growth law, this is not true at large times. We find that as time increases, $\langle r(t)\rangle$ shows a crossover to a regime where it grows with an exponent $1/3$, as in $\epsilon = 0$ case. This phenomenon can be explained from the fact that the KLS medium has a finite correlation length and hence for large enough time when a probe particle explores a region larger than this correlation length, its behavior is same as in $\epsilon = 0$ case (uncorrelated medium).

For a finite density of probes, our scaling analysis shows that the dynamics of the probes is governed by a crossover time-scale. As the probe concentration vanishes, this time-scale diverges as $\rho_0^{-z_0/(2-\lambda)}$. Our numerical simulations show that $z_0/(2-\lambda) = 3$. According to [35] $\lambda = b(\epsilon)$ and this leads to $z_0 < 1$ for large ϵ. A dynamical exponent smaller than unity seems implaussible. On the other hand, if we follow the argument given the end of the previous paragraph and substitute $b = 3/2$ for all values of ϵ, then z_0 takes the value $3/2$ as in $\epsilon = 0$ case. This is in agreement with the large time crossover of $\langle r(t)\rangle$. Note that $b = 3/2$ is also in conformity with the observed domain size distribution. But at present we do not have any clear understanding of why the ZRP mapping would yield such a value of b.

Chapter 10

ASEP with Time Dependent Bias

In this chapter we study a simple but interesting variation of asymmetric simple exclusion process (ASEP) in one dimension. As we have seen before, ASEP describes a set of hard-core random walkers which perform a biased motion on a lattice. We consider the case when this bias itself is a function of time. We would be interested only in the case when the bias changes periodically with time. We find that even in this case of time-dependent bias, the steady state measure can be obtained analytically and turns out to be the same as in an ordinary ASEP. However, the dynamical correlation functions of the density variable show some interesting crossover across the time-period of the bias. For a bias which varies sinusoidally with time, we find that the system shows hysteresis.

The model is defined on a one dimensional periodic lattice. An occupied site is denoted by 1 and an empty site by 0. Any particular configuration is therefore written as a string of 1's and 0's. The exchange rules are :

$$\begin{aligned} 10 &\xrightarrow{\mathrm{p}} 01 \\ 01 &\xrightarrow{\mathrm{q}} 10 \end{aligned} \tag{10.1}$$

where the bias $(p-q)$ is a periodic function of time. For example, for a square-wave bias of period T, one has

$$\begin{aligned} p-q &= +1 \qquad \text{if } t < T/2 \\ p-q &= -1 \qquad \text{if } t > T/2. \end{aligned} \tag{10.2}$$

In the next section, we derive the steady state measure of the model. In section 10.2 we discuss our results for density auto-correlation and mean squared displacement of the tagged particles. In section 10.3 we discuss the existence of hysteresis for a sinusoidal bias.

10.1 Stationary State Distribution

From the above dynamical rules shown in Eq. 10.2, we first construct the time evolution operator for an ordinary ASEP by mapping the process onto a spin half problem. Let us denote an occupied site by an up-spin ($\uparrow$) and an empty site by a down-spin ($\downarrow$), then the possible configurations of a nearest neighbor pair are: $|\uparrow\downarrow\rangle$, $|\downarrow\uparrow\rangle$, $|\uparrow\uparrow\rangle$ and $|\downarrow\downarrow\rangle$. Then according to Eq. 10.2 the time-evolution of these states can be written as:

$$\begin{aligned}
|\uparrow\downarrow\rangle &\xrightarrow{dt} (1-pdt)|\uparrow\downarrow\rangle + pdt|\downarrow\uparrow\rangle \\
|\downarrow\uparrow\rangle &\xrightarrow{dt} (1-qdt)|\downarrow\uparrow\rangle + qdt|\uparrow\downarrow\rangle \\
|\uparrow\uparrow\rangle &\xrightarrow{dt} |\uparrow\uparrow\rangle \\
|\downarrow\downarrow\rangle &\xrightarrow{dt} |\downarrow\downarrow\rangle
\end{aligned} \tag{10.3}$$

where dt is the time interval. It is easy to verify that the time-evolution operator which satisfies Eq. 10.3 is given by

$$\mathcal{H} = \sum_{\langle ij\rangle} [(p+q)(\vec{S}_i.\vec{S}_j - \frac{1}{4}) + i(p-q)(S_{kx}S_{ly} - S_{ky}S_{lx})]. \tag{10.4}$$

Then the time-evolution equation reads

$$\frac{\partial |P\rangle}{\partial t} = \mathcal{H}|P\rangle \tag{10.5}$$

In other words, if the initial state of the system is written as $|\mathcal{P}(0)\rangle$, where different components of the vector correspond to probability of different configurations, then state at time t will be

$$|\mathcal{P}(t)\rangle = e^{\mathcal{H}t}|\mathcal{P}(0)\rangle. \tag{10.6}$$

Now, consider a time-dependent bias which varies with time as a square-wave, as shown in Eq. 10.3. The problem can be mapped onto a spin half problem as before, with the Hamiltonian

$$\mathcal{H}(t) = \sum_{\langle ij \rangle} [\theta(p-q) S_i^+ S_j^- + \theta(q-p) S_i^- S_j^+ + S_i^z S_j^z - \frac{1}{4}] \qquad (10.7)$$

where $\theta(p-q)$ is a step function of the bias $(p-q)$. In two half-periods, the $\mathcal{H}$ shown in the last equation becomes $\mathcal{H}_1$ and $\mathcal{H}_2$ (say) which are the time-evolution operators for two ordinary ASEP's biased in opposite directions:

$$\begin{aligned} \mathcal{H}_1 &= \sum_{\langle ij \rangle} [S_i^+ S_j^- + S_i^z S_j^z - \frac{1}{4}] \\ \mathcal{H}_2 &= \sum_{\langle ij \rangle} [S_i^- S_j^+ + S_i^z S_j^z - \frac{1}{4}] \end{aligned} \qquad (10.8)$$

The state of the system after one complete cycle T would be

$$\begin{aligned} |\mathcal{P}(T)\rangle &= \exp\left(\int_0^T \mathcal{H}(t) dt\right) |\mathcal{P}(0)\rangle \\ |\mathcal{P}(T)\rangle &= \exp\left[\frac{T}{2}(\mathcal{H}_1 + \mathcal{H}_2)\right] |\mathcal{P}(0)\rangle \end{aligned} \qquad (10.9)$$

Now, $\mathcal{H}_1$ and $\mathcal{H}_2$ are time-evolution operators for ordinary ASEP each of which would lead to the same steady state (which is the right eigenvector with 0 eigenvalue) with homogeneous product measure. Therefore their sum $(\mathcal{H}_1+\mathcal{H}_2)$ should also have the same eigenvector and hence the steady state of the system even in presence of a square-wave bias continues to be a uniform product measure.

This result is simple yet striking. A periodically driven system goes to a steady state which is identical to the steady state of a system under time-independent drive. Above derivation can be extended for any t by writing $t = mT + \delta t$ where even for the left-over time δt the time-evolution operator is that of an ordinary ASEP. This result also holds true for any other periodic or even non-periodic variation of the bias $(p-q)$ provided the time-evolution operator at each instant can be written in the form of Eq. 10.4.

10.2 Dynamical Correlation Functions in Steady State

In the previous section, we have seen that the steady state measure of an ASEP remains unchanged even when the bias changes periodically. As a result, all the static properties remain same as in ordinary ASEP. However, the steady state dynamics shows interesting manifestation of the time-dependence of the bias. Consider a square-wave bias of period T. Since the first reversal of bias takes place at time $T/2$, for $t < T/2$ the system is just an ordinary ASEP. On the other hand, for $t \gg T$, when many bias-reversals have taken place the system has spent, on the average, an equal amount of time under leftward and rightward bias. We find that in this regime, the dynamical properties of the system are same as in an SEP. We demonstrate this by monitoring the density auto-correlation and mean squared displacement of a tagged particle in steady state. Below we discuss our results.

For a square-wave bias, we study the auto-correlation function of local density

$$A(t) = \langle n_i(0)n_i(t)\rangle - \rho^2 \tag{10.10}$$

where $n_i(t)$ is the occupancy of the i-th site at time t which takes the value 1 if the i-th site is occupied and the value 0 if the i-th site is empty. The angular brackets denote averaging over steady state ensemble and ρ is the average density which is taken to be $1/2$. We find that the function $A(t)$ shows two different behavior for $t < T/2$ and $t \gg T$. For $t < T/2$, the system being just an ASEP, $A(t)$ decays as a power law with an exponent $1/z = 2/3$ where z is the dynamical exponent. On the other hand, for $t \gg T$, the system shows diffusive behavior and $A(t) \sim t^{1/2}$. We present our data in fig 10.1.

The mean squared displacement of a tagged particle, as defined in Eq. 6.2, shows similar crossover. For $t < T/2$, we find $C(t) \approx (1-\rho)(p-q)t$, as in an ordinary ASEP [52]. For $t \gg T$, on the other hand, $C(t) \sim t^{1/2}$ as expected for a SEP [44]. Our data has been presented in fig 10.2. Note that in the intermediate regime, $C(t)$ shows oscillation. This can be explained in the following way.

A typical configuration contains a pattern of density fluctuations and these density fluctuations move through the system with the speed of a kinematic wave.

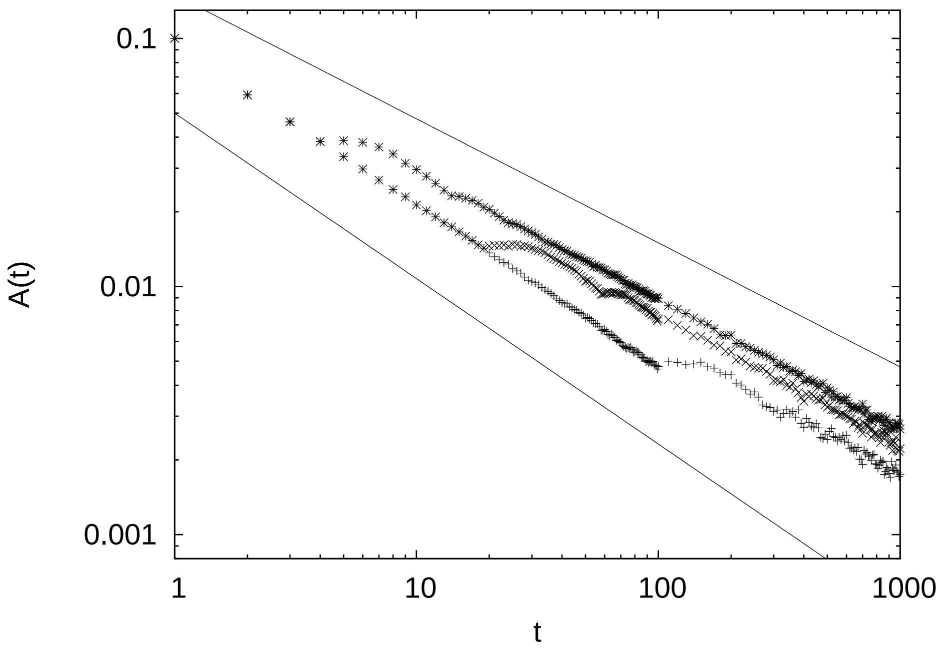

Figure 10.1: *Density auto-correlation in steady state for an ASEP with a bias which varies as a square-wave with* $T = 200, 40, 10$*. The reference lines show* $t^{-2/3}$ *(short-time) and* $t^{-1/2}$ *(asymptotic) decay. We have used* $L = 1024$ *and* $\rho = 1/2$*.*

We have considered $\rho = 1/2$ for which the speed of kinematic wave is zero. But the tagged particle has a finite speed and it moves through this density pattern with an average speed $(p-q)(1-\rho)$. Each density patch contributes a random excess to its average speed and hence the mean squared displacement grows linearly. When the bias is reversed at $t = T/2$, the particle starts moving in the opposite direction, towards its initial density patch. At the end of one complete cycle, the particle reaches its initial density patch and its mean squared displacement then measures the sub-linear dissipation of the density patch which corresponds to a dip in $C(t)$.

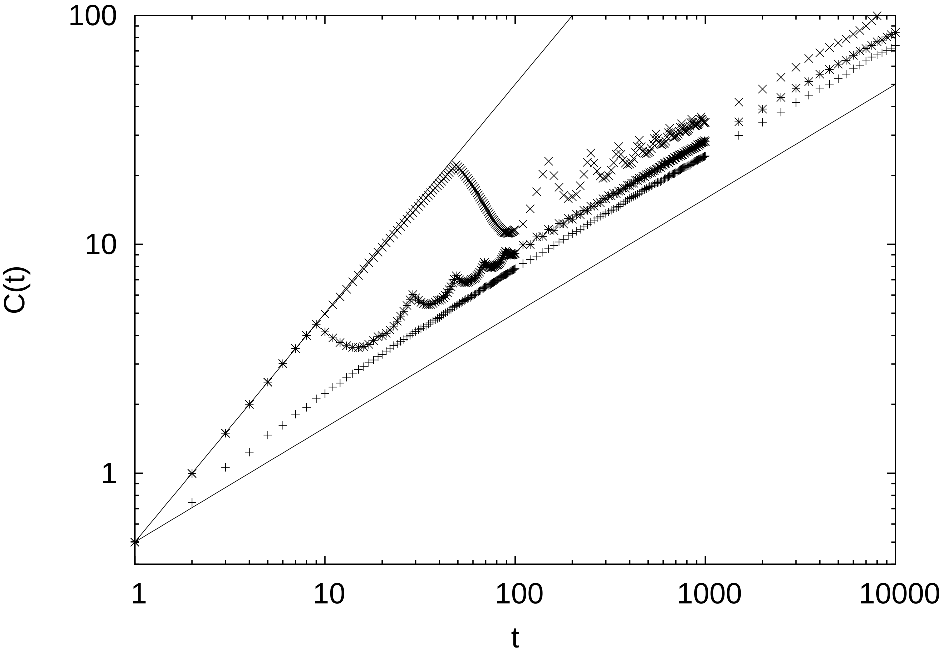

Figure 10.2: *Mean squared displacement of a tagged particle for an ASEP with square-wave bias of time-period $T = 2, 20, 100$ and $L = 256$. The initial linear growth with slope $(p-q)(1-\rho)$ and asymptotic $t^{1/2}$ growth are shown using two reference lines.*

10.3 Hysteresis for Sinusoidal Bias

In this section, we discuss how time-dependent bias in an ASEP gives rise to hysteresis in the system. We will consider a bias that varies sinusoidally with time. At this stage, it would be convenient to map the particle-hole configuration to an inclined interface separating up and down spin regions in a two dimensional nearest neighbor Ising model [74]. Note that in the Ising model, if the field h and inverse temperature $\beta \equiv 1/T$ are assumed to be much smaller than the nearest neighbor exchange coupling J, then there are no overhangs in the interface. We assume that the field h varies sinusoidally with time: $h(t) = \sin \omega t$. The interface evolves under Glauber dynamics in which the rate at which a spin flips, is $min[1, \exp(-\beta \Delta E)]$ where ΔE is the change in the energy due to the flip. In this single-flip Glauber dynamics, and $T, h \ll J$, only the spins at the corner (drawn

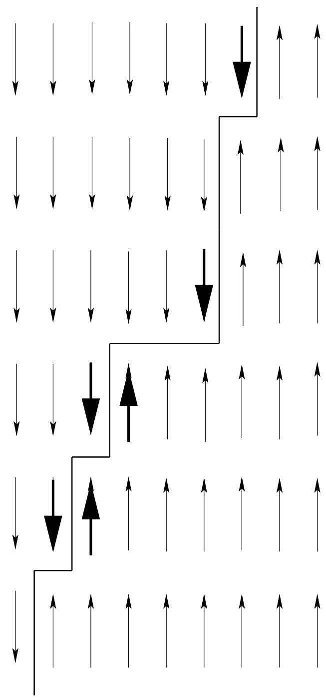

Figure 10.3: *An inclined Ising interface separating the up-spin domain and down-spin domain of a two dimensional Ising model. The exchange coupling being infinite, only the spins marked by bold arrows can flip.*

by bold lines in fig 10.3) have an appreciable probability of flipping. This leads to a flip of the corner, which preserves the length of the interface. The periodic boundary condition is implemented by considering the interface on the surface of a cylinder [see [74] for more details].

The mapping to the exclusion process follows if we associate a particle with each vertical bond of the interface and a hole with each horizontal bond. Corner flip dynamics then corresponds to the particle-hole exchange for the particle system. If p and q be the leftward and rightward hopping in the ASEP, then these rates cane be related to the Ising model parameters on noting that the ratio of the flip-rate of an up-spin to that of a down-spin is $\exp(-2\beta h)$, *i.e.*

$$\frac{p}{q} = \exp[2\beta h(t)] \qquad (10.11)$$

Let us write $p = u\exp(2\beta h)$ and $q = u\exp(-2\beta h)$ for some constant u. Then the current in the particle-hole system is

$$J = (p - q)\rho(1-\rho) = 2u\rho(1-\rho)sinh(\beta \sin \omega t) \tag{10.12}$$

Each time the bias is reversed, the direction of the current is changed and the interface shows a back and forth movement on the surface of the cylinder, changing the magnetisation. If $\Delta M(t_0 \to t)$ be the change in magnetisation as time changes from t_0 to t, then

$$\begin{aligned} \Delta M(t_0 \to t) &= \int_{t_0}^{t} dt' J(t') \\ \Delta M(t_0 \to t) &= 2u\rho(1-\rho) \int_{t_0}^{t} dt' sinh(\beta \sin \omega t') \end{aligned} \tag{10.13}$$

This expression can be evaluated numerically and the magnetisation can be plotted across the field to obtain the hysteresis loop [fig 10.4]. Note that even when the field $h(t)$ completes one half cycle and comes back to its initial value 0, the change in magnetisation remains finite. This gives rise to a hysteresis loop with a finite area.

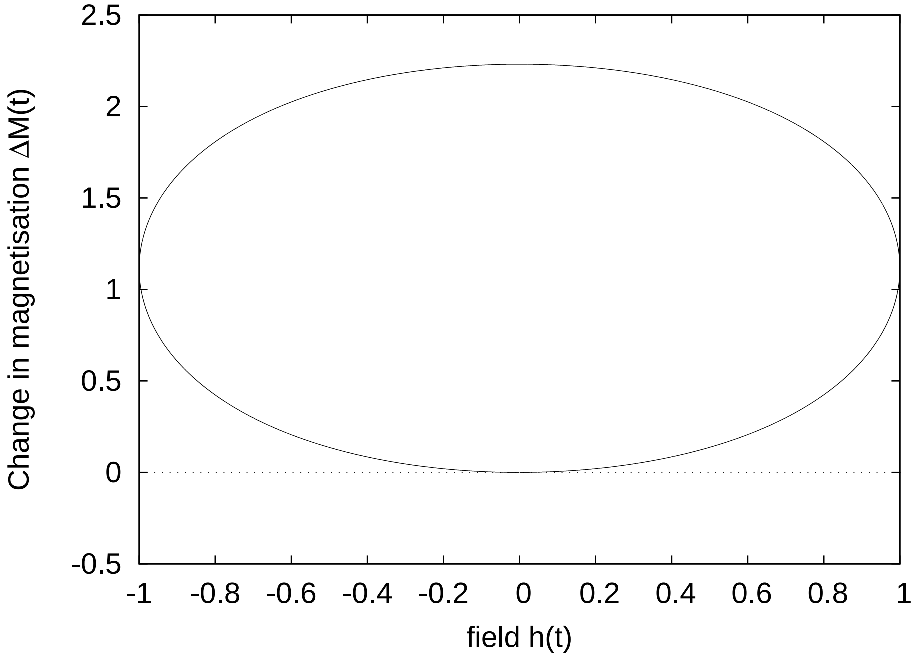

Figure 10.4: *Hysteresis loop for an ASEP under a bias that changes sinusoidally with time.*

Appendix A

Correspondence between Exclusion Process and Surface Fluctuation

In this appendix, we discuss how the lattice model for the exclusion process is related to the continuum equation for the surface fluctuation.

In one dimension, ASEP describes a set of hard-core particles on a lattice. A particle, chosen at random, hops to neighboring site to its right (left) with probability p (q), if the neighboring site is empty. For periodic boundary condition it can be exactly shown that all possible configurations occur with equal probability in the steady state ensemble. The current in an ASEP can be calculated as follows. There is a movement (of particle) to the right, only if the site under consideration is occupied and its right neighbor is empty. This process has a probability $p\rho(1-\rho)$ where ρ is the density of particles. Similarly, probability of having a movement towards left is $q\rho(1-\rho)$ and the total current is $J = (p-q)\rho(1-\rho)$.

One may map the above particle model to a discrete surface model as follows: an occupied site represents an up slope and an empty site represents a down slope. In fig A.1 we show one typical particle configuration and the corresponding surface configuration. Flipping of a hill (valley) to a valley (hill) thus means movement of a particle to the right (left).

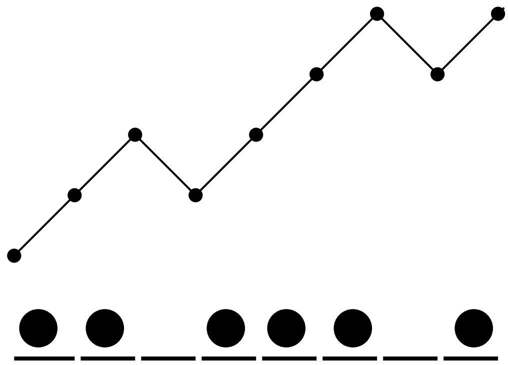

Figure A.1: *Mapping between exclusion process and surface configuration in one-dimension.*

A continuum description of ASEP, obtained by coarse graining over regions which are large enough to contain many sites, involves the local density of particles $\rho(x)$ and the local current $J(x)$. The continuity equation reads

$$\frac{\partial \rho}{\partial t} + \frac{\partial J}{\partial x} = 0 \tag{A.1}$$

with

$$J(x) = \nu \frac{\partial \rho}{\partial x} + j(\rho) + \eta \tag{A.2}$$

where ν is the diffusion co-efficient, η is the Gaussian white noise and $j(\rho)$ is the systematic contribution of the current: $j(\rho) = (p-q)\rho(1-\rho)$.

Since in the discrete model, the presence of a particle is identified with an up slope and an empty site is identified with a down slope, we write

$$\rho(x) = \frac{1}{2}\left(1 + \frac{\partial h}{\partial x}\right) \tag{A.3}$$

and then the continuity equation can be rewritten as

$$\frac{\partial h}{\partial t} = -\frac{1}{2}(p-q) + \nu \frac{\partial^2 h}{\partial x^2} + \frac{1}{2}(p-q)\left(\frac{\partial h}{\partial x}\right)^2 - 2\eta \tag{A.4}$$

which is the KPZ equation (Eq. 2.1) with an additional constant term $-(p-q)/2$ and $\lambda = (p-q)$, $\eta_1 = -2\eta$. Note that the sign of the constant term and λ are opposite. Thus a downward moving surface (corresponding to $p > q$) has a positive λ and an upward moving surface has a negative λ. Although the constant term can be eliminated by a Galilean shift $h \rightarrow h - \frac{1}{2}(p-q)t$, its sign is important in determining the overall direction of motion of the surface.

Appendix B

Sign-Sign Correlation Function for a Gaussian Process

In this appendix, we outline the derivation of the correlation function of the sign of a Gaussian variable.

Consider a Gaussian stationary process $X(t)$ such that the random variables $x(t)$ and $x(t+\tau)$ are jointly normal and their joint distribution is given by

$$f(X_1, X_2) = \frac{1}{2\pi\sigma_1\sigma_2\sqrt{1-r^2}} \exp\left[-\frac{1}{2(1-r^2)}\left(\frac{X_1^2}{\sigma_1^2} + \frac{X_2^2}{\sigma_2^2} - 2r\frac{X_1X_2}{\sigma_1\sigma_2}\right)\right]. \quad \text{(B.1)}$$

Here $X_1 \equiv x(t)$, $X_2 \equiv x(t+\tau)$ and $r = R_x(\tau)/R_x(0)$, where $R_x(\tau) = \langle x(t+\tau)x(t)\rangle$. Then the arc-sine law states that

$$\langle sgnX_1\ sgnX_2\rangle = \frac{2}{\pi}\sin^{-1}\left[\frac{R_x(\tau)}{R_x(0)}\right]. \quad \text{(B.2)}$$

We provide a proof of this below. To start with, define a random variable $Z = X_1/X_2$. Let D_z be the region in X_1X_2 plane such that $X_1/X_2 \leq z$, z being some particular value of Z. The region bounded by the lines $X_1 = X_2z$ and $X_1 = X_2(x+dz)$ is denoted as ΔD_z and shown as the vertically shaded part of fig B.1. Co-ordinate of any point lying in this shaded region is (zX_2, X_2) and the differential area is $|X_2|dzdX_2$. Note that

$$\{Z \leq z\} = \left\{\frac{X_1}{X_2} \leq z\right\} = \{(X_1, X_2) \in D_z\}. \quad \text{(B.3)}$$

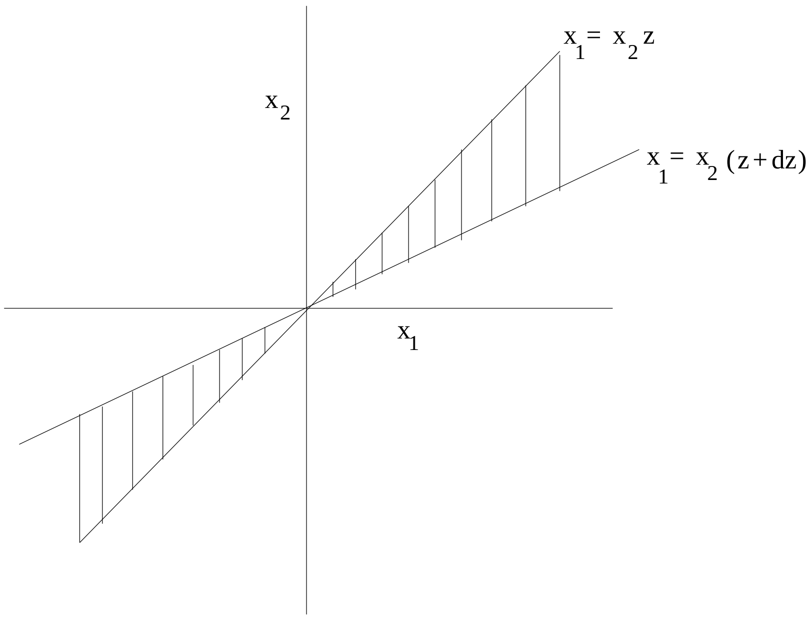

Figure B.1:

Now, consider the cumulative distribution of Z

$$\begin{aligned} F_Z(z) &= P\{Z \le z\} \\ &= P\{(X_1, X_2) \in D_z\} \\ &= \int_{D_z}\int f(X_1, X_2) dX_1 dX_2 \end{aligned} \tag{B.4}$$

Thus, to determine $F_Z(z)$ it suffices to find out D_z for every z and evaluate the integral.

The density of Z can also be determined similarly. Let ΔD_z be the region such that

$$\begin{aligned} \{z < Z < z + dz\} &= \{(X_1, X_2) \in \Delta D_z\} \\ f_Z(z)dz &= \int_{\Delta D_z}\int f(X_1, X_2) dX_1 dX_2 \\ f_Z(z) &= \int_{-\infty}^{\infty} |X_2| f(zX_2, X_2) dX_2 \end{aligned} \tag{B.5}$$

The right hand side can be written as

$$2\int_0^{\infty} dX_2 X_2 \frac{1}{2\pi\sigma_1\sigma_2\sqrt{1-r^2}} \exp\left[-\frac{1}{2(1-r^2)}\left(\frac{X_2^2 z^2}{\sigma_1^2} - 2r\frac{X_2^2 z}{\sigma_1\sigma_2} + \frac{X_2^2}{\sigma_2^2}\right)\right]$$

after carrying out the integration which yields

$$f_Z(z) = \frac{\sigma_1\sigma_2\sqrt{1-r^2}}{\pi\sigma_2^2\left(z - \frac{r\sigma_1}{\sigma_2}\right)^2 + \sigma_1^2(1-r^2)}. \tag{B.6}$$

The cumulative distribution then becomes

$$\begin{aligned} F_Z(z) &= \int_{-\infty}^{z} f_Z(z)dz \\ &= \frac{1}{2} + \frac{1}{\pi}\tan^{-1}\frac{\sigma_2 z - r\sigma_1}{\sigma_1\sqrt{1-r^2}} \\ &= \frac{1}{2} + \frac{1}{\pi}\tan^{-1}\frac{z-r}{1-r^2} \end{aligned} \tag{B.7}$$

where the last step uses the fact that for a Gaussian stationary process $X(t)$, $\sigma_1 = \sigma_2$. Write

$$\alpha = \tan^{-1}\frac{r}{\sqrt{1-r^2}}. \tag{B.8}$$

and Eq. B.7 gives

$$\begin{aligned} F_Z(0) &= \frac{1}{2} - \frac{\alpha}{\pi} \\ &= P[Z \leq 0]. \end{aligned} \tag{B.9}$$

Finally,

$$\begin{aligned} \langle sgnX_1 \; sgnX_2 \rangle &= 1 - 2P[X_1X_2 < 0] \\ &= 1 - 2P\left[\frac{X_1}{X_2} < 0\right] \\ &= 1 - 2P[Z < 0] \\ &= 1 - 2\left(\frac{1}{2} - \alpha\pi\right) \\ &= \frac{2\alpha}{\pi} \\ &= \frac{2}{\pi}\sin^{-1} r \\ &= \frac{2}{\pi}\sin^{-1}\left[\frac{R_x(\tau)}{R_x(0)}\right] \end{aligned} \tag{B.10}$$

which proves the arc-sine law.

Appendix C

Static Correlation Function of Second Class Particles

In this appendix, we outline the calculation by Derrida *et al.* of static correlation function of second class particles in a TASEP.

Steady state measure of the system consisting of macroscopic number of second class particles in a TASEP was calculated in [34] using the matrix product method. It was shown that the steady state weight of one particular configuration is given by trace$[X_1X_2X_3....X_N]$ where X_i is a matrix which is written as D, E or A according as the i-th site contains a medium particle, a hole, or a second class particle. The matrices satisfy the following relations

$$DE = D + E \qquad\qquad A = DE - ED \tag{C.1}$$

Using the stationary distribution, the two-point density-density correlation was obtained and we outline the calculation below.

Consider a finite ring of N sites. We would be mainly interested in the density profile of the medium particles as seen from the frame of a second class particles. For convenience, we assume that the N-th site is occupied by a second class particle. In this appendix, to use the same terminology and notation as in [34], we call the particles in the medium as "first class particles" and denote their density by ρ_1. The density of the second class particles is denoted as ρ_2. Although the numbers of first and second class particles are conserved, it is more convenient to carry out the calculation in the grand canonical ensemble. Let x, y and z denote the fugacities for the first class particles, second class particles and holes. Define a matrix G as

$$G = xD + yA + zE \tag{C.2}$$

Then the densities of the first class particles, second class particles and holes, as seen from one particular second class particle are given by

$$\begin{aligned} d_i(N) &= x\frac{\langle 1|G^{i-1}DG^{N-i-1}|1\rangle}{\langle 1|G^{N-1}|1\rangle} && \text{(C.3)}\\ a_i(N) &= y\frac{\langle 1|G^{i-1}AG^{N-i-1}|1\rangle}{\langle 1|G^{N-1}|1\rangle} && \text{(C.4)}\\ e_i(N) &= z\frac{\langle 1|G^{i-1}EG^{N-i-1}|1\rangle}{\langle 1|G^{N-1}|1\rangle} && \text{(C.5)} \end{aligned}$$

where $\langle 1| = [1,0,0,...]$. The matrix G can be shown to obey a recursion relation

$$\langle 1|G^n|1\rangle = \frac{(y+x)(y+z)}{y}\langle 1|G^{n-1}|1\rangle - \frac{xz}{y}\langle 1|C^{n-1}|1\rangle \tag{C.6}$$

with $C = xD + zE$. Moreover, since $D|1\rangle = |1\rangle$

$$d_{N-1}(N) = x\frac{\langle 1|G^{N-2}|1\rangle}{\langle 1|G^{N-1}|1\rangle} \tag{C.7}$$

A consequence of the matrix algebra yields

$$x(DG - GD) = (x+y)(z+y)A - yAG \tag{C.8}$$

Eq. C.4, C.8 and C.6 imply that for $i > 1$

$$d_i(N) - d_{i+1}(N) = xz\frac{\langle 1|G^{i-1}|1\rangle\langle 1|C^{N-i-2}|1\rangle}{\langle 1|G^{N-1}|1\rangle} \tag{C.9}$$

This equation together with Eq. C.7 determine all the $d_i(N)$.

Now we consider infinite volume limit of these densities. The large n behavior of $\langle 1|G^n|1\rangle$ for $y^2 > xz$ is given by

$$\langle 1|G^n|1\rangle \simeq \left(1 - \frac{xz}{y^2}\right)\left[\frac{(y+x)(y+z)}{y}\right]^n. \tag{C.10}$$

From this, we may determine $x, y.z$ such that in the large N limit, the density of first class particles ρ_1, the density of the second class particles ρ_2 and the density of holes $1-\rho_1-\rho_2$ are recovered.

$$\rho_1 = \lim_{N\to\infty} \frac{x}{N}\frac{d}{dx} log\langle 1|G^N|1\rangle = \frac{x}{y+x} \tag{C.11}$$

$$\rho_2 = \lim_{N\to\infty} \frac{y}{N}\frac{d}{dy} log\langle 1|G^N|1\rangle = \frac{y^2-xz}{(y+x)(y+z)} \tag{C.12}$$

$$1-\rho_1-\rho_2 = \lim_{N\to\infty} \frac{z}{N}\frac{d}{dz} log\langle 1|G^N|1\rangle = \frac{z}{y+z} \tag{C.13}$$

It is clear from these equations that $y^2 > xz$ leads to a consistent determination of x, y, z, unique upto an overall factor.

Now, define $d_i = \lim_{N\to\infty} d_i(N)$ and $d_{-i} = \lim_{N\to\infty} d_{N-i}(N)$ for $i > 0$. From Eq. C.7, C.10, C.12 and C.13

$$d_{-1} = \frac{xy}{(y+x)(y+z)} = \rho_1(\rho_1+\rho_2) \tag{C.14}$$

while the Eq. C.9 yields

$$d_{-i} = \rho_1(\rho_1+\rho_2)+\sum_{n=1}^{i-1}\sum_{p=0}^{n-1}\frac{1}{p+1}\binom{n}{p}\binom{n-1}{p}\times[\rho_1(\rho_1+\rho_2)]^{p+1}[(1-\rho_1)(1-\rho_1-\rho_2)]^{n-p} \tag{C.15}$$

Also, from Eq. C.9 for all $i > 0$ $d_i = \rho_1$. Following similar steps, it can be shown for the hole densities that for $i > 0$, $e_{-i} = 1-\rho_1-\rho_2$ and

$$e_i = (1-\rho_1)(1-\rho_1-\rho_2)+\sum_{n=1}^{i-1}\sum_{p=0}^{n-1}\frac{1}{p+1}\binom{n}{p}\binom{n-1}{p}\times[\rho_1(\rho_1+\rho_2)]^{p+1}[(1-\rho_1)(1-\rho_1-\rho_2)]^{n-p} \tag{C.16}$$

Notice that in the infinite volume limit, the density profile of the holes to the left of a second class particle and that of the particles to the right of a second class particle are constant. Also, $\lim_{i\to\infty} d_{-i} = \rho_1$ and this approach is exponential:

$$d_{-i-1} - d_{-i} = \tfrac{1}{2\sqrt{\pi}i^{3/2}}[\rho_1(\rho_1+\rho_2)(1-\rho_1)(1-\rho_1\rho_2)]^{1/4} \tag{C.17}$$

$$\times\{[\rho_1(\rho_1+\rho_2)]^{1/2} + [(1-\rho_1)(1-\rho_1-\rho_2)]^{1/2}\}^{2i+1} \tag{C.18}$$

From the above expression, it follows that as $\rho_2 \to 0$, the characteristic length of the exponential decay is asymptotically $4\rho_1(1-\rho_1)/\rho_2^2$.

Appendix D

Steady State Measure of Katz-Lebowitz-Spohn Model

In this section we provide a detailed derivation of the stationary measure of KLS model following the calculation in [68].

The system is defined on a one dimensional periodic lattice each site of which is occupied by either species A or species B. We are interested in the totally asymmetric version of KLS model, where the species A moves only to the right and B moves only to the left. There is a nearest neighbor interaction present in the system. The dynamical moves are listed in Table D.1.

The aim is to construct the nonequilibrium dynamics by determining the values of the above rates such that the stationary state measure is given by Boltzmann-Gibbs distribution with the Hamiltonian

$$\mathcal{H} = -J \sum_n s_n s_{n+1}. \tag{D.1}$$

Move	Rate
$AABA \to ABAA$	w_{AA}
$AABB \to ABAB$	w_{AB}
$BABA \to BBAA$	w_{BA}
$BABB \to BBAB$	w_{BB}

Table D.1: *List of moves in KLS model.*

Let the number of AA pairs (*i.e.* the number of times two A's occupy the nearest neighbor sites) in a particular configuration be denoted by N_{AA}. Similarly, one can define N_{BB}, N_{AB} and N_{BA}. These numbers obey the sum rules

$$N_A = N_{AA} + N_{AB} = N_{AA} + N_{BA}, \qquad N_B = N_{BA} + N_{BB} = N_{AB} + N_{BB} \quad \text{(D.2)}$$

where N_A and N_B are the total number of particles of type A and type B, respectively. Note that the four pair numbers obey three independent equations, leaving one single free quantity. It is convenient to take the latter as being the Hamiltonian in Eq. D.1. The pair numbers N_{AA}, N_{BB}, N_{AB} can be expressed in terms of $\mathcal{H}$ and the particle numbers N_A and N_B:

$$\begin{aligned} N_{AA} &= \tfrac{1}{4}(3N_A - N_B - \mathcal{H}/J) && \text{(D.3)}\\ N_{BB} &= \tfrac{1}{4}(3N_B - N_A - \mathcal{H}/J) && \text{(D.4)}\\ N_{AB} &= N_{BA} = \tfrac{1}{4}(N + \mathcal{H}/J) && \text{(D.5)} \end{aligned}$$

The quantity N_A can be rewritten as

$$N_A = \frac{1}{2}\sum_n (1 + s_n) = \frac{N}{2}(1 + \langle s_1 \rangle) \quad \text{(D.6)}$$

N being the system size. Here, and in the following the angular brackets $\langle ... \rangle$ denote spatial averaging for a fixed generic configuration $\mathcal{C}$. Then the pair numbers and the Hamiltonian read

$$\begin{aligned} N_{AA} &= \tfrac{N}{4}(1 + 2\langle s_1 \rangle + \langle s_1 s_2 \rangle), \quad & N_{BB} &= \frac{N}{4}(1 - 2\langle s_1 \rangle + \langle s_1 s_2 \rangle) && \text{(D.7)}\\ N_{AB} &= N_{BA} = \tfrac{N}{4}(1 - \langle s_1 s_2 \rangle), & \mathcal{H} &= -NJ\langle s_1 s_2 \rangle. && \text{(D.8)} \end{aligned}$$

Now, the total exit rate $W_{out}(\mathcal{C})$ from a generic configuration $\mathcal{C}$ to any other configuration $\mathcal{C}'$ can be read off off from table D.1:

$$W_{out}(\mathcal{C}) = w_{AA} N_{AABA} + w_{AB} N_{AABB} + w_{BA} N_{BABA} + w_{BB} N_{BABB}. \quad \text{(D.9)}$$

A similar expression can be derived for the total entrance rate $W_{in}(\mathcal{C})$ from any other configuration $\mathcal{C}'$ to $\mathcal{C}$. Now, to express the stationary state weight $P_{st}(\mathcal{C}')$ as

$$P_{st}(\mathcal{C}') = P_{st}(\mathcal{C}) \exp(\Delta\mathcal{H}) \quad \text{(D.10)}$$

where $\Delta\mathcal{H}$ is the energy difference

$$\Delta\mathcal{H} = \mathcal{H}(\mathcal{C}) - \mathcal{H}(\mathcal{C}') \tag{D.11}$$

we must have

$$W_{in}(\mathcal{C}) = w_{AA}N_{ABAA} + e^{4J}w_{AB}N_{ABAB} + e^{-4J}w_{BA}N_{BBAA} + w_{BB}N_{BBAB}. \tag{D.12}$$

In the stationary state, we must have

$$W_{in}(\mathcal{C}) - W_{out}(\mathcal{C}) = 0 \tag{D.13}$$

for every configuration $\mathcal{C}$. In order to determine the number of independent conditions on the rates, it is convenient to rewrite the Eq.s D.9 and D.12 in terms of spin correlations, *i.e.* spatial averages of product of spin variables. This gives

$$\begin{aligned} W_{out}(\mathcal{C}) - \quad W_{out}(\mathcal{C}) &= \tfrac{N}{16}[(e^{-4J}-1)(1+\langle s_1s_2s_3s_4\rangle)R_1 + \langle s_1(s_3-s_2)s_4\rangle R_2 \\ &\quad + \left\{\langle s_1(3s_2-2s_3+s_4)\rangle + e^{-4J}\langle s_1(s_2-2s_3-s_4)\rangle\right\} R_1], \end{aligned} \tag{D.14}$$

where R_1 and R_2 stand for the following linear combination of the rates:

$$\begin{aligned} R_1 &= e^{4J}w_{AB} - w_{BA} \\ R_2 &= (1+e^{4J})w_{AB} + (1+e^{-4J}) - 2(w_{AA}+w_{BB}). \end{aligned} \tag{D.15}$$

This condition therefore gives two linear relations

$$R_1 = R_2 = 0. \tag{D.16}$$

Let us choose the time unit by setting

$$w_{AA} + w_{BB} = 1 \tag{D.17}$$

This gives

$$\begin{aligned} w_{AA} = \frac{1}{2}, &\qquad w_{AB} = \frac{1}{1+e^{4J}} \\ w_{BA} = \frac{e^{4J}}{1+e^{4J})}, &\qquad w_{BB} = \frac{1}{2} \end{aligned} \tag{D.18}$$

For the above choice of rates, the stationary measure is given by the Boltzmann-Gibbs measure with the Hamiltonian in Eq. D.1.

Appendix E

Algorithm for Generating Steady State Ensemble for $\epsilon = 0$

In this appendix, we describe in detail the algorithm prescribed by Angel for generating a steady state configuration for second class particles in a TASEP.

In a one dimensional periodic lattice, the sites can either be empty or occupied by a first class or second class particle. A first class or second class particle jumps to the position to its right with rate 1 if that position is empty. In addition, whenever a first class particle has a second class particle to its right, the two swap places with rate 1 (thus the second class particle may move in both directions).

The above process can be reinterpreted as follows. Non-empty sites of a graph are occupied by either a particle or an anti-particle. Each edge is chosen with rate 1. A particle (anti-particle) can move right (left) across the edge to an empty spot. In addition, a particle can exchange with an anti-particle to its right. Thus there are particles moving to the right, anti-particles moving to the left but the movements occur with rate 1 at each edge, rather than each particle. This is equivalent to the process described in the previous paragraph, with anti-particles representing empty spaces and empty spaces representing second class particles. When writing out states of the process, we will use 1's for the particles, 0's for anti-particles and $*$'s for empty spaces.

Angel has been able to construct the steady state ensemble for such a process, using a *collapsing procedure* between two sets.

E. ALGORITHM FOR GENERATING STEADY STATE ENSEMBLE FOR $\epsilon = 0$

Two sets of positions S and T (not necessarily disjoint), defined on $\mathbb{Z}$ and $\mathbb{Z}_N$ are said to collapse to a state x of the TASEP if x is the result of the following collapsing procedure: anti-particles are placed at the locations specified by T. Next, the locations in S are checked (in an arbitrary order). If a location is empty, a particle is placed there. Otherwise, a particles is placed in the nearest empty position to the left of the specified location.

For example, consider a lattice of size 10 with 3 particles and 3 anti-particles. If T is $\{5, 7, 8\}$ and S is $\{3, 4, 5\}$, then the location of anti-particles would be given by T; the particles would be at the locations $\{2, 3, 4\}$ and the empty sites are at $\{1, 6, 9, 10\}$.

The stationary measure for the exclusion process on $\mathbb{Z}_N$ with a particles and b anti-particles is the image by collapsing of the uniform measure on pairs of sub-sets S and T of the cycle of sizes a and b, respectively.

The above statement can be proved using combinatorial results on binary sequences (*i.e.* sequences made up of 1's and 0's). These sequences are related to the exclusion process under consideration since a binary sequence describes a segment with no empty site. Consider two such finite binary sequences A and B of the same length n. The sequence A is said to dominate B ($A \succcurlyeq B$) if it is possible to go from A to B by moving 1s to the right. The weight of a binary sequence A is defined as the number of binary sequences dominated by it:

$$W(A) = |\{B : A \succcurlyeq B\}|. \tag{E.1}$$

Thus, for example, $W(1010) = 5$.

Consider a state x of the exclusion process on a ring. How many pairs of sets S, T collapse to x? Since a collapsing procedure begins by placing the anti-particles at T, the unique T is given by the set of positions of anti-particles in x. There may be a number of different sets S that (together with T) collapse to the state x. In order for the collapsing procedure to reach x, it is necessary that S contains none of the empty positions of x (positions marked with $*$'s). The empty positions in x can break up the cycle into a number of segments each containing a sequence of particles (1s) and anti-particles (0's). Denote the binary sequences by $A_1, A_2, .., A_l$.

During the collapsing procedure, if an element $p \in S$ results in a particle being placed in a position q, then clearly there can be no empty position in the interval $[q, p]$, since otherwise, the particle would have been placed there instead. Thus the elements of S in each such binary segment must collapse into the positions marked by the particles in that segment. Also, for each binary segment A_i, any sequence having 1's at the elements of S in that segment is dominated by A_i. Hence there are $W(A_i)$ possibilities for the intersection of S with that segment. The total number of possibilities of the set S is therefore $\prod W(A_i)$, and the collapsed measure of the of the state x is

$$P(x) = \frac{\prod W(A_i)}{\binom{N}{a}\binom{N}{b}} \tag{E.2}$$

For example, the cyclic state $*10 * *10100 * 0101$ may be reached from

$$W(10)W(\phi)W(10100)W(0101) = 2 \times 1 \times 9 \times 2 = 36 \tag{E.3}$$

sets S and so its probability is $36/\binom{15}{5}\binom{15}{6}$.

To show the stationarity of this measure assign a mass $m(x) = \prod W(A_i)$ to each x. Let the mass flow according to the transition kernel of this process, so that when the process goes from x to y with a rate r, mass flows from x to y with a rate $rm(x)$. It is sufficient to show that the derivative of mass at any state x is zero.

Let $x \to_e y$ denote an exchange along the edge e that leads from state x to state y. The time-evolution of the mass therefore follows

$$\frac{d}{dt}m(x) = \sum_{y \to_e x} m(y) - \sum_{x \to_e z} m(x) = m(x) \sum_{y \to_e x} \left(\frac{m(y)}{m(x)} - \sum_{x \to_e z} 1 \right). \tag{E.4}$$

First consider the case when $y \to_e x$, and the end-points of e are $0*$ in x and $*0$ in y. In this case, the binary sequences in y are same as those in x, except for two. If A_i and B_i denote the binary sequences in x and y, respectively, then $A_j = B_j 0$ and $B_{j+1} = 0A_{j+1}$, where j-th and $(j+1)$-th sequences are affected by the exchange through e. Since $W(0A) = W(A)$, it follows that

$$\frac{m(y)}{m(x)} = \frac{W(B_j)}{W(A_j)} \tag{E.5}$$

where B_j is A_j with a terminating 0 removed.

Similarly, when the end-points of e are marked by $*1$ in x and $1*$ in y, then $A_j = 1B_j$ and $B_{j-1} = A_{j-1}1$. Since $W(A1) = W(A)$, we find that Eq. E.5 holds B_j being same as A_j with an initial 1 removed.

Finally, if the edge e is marked by 01 in x and 10 in y, then splitting around that edge, we have $A_j = X01Y$ and $B_j = X10Y$, with all other sequences being identical. Even in this case, Eq. E.5 holds.

Let us write $A \to B$ if it is possible to pass from A to B by either removing an initial 0, or by removing a terminating 1, or by replacing a 10 by 01 somewhere in A. Then the RHS of Eq. E.4 becomes

$$m(x)\left(\sum_{B\to A_i}\frac{W(B)}{W(A_i)} - \sum_{A_i\to C} 1\right). \tag{E.6}$$

So it is sufficient to show that for an arbitrary sequence A

$$\sum_{B\to A} W(B) = \sum_{A\to C} W(A). \tag{E.7}$$

Now, consider a pair of sequences $B \to A$, where $A = X01Y$ and $B = X10Y$. Since $B \succcurlyeq A$, any sequence dominated by A is also dominated by B. The difference $W(B) - W(A)$ corresponds to sequences that B dominates bot A does not. Such a sequence must have the form $X'10Y'$, where $X \succcurlyeq X'$ and $Y \succcurlyeq Y'$ and hence $W(B) = W(A) + W(X)W(Y)$. Substituting this in Eq. E.7 results in the following identity which can be proved by the method of induction

$$W(A) = W(X)\mathbb{1}_{A=X0} + W(Y)\mathbb{1}_{A=1Y} + \sum_{X01Y=A} W(X)W(Y). \tag{E.8}$$

If A ends (starts) with a 0 (1) the RHS gets a contribution from the first (second) term. The sum in the RHS has a term in the sum for each representation of A as $X01Y$.

References

[1] B. Schmittmann and R. K. P. Zia in *Phase Transitions and Critical Phenomena*, vol 17 eds. C. Domb and J. L. Lebowitz (Academic, N.Y.). 1

[2] N.G. van Kampen in *Stochastic Processes in Physics and Chemistry* (North Holland). 1

[3] P. Bak, C. Tang and K. Wiesenfeld, Phys. Rev. Lett. **59** 381 (1987). 2

[4] H. Takayasu, Phys. Rev. Lett. **63** 2563 (1989). 2

[5] A.-L. Barabasi and H.E. Stanley in *Fractal Concepts in Surface Growth* (Cambridge Univ. Press). 2, 13

[6] B. Derrida, E. Domany and D. Mukamel, J. Stat. Phys. **69** 667 (992). 3

[7] M. Prähofer and H. Spohn in *Progress in Probability* vol 51, ed. V Sidoravicius (Boston, MA: Birkhauser). 2

[8] D. Chowdhury, L. Santen and A. Schadschneider, Current Science **77** 411 (1999). 2

[9] R. Lipowsky, S. Klumpp and T.M. Nieuwenhuizen, Phys. Rev. Lett. **87** 108101 (2001). 2

[10] M.R. Evans, Y. Kafri, H.M. Koduvely and D. Mukamel, Phys. Rev. E **58** 2764 (1998). 3

[11] A. Kunwar *et al.*, J. Phys. Soc. Japan **73** 2979 (2004). 4, 9

[12] W.B. Russel, D.A. Saville and W.R. Schowalter in *Colloidal Dispersions* (Cambridge Univ. Press). 4

[13] J. Happel and H. Brenner in *Low Reynolds Number Hydrodynamics* (Prentice-Hall, NJ). 4

[14] S. Ramaswamy, Adv. Phys. **50** 297 (2001). 4

[15] B.I. Shraiman and E.D. Siggia, Nature **405** 639 (2000). 5

[16] E. Balkovsky, G. Falkovich and A. Fouxon, Phys. Rev. Lett. **86** 2790 (2001). 5

[17] K. Gawędzki and M. Vergassola, Physica D **138** 63 (2000). 5, 7

[18] J.M. Deutsch, J. Phys. A **18** 1449 (1985). 6

[19] M. Wilkinson and B. Mehlig, Phys. Rev. E **68** 040101(R) (2003). 6

[20] M. Wilkinson and B. Mehlig, Europhys. Lett. **71** 186 (2005). 6

[21] G. Falkovich, A. Fouxon, M.G. Stepanov, Nature **419** 151 (2002). 6

[22] A. Nagar, S.N. Majumdar and M. Barma, Phys. Rev. Lett. **94** 240601 (2005). 7, 8, 51

[23] A. Nagar, S.N. Majumdar and M. Barma, Phys. Rev. E **74** 021124 (2006). 51, 75

[24] D. Das and M. Barma, Phys. Rev. Lett. **85** 1602 (2000). 4, 7, 8, 18, 21, 42

[25] D. Das, M. Barma and S.N. Majumdar, Phys. Rev. E **64** 046126 (2001). 4, 7, 8, 18, 28, 42

[26] D. Mitra and R. Pandit, Phys. Rev. Lett. **95** 144501 (2005). 8, 49, 50

[27] A.J. Bray, Adv. Phys. **43** 357 (1994). 8, 20, 31

[28] R. Lahiri and S. Ramaswamy, Phys. Rev. Lett. **79** 1150 (1997). 3, 4, 8

[29] D. Ertaş and M. Kardar, Phys. Rev. Lett. **69** 929 (1992); Phys. Rev. E **48** 1228 (1993). 4, 9

[30] A.-L. Barabási, Phys. Rev. E **46** 2977 (R) (1992). 9

[31] D. Weihs, T.G. Mason, and M.A. Teitell, Biophys. J. **91** 4296 (2006). 9

[32] H. Oikawa and H. Nakanishi, J. Chem. Phys. **115** 3785 (2001). 9

[33] G.V. Soni *et al.*, Biophys. J. **84** 2634 (2003). 9

[34] B. Derrida, S.A. Janowsky, J.L. Lebowitz and E.R. Speer, J.Stat. Phys. **73**, 813 (1993). 10, 54, 72, 73, 91, 121

[35] E. Levine, D. Mukamel and G.M. Schütz, Europhys. Lett. **70** 565 (2005). 10, 91, 92, 94, 95, 98, 100, 101

[36] K. Mallick, J. Phys. A: Math. Gen. **29** 5375 (1996). 10

[37] E. Medina, T. Hwa and M. Kardar, Phys. Rev. A **39** 3053 (1989). 14

[38] S.F. Edwards and D.R. Wilkinson, Proc. R. Soc. London, Ser. A **381** 17 (1982). 14

[39] A.-L. Barabási and H.E. Stanley in *Fractal Concepts in Surface Growth* (Cambridge Univ. Press, New York, 1995). 15

[40] P. Meakin *et al.*, Phys. Rev. A **34** 5091 (1986). 16, 25

[41] M. Plischke, Z, Racz and D. Liu, Phys. Rev. B **35** 3485 (1987). 16

[42] G. Porod in *Small Angle X-ray Scattering*, edited by O. Glatter and L. Kratky (Academic Press, New York, 1983). 20

[43] W. Feller in *An Introduction to Probability Theory and Its Application* (Wiley, 2000). 43

[44] T.M. Liggett in *Interacting Particle Systems* (Springer, Berlin, 1985). 58, 106

[45] P.F. Arndt, T. Heinzeland V. Rittenberg, J. Phys. A: Math. Gen. **31** L45 (1998); J. Stat. Phys. **97** 1 (1999). 57, 64, 65

[46] N. Rajewsky, T. Sasamoto and E.R. Speer, Physica A **279** 123 (2000).

[47] B. Derrida, J.L. Lebowitz and E.R. Speer, Phys. Rev. Lett. **87** 150601 (2001); J. Stat. Phys. **107** 599 (2002). 61

[48] P.M. Binder, M. Paczuski and M. Barma, Phys. Rev. E **49** 1174 (1994). 65

[49] F. Hayot and C. Jayaprakash, Phys. Rev. E **54**, 4681 (1996). 38

[50] U. Frisch in *Turbulence*, Cambridge University Press (Cambridge,1995). 38

[51] J. Krug and H. Spohn in *Solids Far from Equilibrium*, vol. 1, edited by C. Godrèche (Cambridge, 1992). 70

[52] A. De Masi and P.A. Ferrari, J. Stat. Phys. **38**, 667 (1984). 70, 106

[53] M.J. Lighthill and G.B. Whitham, Proc. R. Soc. London A **229**, 281 (1955). 70

[54] G.M. Schütz in *Phase Transitions and Critical Phenomena* , vol. 19, edited by C. Domb, J.L. Lebowitz (Academic, London, 2001). 70

[55] M. Paczuski *et al.*, Phys. Rev. Lett. **69**, 2735 (1992). 71

[56] S.N. Majumdar and M. Barma, Physica A **177**, 366 (1991). 71

[57] P.A. Ferrari, C. Kipnis and S. Saada, Ann. Prob. **19**, 226 (1991). 72

[58] P.A. Ferrari and L.R.G. Fontes Prob. Theory Related Fields **99**, 305 (1994). 74

[59] C. Boutillier *et al.*, J. Phys. A: Math. Gen. **35**, 9703 (2002). 74, 79, 81, 82

[60] O. Angel J. Comb. Theory, Ser.A **113**, 625 (2006). 76

[61] B. Derrida and M.R. Evans J. Phys. A: Math. Gen. **32**, 4833 (1999). 76

[62] H.van Beijeren J. Stat. Phys. **63**, 47 (1991). 72, 78

[63] S. Gupta *et al.* cond-mat/070346. 72

[64] K. Mallick, J. Phys. A: Math. Gen **29**, 5375. 79, 81

[65] T. Sasamoto, Phys. Rev. E **61** 4980 (2000). 79, 80

[66] S. Katz, J.L. Lebowitz, H. Spohn, J. Stat. Phys. **34** 497 (1984). 85, 86

[67] J.S. Hagger *et al.*, Phys. Rev. E **63** 056110 (2001). 86

[68] J.M. Luck and C. Godrèche, J. Stat. Mech. P08009 (2006). 125

[69] Y.Kafri *et al.*, Phys. Rev. E **68**, 035101(R) (2003). 86, 88, 97, 100

[70] M.R. Evans, Brz. J. Phys. **30**, 42 (2000). 87

[71] M.R. Evans *et al.* Eur. Phys. J. B **41**, 223 (2004). 88, 100, 101

[72] Y. Kafri *et al.* J. Phys. A: Math. Gen. **35**, L459 (2002). 88

[73] A. Rakos *et al.* J. Stat. Mech P11001 (2006). 91, 92, 94, 98, 100, 101

[74] M. Barma, J. Phys. A: Math. Gen. **25** L693 (1992). 108, 109